ANKARA YILDIRIM BEYAZIT UNIVERSITY

GRADUATE SCHOOL OF NATURAL AND APPLIED SCIENCES

GROWTH AND CHARACTERIZATION OF UNDOPED AND INDIUM DOPED ZINC OXIDE THIN FILMS GROWN BY HYDROTHERMAL METHOD

M.Sc. Thesis by

Tuğçe BAYRAKTAR

Department of Materials Engineering

August, 2020

ANKARA

GROWTH AND CHARACTERIZATION OF UNDOPED AND INDIUM DOPED ZINC OXIDE THIN FILMS GROWN BY HYDROTHERMAL METHOD

A Thesis Submitted to
The Graduate School of Natural and Applied Sciences of
Ankara Yıldırım Beyazıt University
In Partial Fulfillment of the Requirements for the Degree of Master of Science
in Materials Engineering, Department of Material Engineering

by
Tuğçe BAYRAKTAR

August, 2020
ANKARA

M.Sc. THESIS EXAMINATION RESULT FORM

We have read the thesis entitled **"GROWTH AND CHARACTERIZATION OF UNDOPED AND INDIUM DOPED ZINC OXIDE THIN FILMS GROWN BY HYDROTHERMAL METHOD"** completed by **Tuğçe BAYRAKTAR** under supervision of **Prof. Dr. Aytunç ATEŞ** and we certify that in our opinion it is fully adequate, in scope and in quality, as a thesis for the degree of Master of Science.

Prof. Dr. Aytunç ATEŞ

(Supervisor)

Prof. Dr. Selim ACAR

(Jury Member)

Assoc. Prof. Ramazan KARSLIOĞLU

(Jury Member)

Prof. Dr. Ergün ERASLAN

(Director)

Graduate School of Natural and Applied Sciences

ETHICAL DECLARATION

I hereby declare that, in this thesis which has been prepared in accordance with the Thesis Writing Manual of Graduate School of Natural and Applied Sciences,

- All data, information and documents are obtained in the framework of academic and ethical rules,
- All information, documents and assessments are presented in accordance with scientific ethics and morals,
- All the materials that have been utilized are fully cited and referenced,
- No change has been made on the utilized materials,
- All the works presented are original,

and in any contrary case of above statements, I accept to renounce all my legal rights.

Date: **Signature:**

Name & Surname: Tuğçe BAYRAKTAR

ACKNOWLEDGEMENTS

I would like to express my sincere thanks to my supervisor Prof. Dr. Aytunç ATEŞ for his guidance, advices and supports. I am grateful to him for sharing his knowledges and experiences with me from the beginning to the end of this project. It has been a pleasure for me to work with him.

I would like to state my gratefulness to Prof. Dr. Selim ACAR from Gazi University, because of his kind help, patience and enabling me to use his laboratory facilities. I also would like to thank Dr. Sezen TEKİN and Dr. Ahmet KARATAY from Ankara University for providing an opportunity to use the laboratory for photoluminescence measurement. I owe a thank to R.A. Semih Ağca and R.A. Bahadır AYDAŞ for their cooperation for the XRD and SEM measurements.

I am also thankful to my labmate and project partner İrem Ayça YILDIZ for her all support and warm partnership for two years.

Last, but not least, I would like to express my deepest gratitude my mother, brother and late father who gave me strength in every moment of my life.

July 2020 **Tuğçe BAYRAKTAR**

GROWTH AND CHARACTERIZATION OF UNDOPED AND INDIUM DOPED ZINC OXIDE THIN FILMS GROWN BY HYDROTHERMAL METHOD

ABSTRACT

Zinc oxide is a widely used semiconductor metal oxide in optoelectronic applications and it is very advantageous material for transparent conductive oxides (TCO). Recently, to investigate and enhance the properties of ZnO thin films, researchers have been carrying out many researches. In this study, undoped ZnO and indium doped ZnO (IZO) films with different indium percentages (1%, 3%, 5%, 7%) were produced by hydrothermal method on glass substrates. The influence of In doping on the structural, surface and optical properties of ZnO films were investigated. On the other hand, as the parameters of hydrothermal method; growth time, growth temperature effects on the properties of the ZnO and In doped ZnO film were analyzed. For this purpose, the growth time of ZnO films were changed as 3h, 5h, 7h, 9h and 24h. Also, growth temperatures were varied as 90℃, 120℃ and 150℃ too. After the film growth process X-Ray Diffraction (XRD), Scanning Electron Microscopy (SEM), Photoluminescence Spectroscopy (PL) and UV-VIS Spectroscopy measurements were carried out to characterize films' structural, optical, and surface properties. By these characterization methods, the best growth parameters of the films were decided. According to characterization results, all the ZnO and IZO films successfully were grown by hydrothermal method. Hexagonal wurtzite structure and well adhesion to substrate were observed. For the crystallite size, XRD intensity at preferred growth plane, dislocation density and microstrain, a good compromise was reached for 9h growth time, 3% In percentage, and 90°C growth temperature. From the PL, the lowest defect and highest crystallization quality were obtained for 3% In, 9h and 90°C films. As a result, for this work, 9 h growth time, 90°C growth temperature and 3% In doping concentration were defined as the best growth parameters.

Keywords: ZnO, IZO, Films, Doping, Hydrothermal Method, Characterization

KATKISIZ VE İNDİYUM KATKILI ÇİNKO OKSİT İNCE FİLMLERİN HİDROTERMAL METOT İLE BÜYÜTÜLMESİ VE KARAKTERİZASYONU

ÖZ

Çinko oksit optoelektronik uygulamalarda çokça kullanılan bir yarıiletkendir ve şeffaf iletken oksit (TCO) olarak oldukça avantajlı bir malzemedir. Son zamanlarda, araştırmacılar ZnO ince filmleri incelemek ve özelliklerini geliştirmek adına, birçok araştırma yürütmektedirler. Bu çalışmada katkısız ZnO ve farklı oranlarda katkılanmış (%1, %3, %5, %7), indiyum katkılı ZnO (IZO) filmler cam alt taş üzerinde hidrotermal metot ile üretildi. İndiyum katkısının, ZnO filmlerin yapısal, yüzey ve optik özelliklerine etkisi incelendi. Bunun yanı sıra, hidrotermal metodun parametreleri olan, büyütme süresin ve büyütme sıcaklığının ZnO ve IZO filmlerin özelliklerine olan etkisi analiz edildi. Bu amaç ile, ZnO filmlerin büyütme süreleri 3h, 5h, 7h, 9h ve 24h olarak değiştirildi. Ayrıca, büyütme sıcaklıkları da 90℃, 120℃ and 150℃ olarak değiştirildi. Film büyütme işleminden sonra, filmlerin optik, yapısal ve yüzey özelliklerinin karakterizasyonu için X-Işını Difraktometresi (XRD), Taramalı Elektron Mikroskopisi (SEM), Fotolüminesans spektroskopisi (PL) ve Ultraviyole-Görünür Işık (UV-Vis) absorpsiyon spektroskopi ölçümleri uygulandı. Bu Karakterizasyon metotlarıyla filmler için en uygun büyütme parametreleri belirlendi. Karakterizasyon sonuçlarına göre, tüm ZnO ve IZO filmler hidrotermal metot kullanılarak başarıyla üretildi. Hekzagonal vürtzit yapı ve alt taşa iyi yapışma gözlemlendi. Kristalit büyüklüğü, büyüme düzlemindeki XRD şiddeti, dislokasyon yoğunlıuğu ve mikro gerinim değerleri göz önüne alındığında, en iyi uzlaşmaya 9h büyüme süresi, %3In yüzdesi ve 90°C büyütme sıcaklığında ulaşıldı. PL sonucuna göre, en düşük kusur ve en yüksek kristalleşme kalitesi %3In, 9h ve 90°C filmlerde elde edildi. Sonuç olarak, bu çalışma için en iyi büyütme parametreleri, 9h büyütme süresi, 90°C büyütme sıcaklığı ve %3 In katkılama yüzdesi olarak bulundu.

Anahtar Kelimeler: ZnO, IZO, Film, Katkılama, Hidrotermal Metot, Karakterizasyon

CONTENTS

ABBREVIATIONS

Acronyms

CVD	Chemical Vapor Deposition
DI	Deionized
FWHM	Full Width at Half Maximum
HMTA	Hexamethylenetetramine
IDLE	Intensity of Deep Level Emission
ITO	Indium Tin Oxide
IUV	Intensity of Ultraviolet Emission
IZO	Indium Doped Zinc Oxide
MBE	Molecular Beam Epitaxy
MOCVD	Metal Organic Chemical Vapor Deposition
NBE	Near Band Emission
NFs	Nanofibers
NIR	Near Infrared
NPs	Nanoparticles
NRs	Nanorods
NWs	Nanowires
PL	Photoluminescence
PLD	Pulsed Laser Deposition
SEM	Scanning Electron Microscopy
SILAR	Successive Ionic Layer Adsorption and Reaction
TCO	Transparent Conductive Oxides
TEM	Transmission Electron Microscopy
TFs	Thin Films
UV	Ultraviolet
UV/ VIS	Ultraviolet-Visible Spectroscopy
XPS	X-ray Photoelectron Spectroscopy
XRD	X-Ray Diffraction
ZnO	Zinc Oxide

LIST OF TABLES

LIST OF FIGURES

LIST OF SYMBOLS

d	Distance Between the Layers
D	Grain Size
δ	Dislocation Density
ε	Micro Strain
2θ	Diffraction angle
nm	Nanometer
α	Absorption Coefficient
n	Refractive Index
ε_∞	High Frequency Dielectric Constant
$\varepsilon_\circ$	Static Dielectric Constant
$S\rho$	Film Density
β	Full Width at Half Maximum
h	Hour

CHAPTER 1

INTRODUCTION

1.1 ZnO Thin Films

Metal oxide semiconductors have been very popular in optoelectronic applications and researches due to their advantageous electrical and optical properties. Zinc Oxide (ZnO) is one of the attractive metal oxides which can be used as alternative material for transparent conductive oxide thin films [1].

1.1.1 Structure and Properties of ZnO

Zinc oxide (ZnO) is a semiconductor material, as in most of II-IV group binary compounds and its ionicity exist between ionic and covalent semiconductor. Its stable preferential orientation is along to c-axis which resulted in rod shape. ZnO has a tetrahedral bonding configuration. In the structure, each cation is surrounded by four anions at the corners of a tetrahedron, and each anion enclosed by four cations. A typical sp3 covalent bonding is shown in these tetrahedral structures [2]. Besides, ZnO exhibits large ionicity, this situation increases the energy bandgap more than expected from the covalent bonding.

Although its thermodynamically stable phase is wurtzite at ambient conditions; ZnO has three different crystal structures like, hexagonal wurtzite, zinc blend and salt rock. The possible three crystal structures of ZnO is shown in Figure 1.1. The wurtzite crystal structure of ZnO has a hexagonal unit cell and two lattice parameters which are *a* and *c*. The ration of lattice parameters is $c/a=1.633$.

The existence of intrinsic defects like O vacancies and Zn interstitials causes a deviation of stoichiometry. Due to this deviation, wurtzite structural ZnO is naturally an n-type semiconductor. Even though ZnO shows n-type behavior in intrinsic state, it is possible to convert it to p-type by controlling the doping level and defect [3,4].

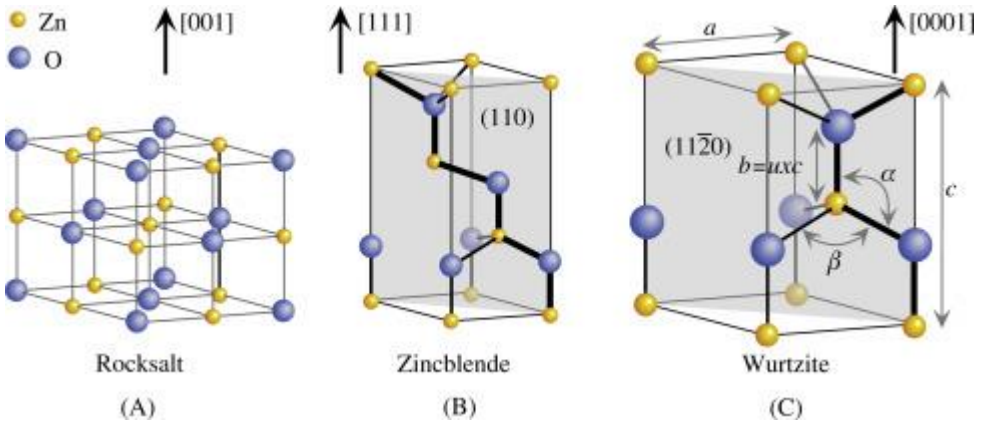

Figure 1. 1 Different crystal structures of ZnO [4]

ZnO has become an excellent material, because of its wide and direct band gap (3.37 eV) also massive excitonic binding energy (60 meV) at room temperature [5,6].

ZnO shows high transparency in visible range where the transmittance is nearly 80-90%. They can show also low electrical resistivity nearly 10^{-5}- 10^{-3} Ω.cm [7,8].

Moreover, ZnO can be produced in several structures and shapes as like nanoparticles (NPs), nanowires (NWs), nanofibers (NFs), nanorods (NRs) and thin films (TFs). ZnO TFs have many outstanding properties such as conductivity, low cost, electron mobility, and high transparency [9,10].

1.1.2 Application of ZnO Films

As a transparent conductive oxide, ZnO is well known and widely used semiconductor. Due to its conductive and transparent properties, it used in industry as transparent electrodes, touch screens, thin film solar cells and low emissivity coatings etc. Besides its well electrical and optical properties, it is an alternative material to ITO material with its high abundancy, low cost, and nontoxicity [11-13].

High refractive index and transparency in visible region allows the ZnO films to be antireflection coating, and window layer in solar cells [14].

In addition to high transmittance in the visible range, their low electrical resistivity makes them important in the optoelectronic devices and photovoltaic conversion field [8]. Besides excellent optical and electrical properties, ZnO also non-toxic, suitable to doping, stable at high chemical, mechanical [15] and high thermal [16] and low-cost material [15]. Depending on these features, it is suitable for optoelectronic applications, [17], varistors [18], light emitting diodes [19], nano lasers [20], heat mirrors [21], gas sensors [22] and acoustic wave filters [23].

1.2 IZO Films

Nowadays, Researchers have been working on n-type transparent oxide semiconductors and TCOs materials which have excellent properties. Investigation and fabrication of ZnO based films started to gain importance due to their properties and became candidate material for transparent conductive oxides (TCO). For the use of ZnO in optoelectronic devices and transparent electrode, high electrical conductivity and optical transparency in visible region are expected [24]. Doping of ZnO with different elements is a method to improve electrical and optical property, conductivity and also photoluminescence (PL) properties of the ZnO films. Thank to doping of ZnO film, alternative materials for TCO may be produced [7]. Multi-component oxide, ternary and quaternary systems like indium doped zinc oxide (IZO) may be a potential alternative to TCO. IZO have been researched for not only TCO materials but also for transparent electrodes, semiconducting oxide layer for thin film transistors, and solar cells [25]. IZO have advantage over the conventional TCO like tin oxide and indium tin oxide. ZnO based thin films are stands out among the others with high abundancy, low cost, non-toxicity and hydrogen plasma stability [26,27].

With the addition of impurities and different ions into the crystal lattice of wide band gap semiconductor, the structural, electrical, and optical properties of can be altered. ZnO doping process is carried out by replacing Zn 2+ ions with higher valency ions. The ionic radius and electronegativity are the parameters that affect the efficiency of doping process [28].

With the different oxidation condition, ZnO conductivity range changes. By doping the ZnO films with group II, III and VII elements like Indium (In), Cadmium (Cd), Aluminum (Al), Fluorine (F), Copper (Cu), etc., conductivity, stability and transparency of ZnO film can be increased [29-30].

A decrease of excitation intensity in the ZnO nanostructures may be seen with the sufficient amount doping. This is because of the increase in the number of shallow states. For this purpose, researchers work at doping the ZnO nanostructures by various impurities like In, Al, Ga, Sn, Sb, and Cu [31].

Recently, for the doping of ZnO, basically group III elements are used. The opinion is that, group III elements like indium (In) have lower vapor pressure than group IV elements for substitutional doping on the oxygen lattice site [32].

Besides electrical and optical properties, indium (In) doping dominates UV and visible emission. According to Jie et al. (2004) [33], with the indium doping of ZnO nanobelts, the UV and Visible emission shifted toward higher wavelength and this phenomenon is defined by bandgap energy decreasing and existence of extrinsic or intrinsic defects. Exciton emission peak of indium doped ZnO nanowires which prepared by Xu et al. (2006) [34], showed red shifting because of indium doping. It is explained by decrease of band gap energy again. On the other hand, when Liu et al. (2006) [35] noticed that the bandgap energy of indium doped ZnO disk increased and the exciton emission peak shifted to blue; Pál, E et al. (2009) showed that band gap energies of In doped, prism-like and flower-like ZnO decreased and visible emission peaks shifted blue with increasing indium concentration [36].

1.3 Thin Film Growth Methods

Thin film is a layer of material on a substrate whose thickness changes from several nanometer to few micrometers. According to the material nature and deposition condition, the structure of thin film can vary such as amorphous and polycrystalline [37]. Also, all properties of thin film can be alternated by deposition process. In other word, optical, electrical, tribological properties, microstructure and surface morphologies are highly affected from deposition methods [38]. To get the properties which expected from the film, choosing the proper growth method is very important [39].

Thin film deposition method divided into two main categories which called as chemical deposition and physical deposition [40].

Physical film production methods based on moving of particle and gathering on the substrate. Physical film production methods are predicated on just physically moving of particle and depositing on a substrate [41]. A target is used as the source of thin film and with an energy, materials dislodged and moved onto substrate surface at which point the atoms stick and form a film. On the other hand, in chemical film deposition method, a chemical reaction of film precursor happening on the substrate surface is expected [42].

Nanostructured ZnO TFs have been grown by several methods like sputtering [43] metal organic chemical vapor deposition (MOCVD), electrochemically [44], spray pyrolysis [45], molecular beam epitaxy [46], pulsed laser deposition [47], the sol-gel method [48], optical thermal evaporation, hydrothermal synthesis, Successive Ionic Layer Adsorption and Reaction (SILAR) [3] etc. The wide classification of thin film deposition methods is given in Figure 1.2.

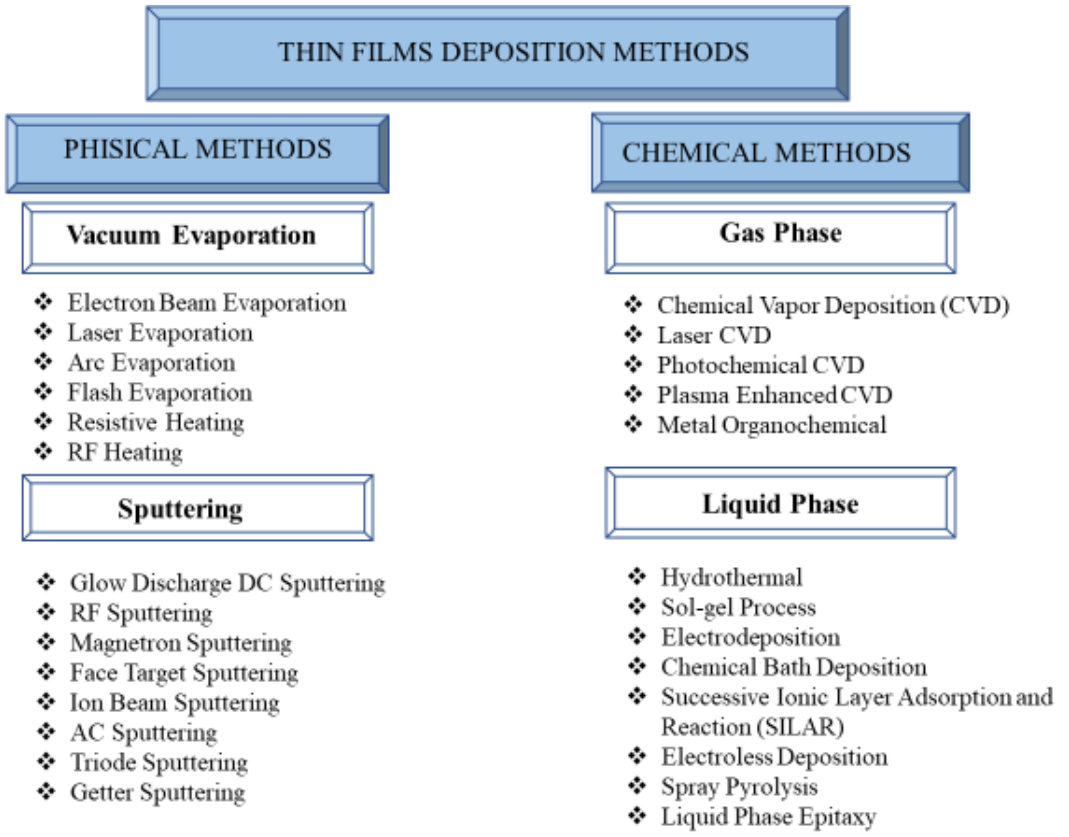

Figure 1. 2 Wide classification of thin film deposition methods

High quality ZnO crystals and large area growth is important for device application. According to reports, ZnO deposition by magnetron sputtering [49] and chemical vapor deposition (CVD) growth techniques [50]; achieved mainly polycrystalline films. Fallowing studies showed that films grown by rf magnetron sputtering [51], molecular-beam epitaxy (MBE) [52], pulsed-laser deposition (PLD) [53], and metalorganic chemical-vapor deposition (MOCVD) [54] led to single crystal and high-quality ZnO films. In addition to that, these techniques allow good deposition procedure control. The diagram of material processing techniques according to temperature and pressure is shown in Figure 1.3.

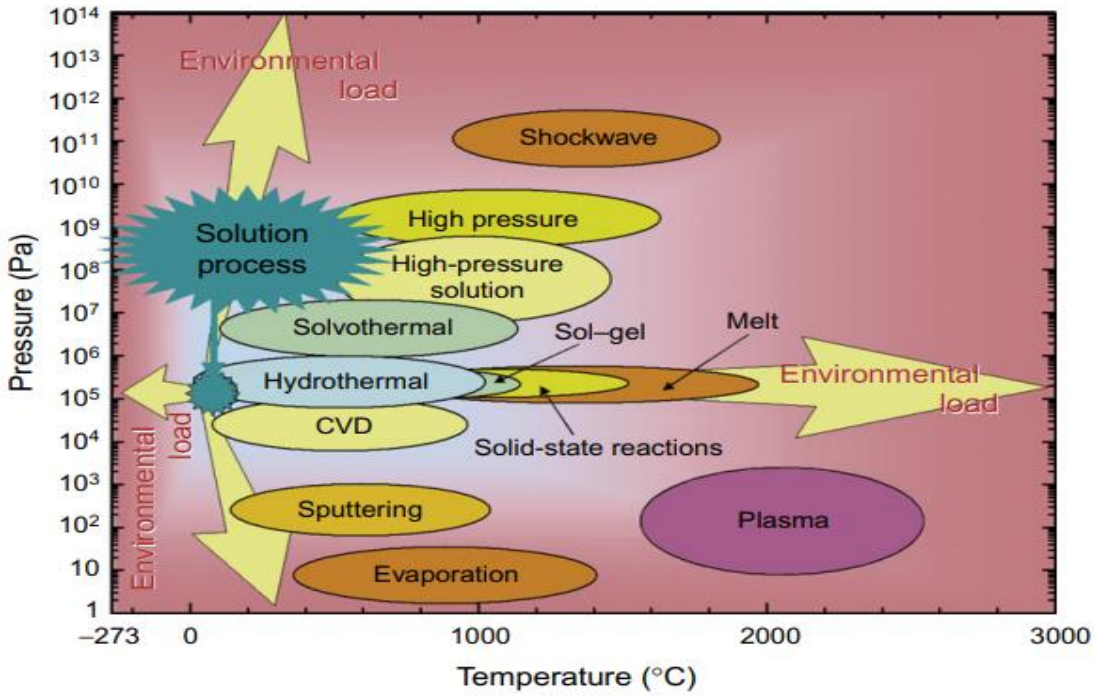

Figure 1. 3 Pressure - Temperature map of materials processing techniques [55]

Hydrothermal method is one of the main film deposition technique to perform bulk ZnO crystal growth. This method has advantage over the melt growth and vapor phase methods by large single crystal ability. Because of the high vapor pressure of melt growth and vapor phase method, they show some challenges in the growth process of ZnO. High vapor pressure causes difficult process control and poor ZnO growth. On the other hand, in hydrothermal reaction, low supersaturation promotes crystal growth. Thus, hydrothermal method is notably proper to ZnO growth for large size and single crystal applications [3].

1.4 Hydrothermal Method

1.4.1 Definition of Hydrothermal Method

Hydrothermal synthesis is one of the substantial branches of inorganic synthesis which allows producing nanomaterials with different structures. Hydrothermal method is used for not only synthesis and growth of material but also treatment of waste [56].

Although it has not definite definition, it explained as a heterogenous reactions to solve and crystallization of materials at high pressure and temperature [57].

Nowadays, the hydrothermal synthesis is described by scientists as heterogenous reaction that occur in a closed system at a temperature which higher than room temperature and 1atm pressure [58].

While Laudise (1970) says the hydrothermal synthesis was a growth reaction that happening in aqueous solution under normal conditions, Rabenau (1985) says this reaction occurred at 1bar pressure and higher than 100℃ [59,60]. Byrappa (1992) defined it as heterogeneous reaction in an aqueous solution which is performed temperatures higher than room temperature and higher 1atm pressure [61]. Also, according to Yosimura et al. (1994) hydrothermal synthesis is a reaction occurring in aqueous media in a closed system at above 100℃ and 1 atm pressure [62].

Hydrothermal synthesis required solution above room temperature and pressure which is closed and heated to synthesis by chemical reactions. Hydrothermal synthesis research began in the middle of the 19th century. After long research, hydrothermal synthesis was obviously outlined as an important materials synthesis technology, especially for single crystal growth, in the 20th century [58].

According to researches, by using hydrothermal method, it is possible to growth ZnO nanorods and nanowires on a substrate [63], patterning [64] and doping with transition metals [65] and changing the growth and physical directions [66].

In hydrothermal synthesis, water is indispensable and act as transformation element of materials. According to the water phase diagram in Figure 1.4, at below of 100℃, the equilibrium vapor pressure of water is lower than 1bar. On the other hand, at higher temperatures, hydrothermal pressure range is more suitable.

Hydrothermal process can be classified into two operation modes: autogenous and high-pressure mode. In the autogenous mode there is no external pressure and the pressure is

provided by the present gas in equilibrium. The pressure of the closed system is due to the temperature. As is seen in the equilibrium line of gas and liquid in Figure 1.4, with the increasing temperature, the gas pressure is increases. In the high-pressure hydrothermal mode, in contrast to autogenous, there is an external pressure which is higher than the equilibrium water vapor pressure. Generally inorganic materials become more soluble under high pressure. As a sum up, in hydrothermal synthesis the effective three parameters are; water pressure, temperature and reaction time [67,68].

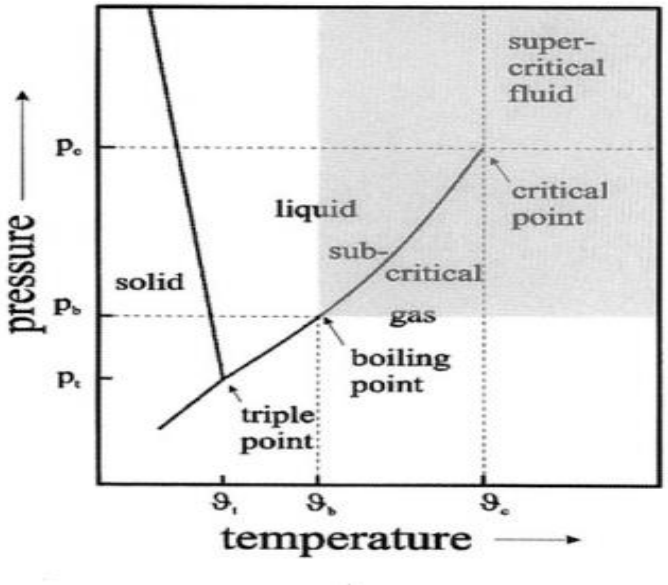

Figure 1. 4 Phase diagram of water [68]

1.4.2 Advantages of Hydrothermal Method

For the processing of advance materials, hydrothermal method provides superb opportunity with its outstanding advantages. By this method, wide range advance materials from bulk single crystals to fine particles and nanoparticles can be processed and high-quality crystals can be obtained.

Hydrothermal method is a low energy consuming, low temperature, and single step production method. With the enablement to in situ fabrication, size, and morphology

control and not to need post synthesis treatment, it is prominent production method. Also, it does not require expensive surfactants, catalyst, or seeds.

The other important advantage of hydrothermal method is the ability of combining with an external energy like microwave, sonar, or mechanochemical, electrical and magnetic. That process is called as multi energy processing [69].

The most significant superiority of hydrothermal method is being environmentally friendly. Because of consuming less energy, wasteless processing (solid, liquid or gas), using nonhazardous materials and closed processing system, hydrothermal method is a green technology [70].

As a sum up, hydrothermal synthesis method has advantages over deposition methods with its low reaction temperature (less than 200°C), simple equipment, high purity, high crystal quality, nontoxicity, hybridizability, low cost, environmentally friendly, ability to control morphology, size and deposit on a three-dimensional structure [69,71].

1.4.3 Components and Apparatus of Hydrothermal Method

Hydrothermal is a technique to dissolve and recrystallize materials under some conditions. This heterogeneous reaction is happening in an aqueous media which involve solvents and mineralizers. The required conditions for hydrothermal synthesis are high temperature and pressure. To provide these conditions used components and apparatus are mineralizer, surfactants, water, autoclave, and liners.

1.4.3.1 Mineralizer

The main expectation from a solvent is to present a medium which provide suitable environment. Solvent also can work as absorber or reactant in hydrothermal reaction. By using proper solvent, the solubility of the materials can be increased so, material synthesis, crystal growth or materials processing can be performed. In hydrothermal, water is the most important solvent and mineralizer. Whereas, even at supercritical temperature, some

compounds can not dissolve in water. Hence, researchers investigated different favorable mineralizers [72].

1.4.3.2 Water

In hydrothermal method, water is foremost constituent. Water shows incomparable properties which used for decomposing toxic organics, recycle and treat waste materials. These properties of water become more unique under supercritical conditions.

Water is used to transform the precursor material in hydrothermal synthesis. It solves most of organic substance at high temperatures and pressures. The dissolved materials in fluid starts to crystallization and material transformation is completed [55,68].

1.4.3.3 Surfactants

In the processing of advance materials by hydrothermal method, the surfactants play important role. Surfactants help to control of the nucleation, crystal growth, crystal size, morphology, shape, and phase homogeneity. It also enhances the surface of materials, disperses the fine particles along the crystallization. Due to this qualification, it called as surface modifier and prompt to produce good dispersed and oriented materials in nanotechnology [55].

In the hydrothermal synthesis process, structures tend to have different sizes and irregular morphology due to high reaction rate. Therefore, by using proper chemical additives like surfactants, the reaction process is taken under control [73]. Hexylamine, butylamine, ethylenediamine and trimethylamine are amin molecules which used for synthesis of ZnO nanostructures [74,75].

Hexamethylenetetramine (HMT) is also a surfactant which used to modify the morphology of nanostructure in the thin film [76].

With the increasing HMT concentration size and diameter of nanorods decreases, hexagonal shape of ZnO shifts to circular shape, grain size decreases and dense growth

occur. Correspondingly, blue shift in UV emission peak, and increasing on the absorbance edge in UV-Vis spectra and a rise in electrical resistivity can be observed [77].

1.4.3.4 Autoclave

Hydrothermal method requires a pressure vessel called as autoclave (in Figure 1.5). Autoclave must withstand to highly corrosive solvents at high pressure and temperature for crystal growth and material processing. These following properties are expected from autoclave:

- Durability to acids, oxidizing agents, and bases.
- Durability to high temperature and pressure for a long time.
- Convenience assemble and disassemble.
- Suitable length to get temperature gradient.
- Impermeability at desired temperature and pressure

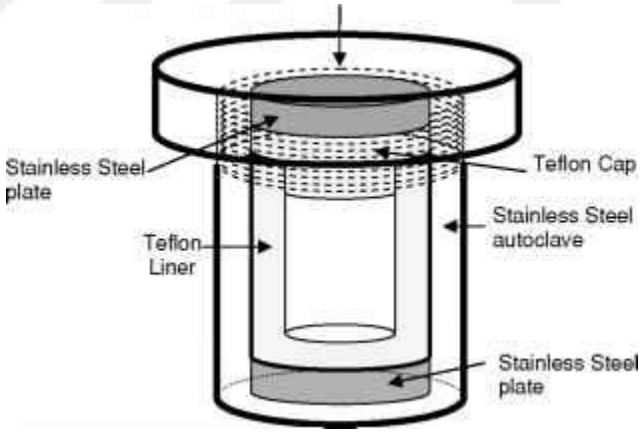

Figure 1. 5 The illustration of autoclave of hydrothermal

For the selection of ideal autoclave, corrosion resistance, experimental pressure and temperature are the prominent parameters. Especially, when the vessel directly used for reaction chamber without using any liner, corrosion resistance factor becomes more serious. Mostly used materials for the autoclave are stainless steel, iron, titanium, nickel,

high strength alloys, cobalt based superalloys, and titanium alloys due to high corrosion resistance properties.

The other critical factors of autoclave materials are ultimate tensile strength, creep rupture strength, and yield strength. The creep rupture strength shows a dramatic decrease with increasing temperature during operation. Although stainless steel - SS 316 has best creep rupture strength and good choice for autoclave material, super alloys are generally stronger than at elevated temperature [78].

1.4.3.5 Liner

In the hydrothermal method, used mineralizers are very corrosive and they generally attack to autoclave. This situation hinders to obtain high quality crystals for advance devices. To prevent this problem, a proper liner is placed into the autoclave. Some metal like silver, copper, nickel, titanium liners can be used as lining according to solvent media, but it is possible to dissolve at higher temperature or at unproper solvent. For alkaline and neutral media noble metal liners can be used. In addition, quartz glass, Pyrex and Teflon are the other mostly used liner materials. The mostly used materials for reactor lining is given in the Table 1.1.

As crystals with high purity are grown in strong corrosive media, Teflon liners or bakers are used. Teflon material is very popular in hydrothermal application as a lining material at below 300 ℃ and 250 bars. The Teflon liner/ baker should be placed into the autoclave strictly without any gap. There are two biggest disadvantages of Teflon liners;

- It is difficult to measure the actual temperature inside liner because there is an obvious temperature decrease in it when compared to vessel without liner.
- Above the 300 ℃, it starts to dissociate and changes the pH of unbuffered solution in it so, it is not suitable at above this temperature [78].

Table 1. 1 The materials used for reactor lining [78]

MATERIAL	T (°C)	SOLUTIONS	REMARKS
Titanium	550	Chlorides, Sulphides, Sulphates, Hydroxides	• Corrosion in NaOH solution
Silver	600	Hydroxides	• Gradual recrystallization • Partial dissolution
Teflon	300	Chlorides, Hydroxides	• Poor thermal conduction
Copper	450	Hydroxides	• Corrosion reduced in the presence of fluoride ions and organic compound
Graphite	450	Sulphates	• Pyrolytic graphite most suitable for lining
Platinum	700	Hydroxides	• Blackening in chloride in the presence of sulpher ion

1.4.3.6 Substrates

Substrate is a base for thin film, and it is required for embodying the film, to provide mechanical endurance and rigidity. For the successful growth of thin film, flatness and smoothness is expected from the substrate materials. Glass, silicon, alumina, aluminum nitride and metals are mostly used substrate for the semiconductor thin film. Deposition on glass is generally preferred for easy measurement of the optical and electrical properties of thin film. In addition, glass substrate is quite economic when compared the others [79,80].

1.4.4 Growth Parameters of Hydrothermal Method

Hydrothermal synthesis method has variety of parameters which affect the properties of grown films. These growth parameters are concentration of the precursor solution, synthesis temperature, growth time, pH of the precursor. Growth rate of particles, crystal

structure, nanoparticle size, nanoparticle density, morphology, optical properties, aspect ratio and orientation are powerfully influenced from the hydrothermal synthesis parameters [81-83].

1.4.4.1 Precursor concentration

There is no doubt about the precursor concentration has an effect on aspect ratio, morphology and the growth rate of nanostructure because, precursor solution works as Zn^{+2} ion source for production of ZnO nanostructure in hydrothermal method [82,84,85].

Wang et al. (2008) and Lee et al. (2007) reported that the increasing precursor and reactant concentration caused increase at average length and diameter of synthesized nanorods [86,87].

Gou et al. (2005) also worked on concentration effect on the structure of ZnO nanorods. They reported that the decreasing concentration caused a nonlinear decrease on the average diameter of ZnO nanorods [81].

According to Bian et al. (2010), when the concentration of precursor was high, the average length of ZnO rods decreased and diameter increased. Also, rods showed uniform distribution on the substrate [85].

H.Q. Le et al. (2006) changed the zinc acetate concentration to observe the precursor effect. When the concentration increased, the diameter of the nanorods shrank and length increased. In addition, aspect ratio increased but density decreased when the concentration increased from 0.01 to 0.33M [84].

Some researchers observed that, diameter of hexagonal nanorods are strongly affected from the precursor concentration. They remarked that the average diameter of rod decreases with diminishing precursor concentration. Nonetheless, this relationship was not linear. This nonlinear relationship was associated with the existence of more nucleation sites when the precursor concentration is high. Thermodynamically, in higher concentration, extra nucleation sites come into existence. Nevertheless, after some point

the relationship changes by reversal. The density starts to decrease while the concentration increases due to lateral growth of rods. Moreover, with the precursor concentration, growth rate of ZnO rods go up not only laterally but also longitudinally [81,83,84,88].

1.4.4.2 Growth Time

Growth time strongly affects the morphology and aspect ratio and optical properties of zinc oxide nanorods in hydrothermal synthesis method. Li et al. (2010) produced hexagonal ZnO nanorods at different growth time. When the growth time increased from 3hours to 5hours, they observed an increasing in the rod size however, they did not observe significant change for 7h and 9h growth time [85].

Akhiruddin et al. (2014) reported that, with the increasing growth time in hydrothermal method, the crystal size of ZnO film and the bandgap energy increased but grain size of particles decreased [89].

Baruah et al. (2009) thought that, at low temperature (~ 95℃) hydrothermal process, growth rate reaches its maximum in the first 5hours, after that time it starts to decrease. [90] According to Xu et al. [88], the first half hour nanorods grows laterally, between 0.5. – 6 hours longitudinal growth is dominant and after 6 hours to 2 days the growth is prominent both laterally and longitudinally. On the other hand, at high temperature condition (~350℃), with increasing growth time, the length of rods increases but diameters remain fairly constant [91].

1.4.4.3 Growth Temperature

In hydrothermal method, growth temperature strongly affects the morphology, structure, and aspect ratio of ZnO nanorods. Polsongkram et al. (2008) produced ZnO nanorods at different temperatures by hydrothermal method. They report that when the temperature is increased to 95℃ from 60℃ the width of nanorods decreased and aspect ratio increased [92].

In the study of H.Q. Le et al (2006) worked on the growth temperature effect on the ZnO nanorods morphology. Samples hydrothermally grown at 60, 80, 100 and 150℃. When the temperature increased from 100 to 150℃ the diameter of nanorods decreased and length of nanorods increased. Also, aspect ratio and density of nanorods showed a decrease with this temperature change [84].

According to Xu et al. (2008), nanorod's growth is related with the presence of OH^- ions in precursor which are formed because of thermal dissociation of hexamine. At high temperature, a sudden dissociation of hexamine happens and many OH^- ions are formed, so lateral and longitudinal growth become faster. With the time, the concentration of OH^- ions decreases and competition for preferential face drops, ions place the top of structure and resulted in hexagonal pyramid. On the other hand, at low temperature, decomposition happens with a uniform mild rate and ion competition remain stable, so as uniform nanorod structure is obtained. Also, in this study it is shown that, when the growth temperature was lowered from 70℃ to 60℃, the aspect ratio decreased [88].

Tang et al. (2008) used zinc acetate as precursor and surfactants to search the relation between growth temperature and morphology of ZnO nanorods. They perform the experiment at 130℃, 150℃, and 180℃ for 5 h. According to results, at 130℃ broad size distribution of spheres, cubes, and other shape structures were obtained. While needle like structures obtained at 150℃, uniform dimensioned ZnO nanorod were synthesized at 180℃ [93].

To investigate the temperature effect on nanoparticle's structure, Li et al. (2008), synthesized flower like and cabbage like single crystal ZnO nano structures at 120℃, 150℃, and 180℃ [94].

Wahab et al. (2009) showed the diversity of the synthesized nanostructures morphology with temperature. While the temperature increased from 40℃ to 60℃, 80℃, and 100℃; morphology varied from particle to star shape, rosette shape and nanorod shape, respectively [95].

1.4.4.4 PH

With thermal decomposition of hexamine, many OH^- ions are formed and an increase is shown in the pH. Rod growth in basic medium is faster than acidic medium. The changing pH causes morphology transformation. With increasing basicity, structures change from rod to flower like shape [83].

According to Alshehri et al. (2018), base concentration affects the aspect ratio of produced NWs. When Na_2CO_3 concentration is increase from 2.673M to 4.717M, average diameter of NWs decreases while their length increases [96].

In the another work which has been done by Kumaresan et al. (2017), it is reported that the crystallite size of hydrothermally grown ZnO increases with increasing pH from 7 to 9, 11 and 13 [97].

1.5 Literature Review

Zinc oxide (ZnO) thin film growth and doping with other elements have been extensively studied by researchers. The hydrothermal method which is useful and easy growth method of ZnO have been widely worked. The growth parameters, optical and structural properties were the most focused area in literature due to application suitability of ZnO in semiconductor industry, optoelectronic, solar cells etc. In addition, doping of ZnO with different elements are also proposed area of research to enhance the properties of ZnO. Although there are satisfying amount of hydrothermal synthesis, ZnO synthesis and doping of ZnO with variety elements, lack of study of indium doped ZnO thin film by hydrothermal method is seen obviously. There is a big deficiency in research of the indium doped ZnO thin film by hydrothermal method, its growth parameters, structural and optical parameters.

Yoshimura and Byrappa (2007) gave an overview of the past, present and future perspective of hydrothermal technology. They described the hydrothermal method and it advantageous, compared hydrothermal method with the conventional material processing methods. They also discussed the multi energy processing of material like mechanochemical, electrochemical and microwave hydrothermal. According to them, hydrothermal technique provides a great opportunity to process of advanced materials for fine particles, nanoparticles or bulk single crystals [69].

Mahmood et al. worked on low temperature hydrothermal growth parameters of ZnO which are growth duration, growth temperature, precursor pH, concentration of solution, role of hexamine and layer deposited on a substrate. According to them, size, morphology, orientation, and growth rate of the one-dimensional nanocrystals of ZnO in the low temperature hydrothermal synthesis, are strongly dependent on these growth parameters. It is reported that synthesis of ZnO nanocrystals which required size, morphology, orientation could be achieved by the adjustment of these growth parameters [83].

Alshehri et al. (2018) synthesized ZnO nanowires by low temperature hydrothermal methods. They investigated the effect of growth temperature, growth time, zinc precursor and base (Na2CO3) concentration on morphology of nanowires. using X-ray diffraction (XRD), scanning electron microscopy (SEM), Transmission electron microscopy (TEM), X-ray photoelectron spectroscopy (XPS) and photoluminescence (PL), the products are characterized. High yield of ZnO nanowires produced by using any of zinc chloride, zinc acetate and zinc nitrate as precursors. A relation between length/diameters of nanowires and growth time and base concentration is specified [96].

Ellmer and Bikowski (2016) reviewed the doping of n-type semiconductor ZnO. They said ZnO normally shows n type conductivity and it used in transparent electrode, thin film solar cell. On the other side, for the electronic devices like UV photodetectors, power devices and LEDs, p type doping is required. By doping of ZnO with IIIB elements (B, Al, Ga, and In), highly doped n type ZnO can be obtained. IIIB elements act as shallow donors [98].

Xu et al. (2020) grew highly c-axis oriented and transparent ZnO nanorod by chemical solution method and investigated the relation between crystallization quality, surface defects, optical properties and growth time of nanorods. As a raw material, they used zinc acetate and urea instead of mostly used zinc nitrate and hexamethylenetetramine. According to study results, as the crystal quality and length of ZnO nanorods increasing, defects that related to oxygen on the surface was reduced with increasing growth time. Also, with the increasing growth time the intrinsic emission of nanorods, the ultraviolet emission and transmittance in the visible range enhanced, and the visible emissions related to the defects are weakened [99].

Sugumaran et al. (2015) prepared 100 nm thickness novel indium zinc oxide (InZnO) thin film onto glass substrate by thermal evaporation method from InZnO nanoparticles. On the optical study, the band gap energy was evaluated about 3.46–3.55 eV by Tauc’s plot, low absorption and high transparency were achieved. The structure and high transparency

with wide band gap energy of produced InZnO thin film, is approved for transparent layer in optoelectronic devices in the future [25].

Kumar at al. (2004) prepared undoped and indium doped zinc oxide thin films by using chemical spray pyrolysis and characterized them by XRD, SEM, optical transmission and absorption spectra, resistivity measurements, x-ray photoelectron spectroscopy and photoluminescence. The optical transmittance was lowered at higher doping concentrations and increased at low doping levels. The 1 at % indium was preferred due to enhance optical transmission and lowest resistivity. According to this study, while ZnO thin films was showing a strong blue-green emission, indium doping process concluded with the rising of three emissions at 408, 590 and 688 nm and the blue-green emission dropped behind of these increased three emissions [28].

Pál et al. (2009), by using hydrothermal method at 150°C, prepared ZnO and indium doped ZnO with different morphologies. By the zinc ion/hydroxide ion molar ratio and presence of l-histidine in the reaction mixture, the structure formation was controlled. According to measurements, during the synthesis the prism like and flower like crystals formed. With the indium doping, a deformation is seen in these crystal shapes. Effect of indium doping on the optical properties (fluorescence, UV-diffuse reflection) of the particles was observed. With increasing indium concentration, they saw a decrease in the band gap energy. Moreover, the decrease becomes more apparent. The visible emission region of particles was 506–565 nm and with increasing indium, visible emission peak of the ZnO shifted toward the shorter wavelength. Also, with increasing indium concentration, photocurrent intensity decreases due to the presence of oxygen vacancies that impede the direct recombination of the photoexcited charge carriers [36].

Wang et al. (2007) grew indium doped ZnO crystal by hydrothermal method. They investigated the effect of impurities especially In3+ on hydrothermal growth mechanism. They analyzed the transmission spectra of pure ZnO and indium doped ZnO crystals. With the doping, transmittance of ZnO crystals are lowered. The absorption edge undoped ZnO was red shifted with doping. In this study which conduct in the presence of In3+, would

promote interpretation growth mechanisms of ZnO crystals in the existence of impurities and the provide conductive substrates from ZnO materials [100].

Morales et al. (2006) synthesized rod like ZnO nanostructures by low temperature hydrothermal process and studied the effect of indium on morphology and optical absorption of the nanostructures. Due to the formation of a new $In(OH)_3$ phase, indium incorporation in nanostructures was not enviable. For the doping of indium into the structures and dissociation of $In(OH)_3$ phase, a thermal annealing process was done at 300 ℃ in inert atmosphere is applied after deposition for 2 hours [31].

1.6 Objective

In this thesis ZnO and indium doped ZnO (IZO) thin films were deposited on the glass substrates with different growth time, growth temperature and indium doping percentage by hydrothermal synthesis method. The aim of the thesis is to determine the optimal film growth parameters such as growth time, growth temperature and indium doping percentage by characterizing structural (crystallite size, dislocation density and microstrain), surface (homogeneity, film density and smoothness) and optical (energy band gap, refractive index and defect level) properties of the films.

CHAPTER 2

EXPERIMENTAL PROCEDURE

2.1. Cleaning Substrate

Substrate cleaning is very important stage before film deposition. Substrate cleaning process is necessary to remove the contaminants from surface of substrate by breaking the bonds between contaminant and substrates. The mentioned contaminants are fingerprints, dust, dirt, oil particle etc. which can affect the morphological, nucleation, electronic properties of films and film-substrate interface. With the substrate cleaning, reproducible films are obtained, porosity, adherence, uniformity, and smoothness of the films are fixed up. The suitable cleaning technique was chosen according to the nature of contaminant and substrate [79].

In this study glass substrates were used. The used ultrasonic cleaner for cleaning the glass substrates can be seen in the Figure 2.1 For the substrate cleaning process, the following steps were applied to remove the contaminants and to obtain smooth and dust free surface;

(i) Washing with detergent and clear rinsing
(ii) First ultrasonic bath in DI-water for 5 minutes
(iii) Ultrasonic bath in Ethanol for 5 minutes
(iv) Final ultrasonic bath in DI-water for 5 minutes
(v) Evaporation of the remaining water by drying machine

Figure 2. 1 The used ultrasonic bath for substrate cleaning

2.2. Solution Preparation

For growth of undoped ZnO films, equimolar solutions were prepared by using Zinc nitrate tetrahydrate [$Zn(NO_3)_2$ $4H_2O$] (EMSURE®) and Hexamethylenetetramine [HMTA] (MERCK) chemical powders. The 0.03M molar solutions were prepared to determine the most suitable growth time for best ZnO thin film. To be used powder amounts were calculated according to solution molarity, and molecular weight of powders. For the power calculation, precision scale was used which can be seen in Figure 2.2) The calculated amount of powders was poured into the 30ml DI water and they mixed on magnetic stirrer (in Figure 2.2) at 180 rpm for 10 minutes until the entire powder dissolve.

For the Indium doped ZnO, differently from undoped ZnO, Indium (III) chloride Anhydrous, +%98 (Alfa Aesar) was extra added with the Zinc nitrate tetrahydrate and Hexamethylenetetramine into DI-Water. Amount of to be added Indium, was determined according to the percentage of doping (1%, 3%, 5%, 7%). Zinc Nitrate tetrahydrate,

hexamethylenetetramine and Indium (III) chloride mixed together in 30ml DI water for 10 minutes at 180rpm.

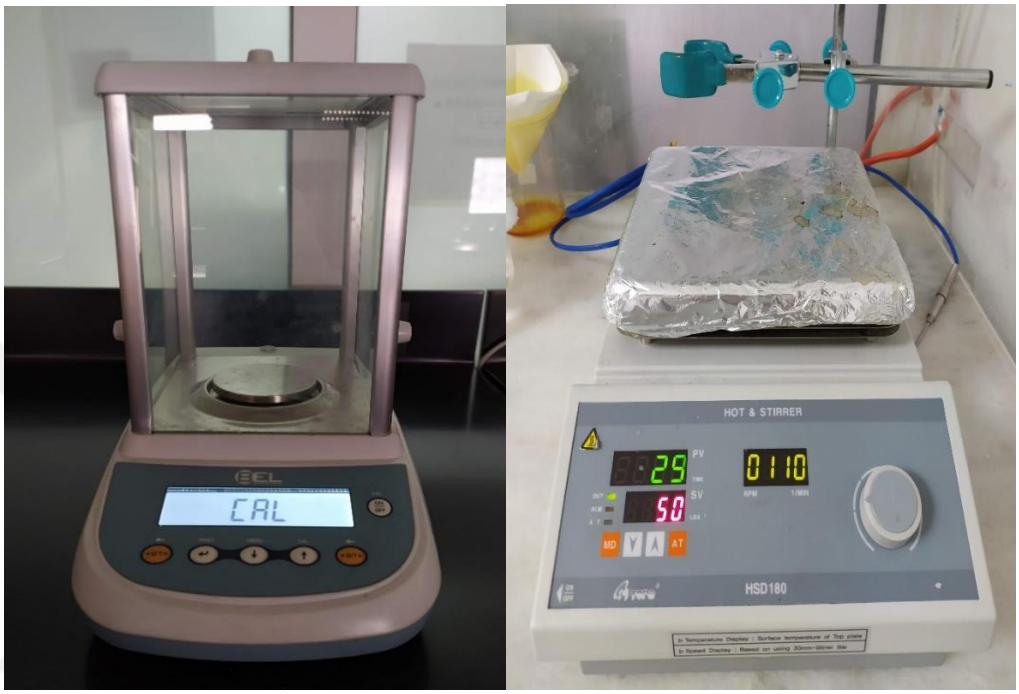

Figure 2. 2 The used precision scale and magnetic stirrer

2.3. ZnO and IZO Films Growth

Prepared solutions were poured into the Teflon liner of autoclave. The glass substrates were placed into the liner and submerged into solution. Seal ring of autoclave of hydrothermal device was controlled, and screws were tightened with allen wrench. The temperature was set to desired temperatures and times. During the autoclave stage dissolution of precursors, crystallization from solution and film formation occurs. At the end of the growth duration, autoclave was slowly cooled to room temperature and samples were kept at room temperature for drying. Films were grown with different growth time (h), In dope percentage (In %) and growth temperature (T). The used autoclave of hydrothermal method can be seen in Figure 2.3.

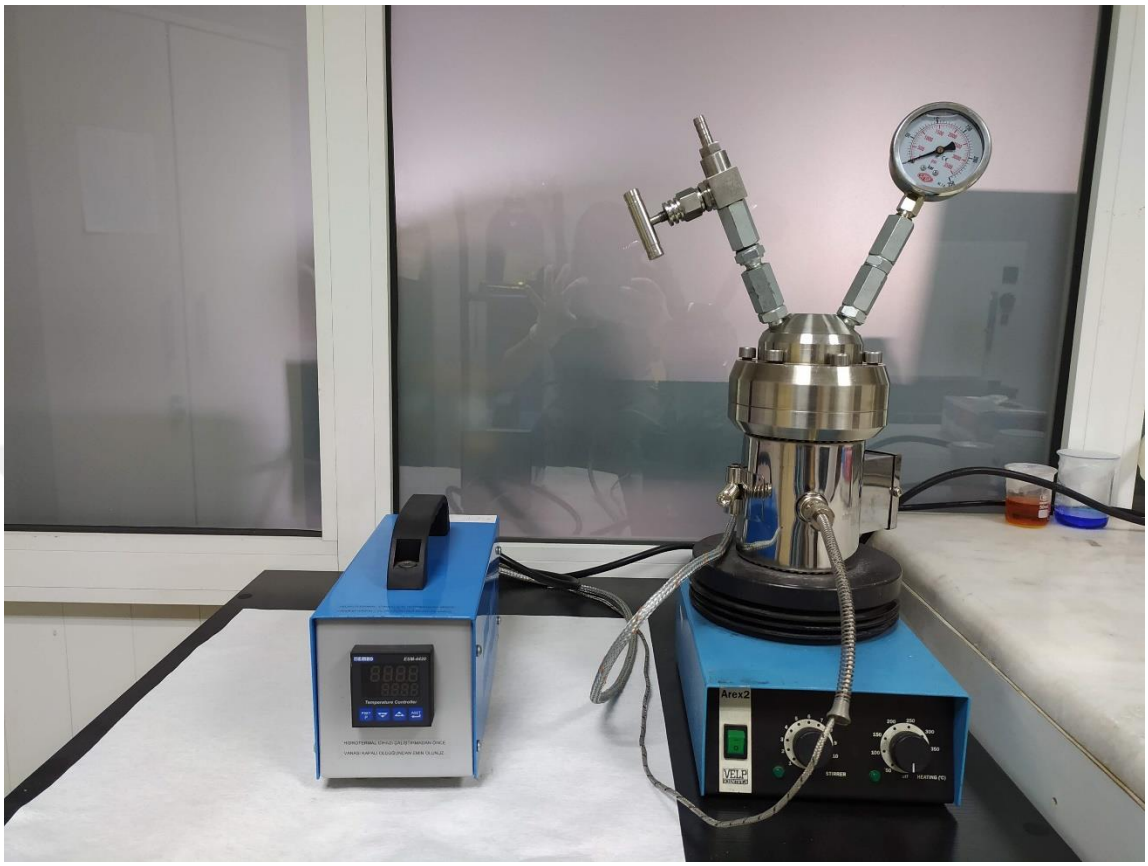

Figure 2. 3 The used autoclave for hydrothermal synthesis

In this study it is aimed that to decide the best combination of hydrothermal synthesis parameters according to characterization results and investigating the effect of these parameters on the produced ZnO and IZO films. For this reason, firstly the most suitable molarity value was sought out from the literature works. By preparing 0.03M ZnO solution thin films were produced for 3h, 5h, 7h, 9h and 24h at 90 ℃. The best growth time value was decided for 0.03M solution, after characterizations.

After the decision of best growth time for 0.03M solution, In doped ZnO thin films were produced. In dope percentage were varied as 1%, 3%, 5%, 7% and the best In dope percentage of ZnO film was detected.

Finally, growth temperature parameter was investigated on 0.03M 5h %5 doped IZO films. The 90℃, 120℃ and 150℃ growth temperatures were applied onto IZO films and

the change of structural properties, surface properties and optical properties were examined.

2.4. Calculation of Film Thickness

The thicknesses of grown ZnO and IZO films were calculated by Gravimetric method. For the calculation of thickness precision scale with a sensitivity of 0,0001 grams were used which can be seen in Figure 2.2. Before the deposition, weights of substrates were weighed and after deposition they were reweighed. The difference between two measurements accepted as the mass of ZnO or IZO films. Using the films' mass, their thicknesses were calculated by,

$$d = \frac{\Delta m}{S\rho} \tag{2.1}$$

Where d is thickness of the film, Δm is film mass, S is the surface area of the film and ρ is the film density which is 5.61 g/cm^3 for the ZnO compound.

2.5. Characterization

2.5.1. X-ray Diffraction (XRD)

XRD is a functional and nondestructive characterization method for solid materials which widely used for researches, material characterization industry and process control. It is mostly used for investigation of crystal structure of material by using lattice geometry and constants. In addition to that, while this method can detect the orientation of defects and single crystals in crystal structure it also can identify the unknown phases and solids [101,102].

Some parameters like crystallite size, dislocation density and microstrain can be obtained from XRD analysis method which gives an opportunity to get information about the material [103].

In this work, the structural properties of hydrothermally produced thin films was examined by X-ray diffractometer (Miniflex 600, Rigaku) which given in Figure 2.4. The crystal

structures were checked between 2θ =20-80 degrees with a step size of 0.002 and rate of 2°/min using Cu-Kα λ = 1.5405 Å radiation. Crystal structures and structural properties of film were analyzed from some XRD patterns. Some used parameters are grain size (D), distance between the layers (d), dislocation density (δ) and the strain (ε) values of the films.

The undoped ZnO film crystal structure and its difference with In doping, growth time and temperature were investigated.

By using Bragg's Law formula, the lattice spacing, d, was calculated:

$$n\,\lambda = 2\,d\,\sin\theta \tag{2.2}$$

where n is the diffraction order which usually n = 1, λ is the wavelength of used X-ray source (1.5405 Å) and 2θ is the diffraction angle. Hence, [104]

$$d = \frac{\lambda}{2\sin\theta} \tag{2.3}$$

The average crystallite size values of ZnO was reached by using a well-known Debye Scherrer's formula:

$$D = \frac{k\,\lambda}{\beta\cos\theta} \tag{2.4}$$

Where k is a constant which was taken as 0.9, λ is the wavelength of the used X-ray source (1.5405 Å), β is the full width half maximum (FWHM), and θ is the angle of diffraction [89,105].

The dislocation density (δ) of the films can be defined as the number of defects in materials. It can be expressed as the length of dislocation lines per unit volume of the crystal. During calculation of dislocation density (δ) of the films the FWHM peaks values are implicitly related which is necessary to get more information about the defects in the produced films. For the dislocation density calculation, the formula below was used: [106-108]

$$\delta = \frac{1}{D^2} \quad \textbf{(2.5)}$$

Where D represents the average crystal size.

The diffraction line broadening due to either crystallite size or strain contribution, according to Williamson and Hall approach. The microstrain (ε) values which cause broadening due to crystal defects and imperfections was calculated using the following formula: [104,109]

$$\varepsilon = \frac{\beta \cos\theta}{4} \quad \textbf{(2.6)}$$

The broadening of the diffraction peaks of materials are caused by the deviation from perfect crystallinity. Peak width (FWHM) is dependent variable to the crystallite size. While the crystallite size decreases, the peaks broaden which means FWHM increases.

Structural disorders, point defects, stacking faults and tensile stress in the material influence crystallinity and grain boundary negatively which result in widening of FWHM value of XRD peak [110-112].

The crystallite size and lattice strain are the main properties which can be obtained from XRD peak width analysis. These properties influence the Bragg peak, cause an increase in the peak intensity, peak width, and shift of 2θ peak position [113].

In XRD patterns, high intensity and narrow width of peaks indicates the good crystallization of films. On the other hands, low intensity and large width peaks signifies the amorphous crystallization of films. To determine the best crystallization of grown films, large crystal size (D), small dislocation density (δ), and the strain (ε) values were considered [106,108].

Figure 2. 4 X-ray Diffraction instrument

2.5.2. Scanning Electron Microscopy (SEM)

Surface properties of undoped and indium doped ZnO films were examined by Scanning Electron Microscopy SEM (FlexSEM 1000 II, HITACHI) which given in Figure 2.5. With the SEM imaging, shapes of nanoparticles, uniformity and homogeneity of the film, surface defects, surface roughness, and particles distribution were analyzed. The surface homogeneity has critical role on the optical properties of the films. Homogeneity improves the optical transmission of the films. It is caused by reduction in the minimum optical loss [25,114].

For defining the suitable growth parameters, SEM is the one of the characterization methods. In this study, it is expected that high uniformity, good particle distribution, density, smoothness and well-adhesion to the substrate [106] and also, changing the film structural parameters with In addition.

Figure 2. 5 Scanning Electron Microscope (SEM)

2.5.3. Photoluminescence (PL)

Photoluminescence spectroscopy (PL) is a noncontact and highly precise characterization method which provides important information about the semiconductor properties of ZnO thin films. It is used to investigate the crystal quality, bandgap, defect types and density and recombination mechanism of semiconductor materials [99,115].

PL spectra generally shows two apparent band which are Near band edge emission (NBE) in UV region and in visible emission region. While the band edge emission attribute to recombination of free exciton between valance and conduction bands, visible emission peak series originated from the different intrinsic and surface defects of semiconductors. With the other words, the UV emission of ZnO result from exciton-related activity [116] however the point defects like oxygen vacancies or zinc interstitials and impurities on the ZnO thin films causes a visible luminescence [117-122].

Generally higher PL intensity of the ultraviolet (UV) emission implies the better crystallization quality of ZnO semiconductor [123,124]. For the improved crystallinity of ZnO, the high NBE emission is expected. Also, the intensity of PL spectra for visible emission indicates the included crystal defects and surface oxygen vacancies of the films. When the PL intensity of visible emission is lower, it can be said that the film may have

less defects, and low oxygen vacancies [125]. On the other hands, high PL intensity is observed when various defects like oxygen interstitials (Oi), oxygen vacancies (Vo), zinc vacancies (VZn) and zinc interstitials (Zni) are included. In brief, lower PL intensity of visible emission peaks indicate the higher crystallization quality of ZnO films because of containing less defect [99].

Optical properties of undoped and In doped ZnO thin films were characterized with the 300 nm excitation light energy by Fluorescence Spectrometer (LS-55, PerkinElmer) which is given in Figure 2.6. By fluorescence spectrometer surface defects and luminescence behavior of films were analyzed. From PL characterization its expected that to get less defects and stronger ultraviolet emission with the increase of crystallization quality of ZnO and IZO films.

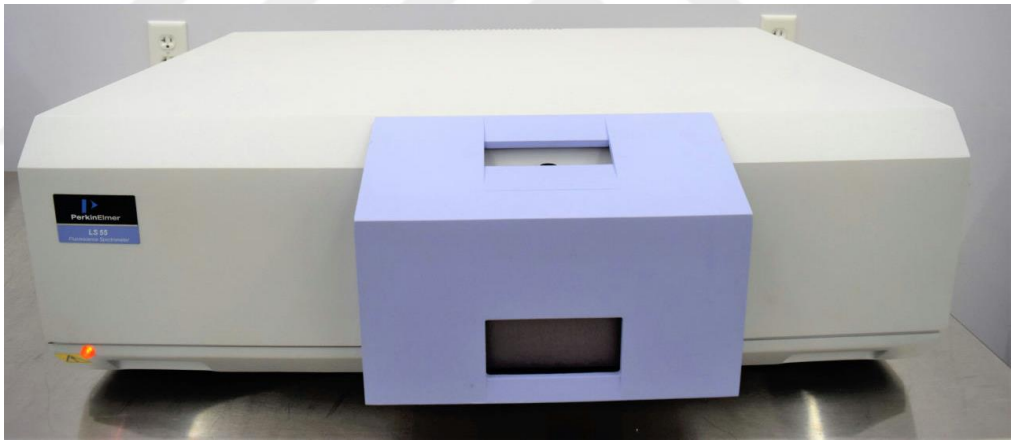

Figure 2. 6 Fluorescence Spectrometer

2.5.4. UV-VIS Spectroscopy

Ultraviolet-visible spectroscopy is an optical characterization method which comprise the photon spectroscopy in UV - visible region and uses the adjacent near ultraviolet (UV), visible and near infrared (NIR) ranges of light. Absorption spectroscopy is quite easy and direct method for investigating the band structure of semiconductors. While for the UV region, 200 - 400nm range is scanned, for the visible part scanning range is between 400

and 800 nm [126]. With UV-Vis spectra study, materials optical properties like UV absorption, transparency and refractive index can be evaluated [127].

In this study, the optical properties of films were investigated by using Shimadzu UV-VIS 2600 Spectrophotometer which given in Figure 2.7 and the wavelength range of used light source was between 200 nm and 1000 nm. The effects of the growth time, indium doping and growth temperature on the optical properties like optical absorption spectrum, optical bandgap (Eg), refractive index (n), high frequency (optical) dielectric constant (ε_∞) and static dielectric constant ($\varepsilon_\circ$) of ZnO and IZO films were investigated.

Figure 2. 7 UV-VIS Spectrometer

The energy gap of the films was evaluated via the Tauc's relation and the bandgap values were obtained from the plotted $(\alpha h\nu)^2$ versus $(h\nu)$ graph. The intersection of the tangent line obtained from the plotted graph with the energy $(h\nu)$ axis, gives the band gap energies of films [128-131].

$$(\alpha\, h\nu) = A(h\nu - Eg)^n \qquad \textbf{(2.7)}$$

Where Eg is band gap energy, α is absorption coefficient, A is a constant which is the function of the refractive index of material, speed of light and reduced mass. Also, hν is the incident photons' energy and n value is $\frac{1}{2}$ due to ZnO material has direct band gap [132].

The absorption coefficient (α) values of the films for the allowed direct transition was detected as a function of photon energy (hν) by following relation [130,131].

$$\alpha = \frac{A}{h\nu}(h\nu - Eg)^{1/2} \quad \textbf{(2.8)}$$

Moss relation was used for the calculation of refractive index of thin films [133,134] and it has direct relation with the energy bandgap (Eg),

$$Egn^4 = k \quad \textbf{(2.9)}$$

where k is a constant value which is 108 eV. Another relation between the refractive index and bandgap energy is presented by Herve and Vandamme in the following formula,

$$n = \sqrt{1 + \left(\frac{A}{Eg+B}\right)^2} \quad \textbf{(2.10)}$$

where A and B are constants whose values are 13.6 and 3.4 eV, respectively. For this study, the Moss relation is more suitable than Herve and Vandamme equations due to better agreement for refractive index in II–VI semiconductors [135,136].

The dielectric behavior of solids is important for several electronic device properties. For the high frequency dielectric constant (ε_∞) calculation, the following relation was used: [137]

$$\varepsilon_\infty = n^2 \quad \textbf{(2.11)}$$

where n is refractive index of the film. The static dielectric constant ($\varepsilon_\circ$) of the films was found by using a relation which indicates connection between the energy band gap and dielectric constant for semiconductors compounds [135,138].

$$\varepsilon_\circ = 18.52 - 3.08Eg \quad \textbf{(2.12)}$$

CHAPTER 3

RESULT AND DISCUSSION

3.1 Film Formation

According to the literature works, for the formation of ZnO nanoparticles and films by chemical methods, zinc salts such as nitrate, acetate etc. are used essentially. These zinc salts are blended with some compound with the OH group (base, alcohol etc.) and water to start a reaction. As a result of this zinc salt and base reaction, hydroxide form of zinc comes into existence. This is the basis of the chemical synthesis.

The obtained hydroxide is thermally oxidized in the hydrothermal autoclave to produce ZnO nanoparticles. This reaction happens in a solvent (water) and the formed ZnO particles can be gathered as powders. To obtain the film form of ZnO, a substrate (glass) is used which placed into the liner of autoclave. In this way, produced ZnO nanoparticles are adsorbed onto the substrate [139].

In this study, to produce ZnO thin films from nanoparticles by hydrothermal synthesis, equimolar Hexamethylenetetramine (HMTA) and nitrate based (Zinc nitrate tetrahydrate) precursor was used. In this reaction, the main function of HTMA (weak base) is to act as pH buffer and producing required amount of OH^- ions [88,140]. On the other hand, Zinc nitrate tetrahydrate is responsible for producing Zn^{+2} ions.

HMTA decomposed to formaldehyde and ammonia with the increasing solution temperature and the produced ammonia reacted with water, as a result, OH^- ions was produced. With the combination of these OH^- ions and Zn^{+2} ions from precursor, zinc-hydroxide complex occurred. By the reaction temperature, this complex hydroxide form decomposed and turned to ZnO formed. The mentioned reaction is shown in the following reactions:

$$C_6H_{12}N_4 + 6H_2O \rightarrow 6HCHO + 4NH_3 \quad \textbf{(3.1a)}$$

$$NH_3 + H_2O \rightarrow NH_4^+ + OH^- \quad \textbf{(3.1b)}$$

$$Zn(NO_3)_2 .4H_2O + 2OH^- \rightarrow 4Zn(OH)_2 + NO^{-2}_3 + H_2O \quad \textbf{(3.1c)}$$

$$Zn(OH)_2 \leftrightarrow Zn^{+2} + 2OH^- \quad \textbf{(3.1d)}$$

$$Zn^{2+} + 2OH^- \rightarrow ZnO + H_2O \quad \textbf{(3.1e)}$$

The composed ZnO adsorbed onto the clean glass substrate in the autoclave and ZnO thin films were obtained [141-144].

With several ions, ZnO can be doped. The doping process occurs by replacing higher valency atoms with Zn^{+2} ions in ZnO crystal lattice. [145] The efficiency of doping process is highly affected from the ionic radius and electronegativity of atoms [146].

The ionic radius of Zn^{2+} and In^{+3} are 74pm and 76 pm respectively. The larger radius of doping atoms can cause lattice deformation [147]. Also, the electronegativity (Allred Rochow) values of Zn^{2+} and In^{+3} are 1.66 and 1.49, respectively [148].

For the In doping process, $InCl_3$ powder was added to equimolar solution by calculating the powder amounts according to doping percentage. In the water medium, added $InCl_3$ dissolved and In^{+3} ions took place. In^{+3} ions from $InCl_3$ acted as dopant and replaced with the Zn^{+2} ions in the ZnO crystal lattice.

3.2 Structural Properties

3.2.1 Growth Time Effect

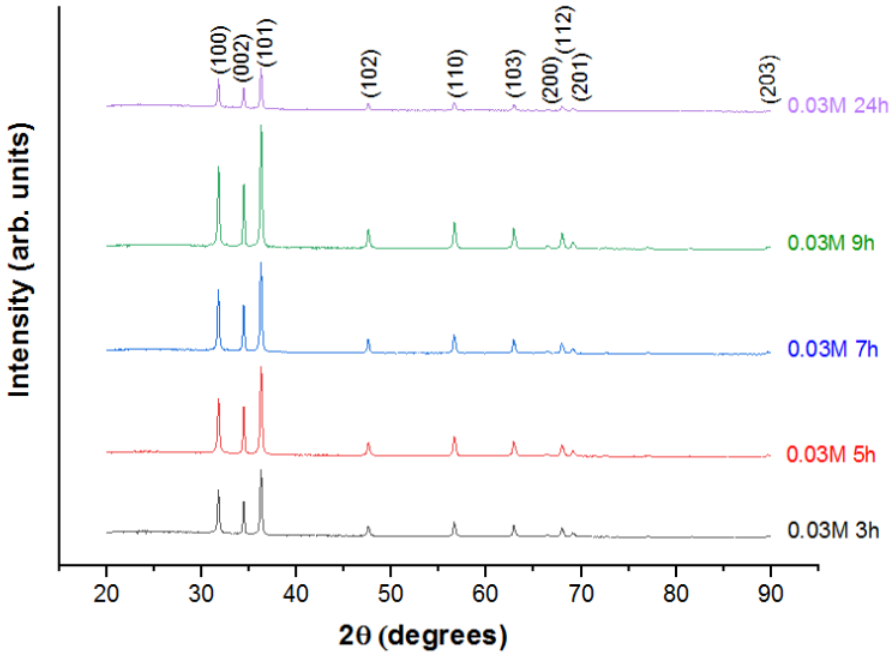

Figure 3. 1 The XRD patterns of ZnO thin films at 3 h, 5 h, 7 h, 9 h and 24 h growth times

The X-ray diffraction patterns of the ZnO thin films with all different growth times are given in Figure 3.1. All films have nearly the same 2θ values of the strongest peaks at 31.78º, 34.4º, 36.28º, 47,52º, 56,62º, 62.86º, 66.72º 67.9º and 69.04º corresponding to the ZnO lattice planes (100), (002), (101), (102), (110), (103), (200), (112), and (201), respectively. [142] When the XRD peaks compared with values in the JCPDS PDF Card No: 00-036-1451, all the peaks compromised with the hexagonal wurtzite ZnO structure [149].

It can be said that the grown ZnO thin films on the glass substrate without any pre deposited seed layer, are highly pure and have no secondary phases, because of no other detected diffraction peaks from XRD patterns [149].

All the thin films obtained at different growth times have polycrystalline structure with orientation along with different planes [150].

The predominantly preferred growth orientation for each growth time was been along the (101) plane and the growth time did not change the preferred growth orientation for ZnO thin films [151-153].

The peak intensities of preferred (101) growth planes in all the films are 6529, 8614, 8809, 11909 and 4221 for 3 h, 5 h, 7 h, 9 h, and 24 h growth times, respectively. The peak intensities of the growth planes increased with growth time up to 9 h and a dramatically reduction in the peak intensities was observed at the film obtained in 24 h growth time. Full Width Half Maximum (FWHM), Dislocation density (δ), Crystallite size (D), Microstrain (ε) and Peak intensity values are given in Table 3.1.

Table 3. 1 The structural parameters of the ZnO thin films obtained at 90℃ with different growth times

Growth Time For ZnO Thin Film	**2θ (101)**	**d (nm)**	**FWHM (β)**	**D (nm)**	**δ $(nm)^{-2}$**	**ε x 10^{-3}**	**Peak Intensity**
3h	36.27	0.2474	0.2463	33.9329	0.000868	1.021	6529
5h	36.27	0.2474	0.2613	31.9907	0.000977	1.083	8614
7h	36.26	0.2475	0.2453	34.0663	0.000861	1.017	8809
9h	36.28	0.2473	0.2421	34.5186	0.000839	1.004	11909
24h	36.26	0.2474	0.2419	34.5538	0.000837	1.003	4221

The lower FWHM and higher crystallite size values indicate better crystallization of the particles. The strain increases due to crystal imperfection and distortion in the film so, for the good crystallization, low microstrain expected from the films [154].

Although the film obtained 24h growth time has lowest FWHM, dislocation density, microstrain value and highest crystallite size; it shows excessively fall in peak intensity. In addition to that, when we look at the XRD pattern of 24h individually, the background indicates the bad crystal quality and tendency to amorphous structure. It can be seen from Figure 3.2

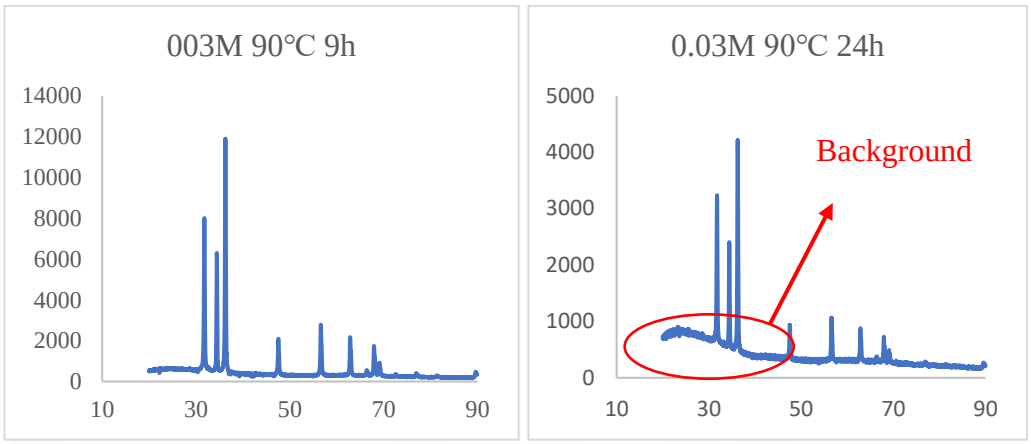

Figure 3. 2 XRD pattern of ZnO thin film obtained at 0.03M and 90 °C for 9h and 24h

The FWHM, dislocation density, microstrain, peak intensity and crystallite size change with the growth time were given in Figure 3.3. According to Figure 3.3, FWHM, dislocation density, microstrain and crystallite size for 24h and 9h are nearly same.

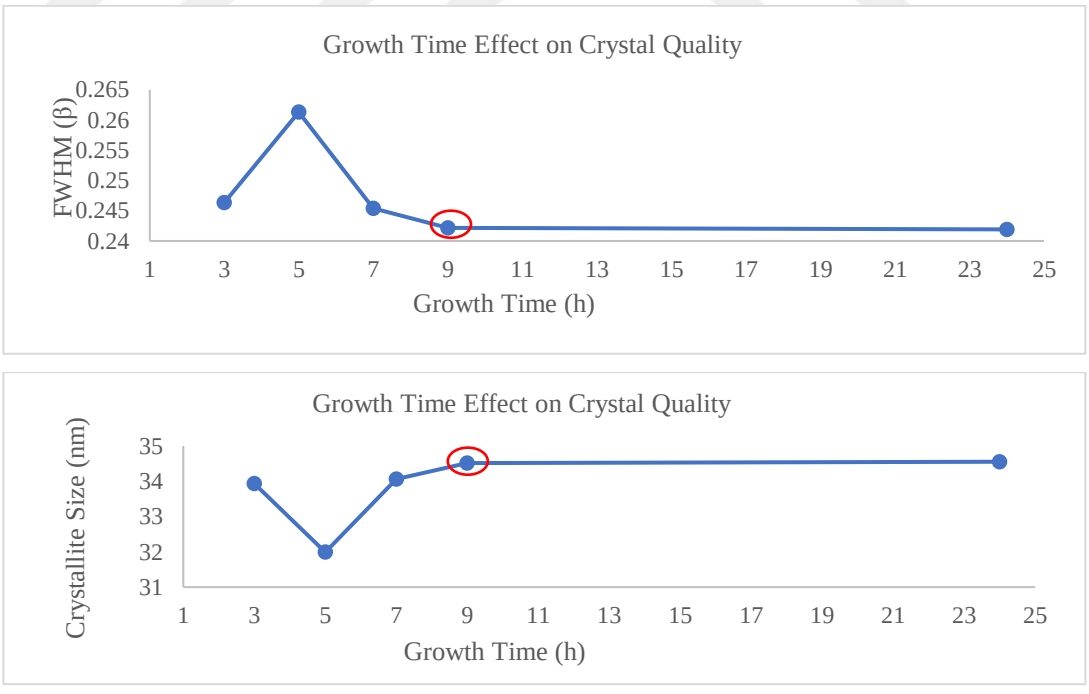

Figure 3. 3 (Continuing): Crystal quality change with growth temperature, a) FWHM b) crystal size c) dislocation density d) microstrain e) peak intensity

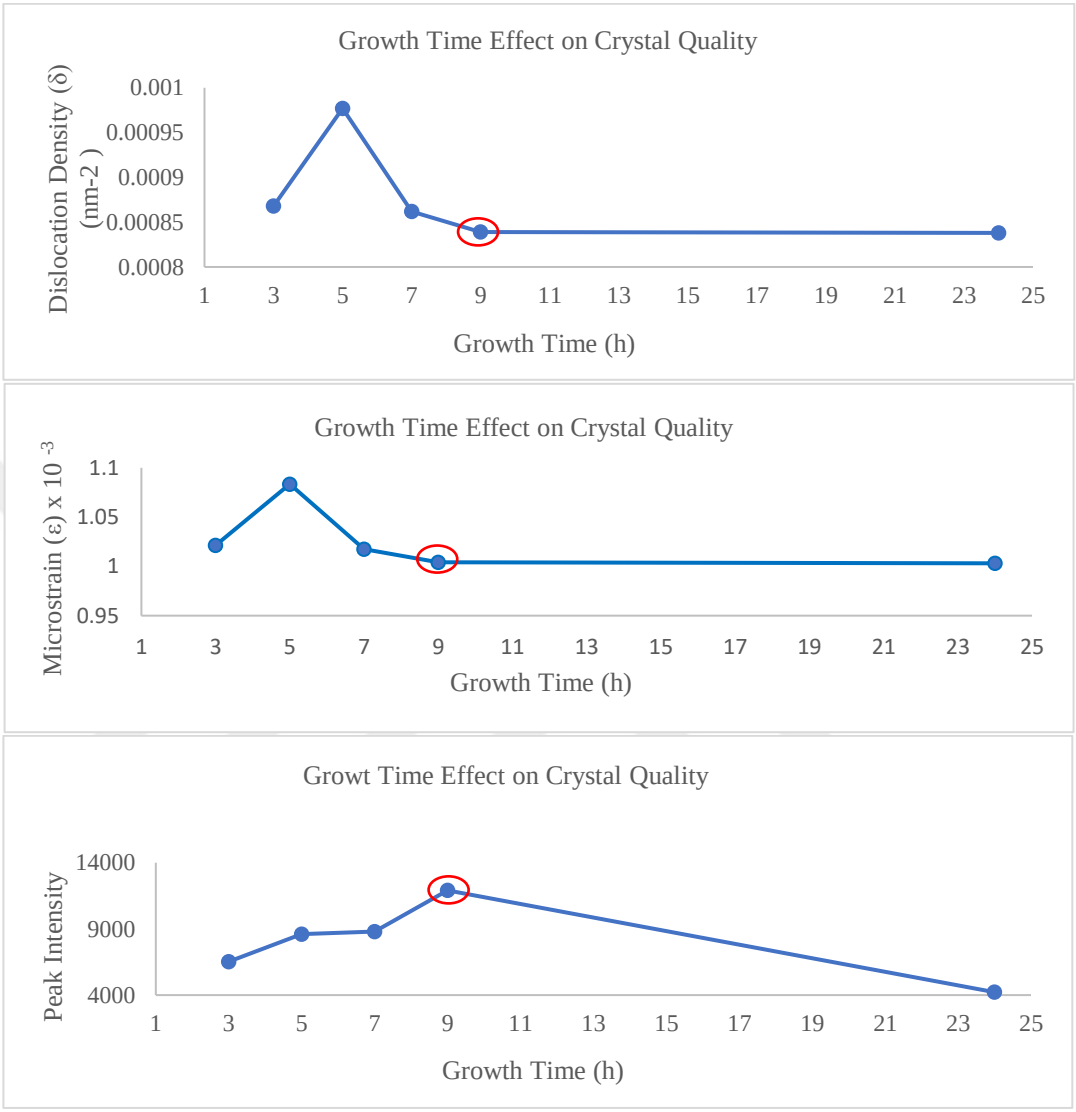

Figure 3. 3 Crystal quality change with growth temperature, a) FWHM b) crystal size c) dislocation density d) microstrain e) peak intensity

It can be seen from Figure 3.3, the turning point of crystal quality, growth time effect and dislocation density are at 9h. With the further examination, it is obvious that there is no remarkable difference between 9h and 24h.

As a result, with increasing growth time from 3h to 9h, the intensity of predominant ZnO peak (101) increased gradually. However, for higher duration such as 24h, this intensity

shows very sharp decreases. Also, FWHM, dislocation density, microstrain and crystallite size values got better with increasing growth time [89].

In other words, XRD analysis indicated that enhanced crystallization is dependent on the growth time up to a certain extent and 9h is best growth time for 0.03M ZnO thin film growth by hydrothermal method in this research.

3.2.2 Indium Doping Effect

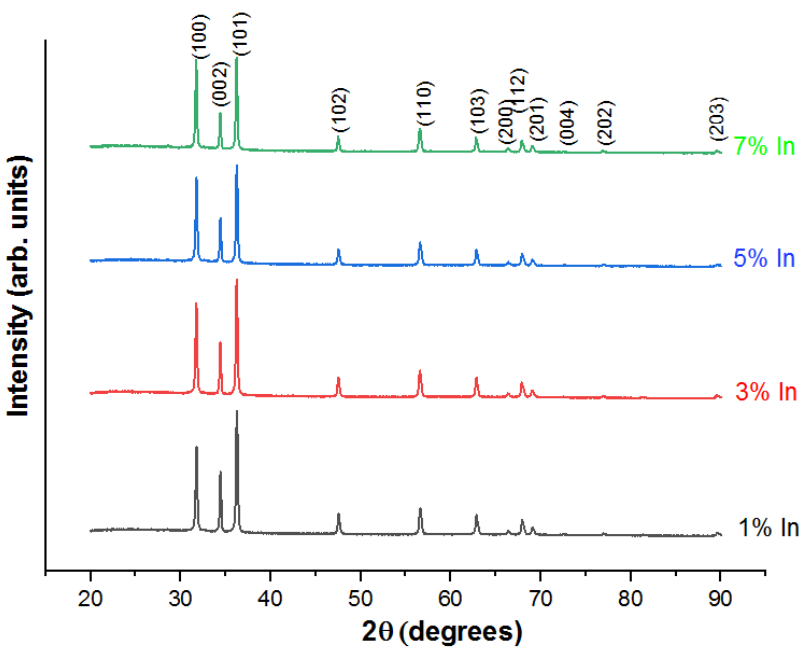

Figure 3. 4 X-ray diffraction patterns of 1%, 3%, 5% and %7 In doped ZnO films

The X-ray diffraction patterns of the films with different In dope percentage are given in Figure 3.4. As seen in the graph, all of the thin films obtained with different In doping percentages have polycrystalline structure with orientation along with different planes [145].

All doped films have nearly same 2θ values, peaks at 31.73º, 34.39º, 36.21º, 47,53º, 56,58º, 62.86º, 66.35º, 67.87º and 69.05º matched with the lattice planes (100), (002), (101), (102), (110), (103), (200), (112), and (201), respectively. When the XRD peaks

compared with values in the JCPDS PDF Card No: 00-036-1451, all the peaks compromised with the hexagonal wurtzite ZnO structure [155,156].

No other phases corresponding to zinc indium or indium oxide compounds were detected even at higher doping [157]. From this point of view it can be said that the In doped ZnO films grown on glass substrate without any pre deposited seed layer, are highly pure.

The strong diffraction peaks indicate high crystallinity of the ZnO thin films, and it locates at $2\theta=36.22^{o}$ which corresponded to (101) planes. The predominantly preferred growth orientation for each doping percentage was been along the (101) plane and the doping percentage did not change the preferred growth orientation for In doped ZnO thin films. Similar results were achieved in relevant study [36,151-153].

Full Width Half Maximum (FWHM), Dislocation density (δ), Crystallite size (D), Microstrain (ε) and Peak intensity values are given in Table 3.2

Table 3. 2 Structural parameters of 1%, 3%, 5% and %7 In doped ZnO (IZO) films

Dope Percentage for IZO Thin Films	**2θ (101)**	**d (nm)**	**FWHM (β)**	**D (nm)**	**δ $(nm)^{-2}$**	**ε x 10^{-3}**	**Peak Intensity**
0.03M- 9h-In %1	36.25	0.2475	0.2387	35.0171	0.000816	0.989	9563
0.03M-9h-In %3	36.22	0.2477	0.2345	35.6403	0.000787	0.972	9119
0.03M- 9h-In %5	36.24	0.2476	0.2386	35.0221	0.000815	0.989	7753
0.03M- 9h-In %7	36.21	0.2478	0.2303	36.2810	0.00076	0.955	7354

The peak intensities of preferred (101) growth planes in all the films (in Table 3.2) are 9563, 9119, 7753, and 7354 for 1%, 3%, 5% and %7 In doping percentages, respectively. The peak intensities of the growth planes decreased with increasing doping concentration. The decrease in peak intensities are probably due to the poor crystallization caused by increasing doping concentration [31,157,158].

Based on the absence of new phase, it has been believed that the doping causes that the indium in ZnO nanostructures substitutes zinc atoms from its lattice sites [31]. It can be clarified by dopant atoms either replace Zn and take up the Zn sites or occupy interstitial spaces within the ZnO crystal lattices [153].

Although the In doping highly impressed the intensity of the diffraction peaks, there was only slightly shift in positions towards lower degrees and width on prominent XRD peaks (in Figure 3.5). This type of small shift in peak position was thought to be caused by the deformation of ZnO lattice which owing to association of lager ionic radius of In $^{+3}$ than Zn $^{+2}$ (r Zn^{2+} = 74 pm and r In^{3+} = 76 pm) [147,159].

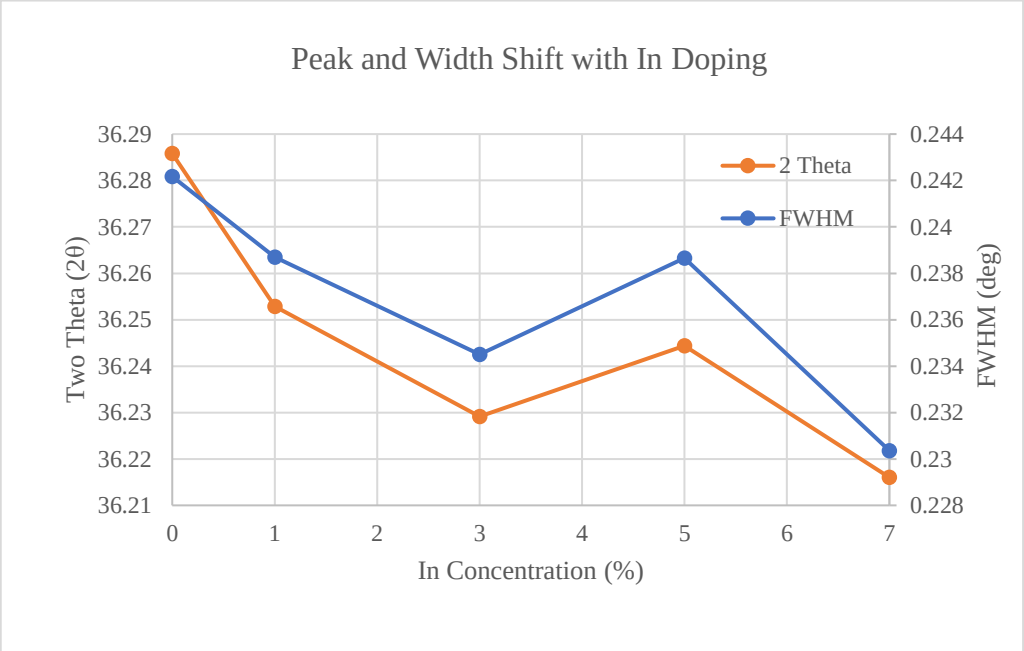

Figure 3. 5 Shift in peak position and width with changing doping concentration

The microstrain is produced by the residual stress in film and affects the crystallinity. 1.004 x10^{-3}, 0.989 x10^{-3}, 0.972 x10^{-3}, 0.989 x10^{-3} and 0.955 x10^{-3} microstrain values belongs to 0%, 1%, 3%, 5% and 7% In concentration, respectively. Microstrain values decreased with increasing doping percentage up to 3%, after that point it exhibited an increase. Simply, the crystal quality started to decrease after 3% In doping. This behavior shows similarity with another related research [158].

Even though 7% In has lowest FWHM, dislocation density, microstrain value and highest crystallite size; it shows the lowest peak intensity. Because of this contrast, the remain dope percentages (%1, 3 and 5) were regarded.

Although 1% In doped ZnO thin film has higher peak intensity than others, 3% In has better FWHM, dislocation density, micro strain and crystallite size. Furthermore, when the SEM images of %1 and 3 In doped ZnO thin films are compared, %3 In doped film has more uniform structure (in Figure 3.6). To get the best percentage of In doped films, a compromise had to be reached. By using these results, it can be said that %3 doping percentage is the best for IZO thin films.

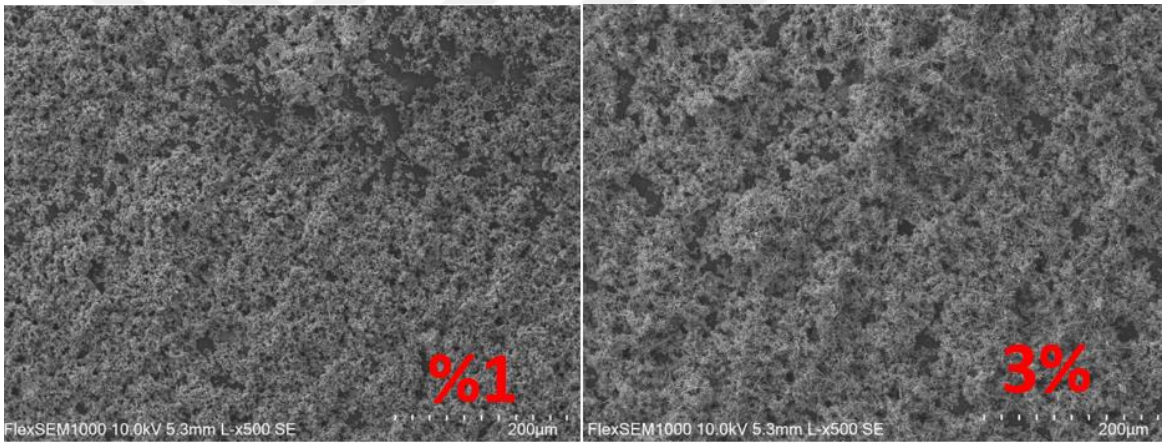

Figure 3. 6 SEM images of 1% and 3% doped IZO films (x500)

The FWHM, dislocation density, microstrain, peak intensity and crystallite size change with the indium doping percentage were given in Figure 3.7.

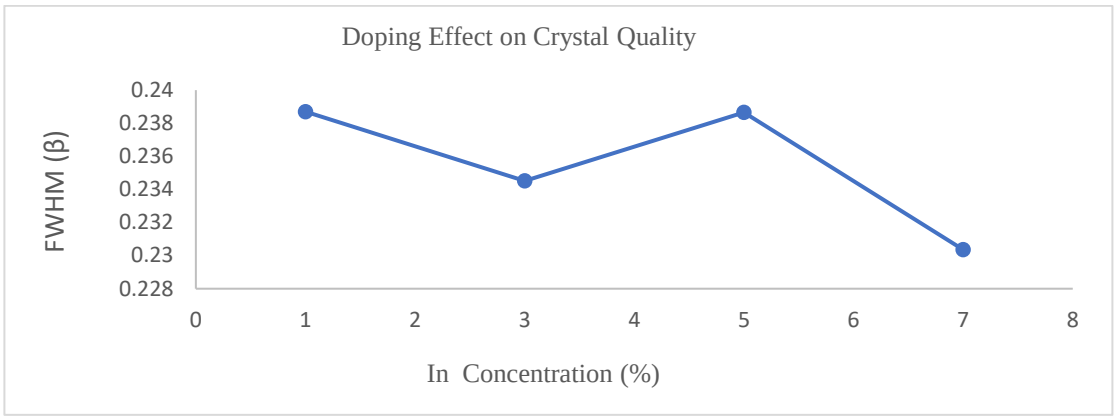

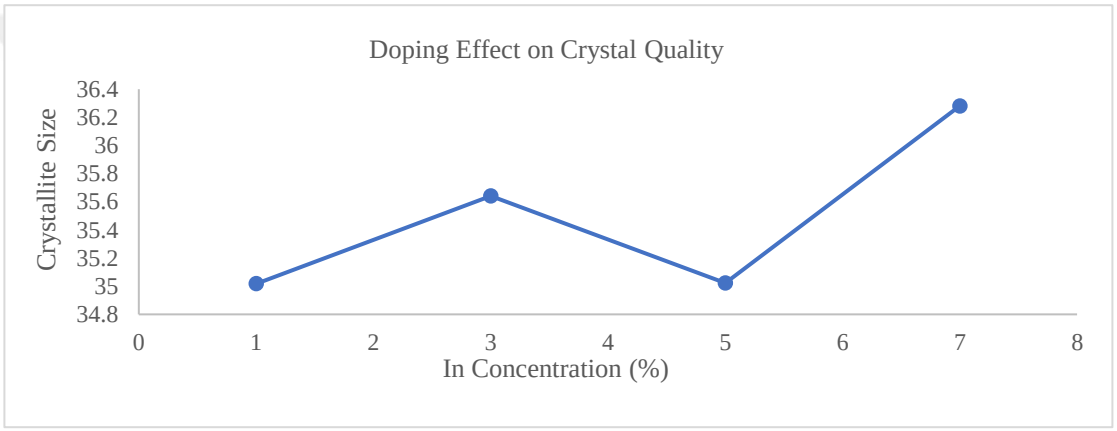

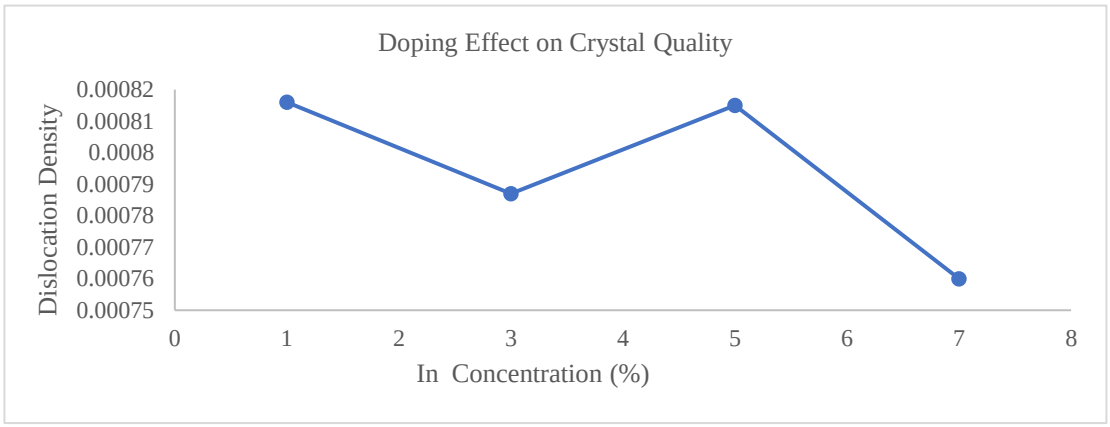

Figure 3. 7 (Continuing): Crystal quality change with doping a) crystal size b) FWHM c) dislocation density d) microstrain e) peak intensity

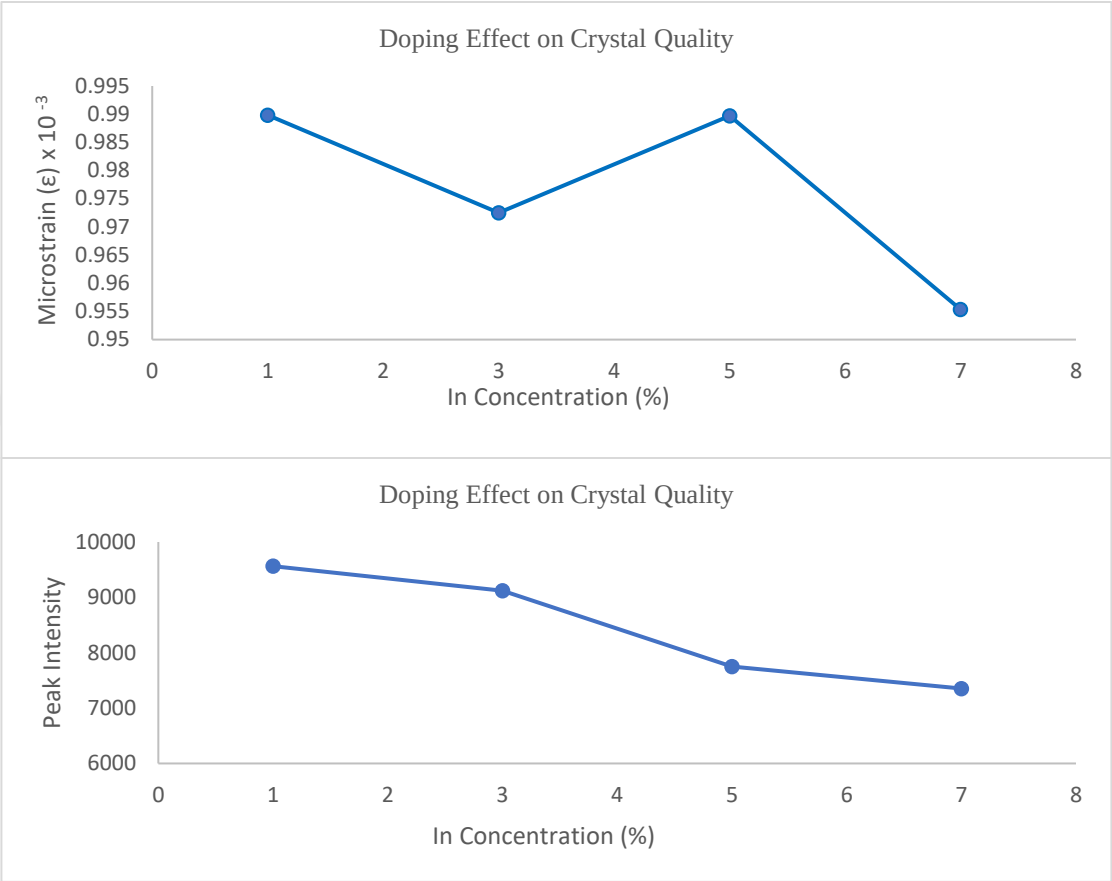

Figure 3. 7 Crystal quality change with doping a) crystal size b) FWHM c) dislocation density d) microstrain e) peak intensity

3.2.3 Growth Temperature Effect

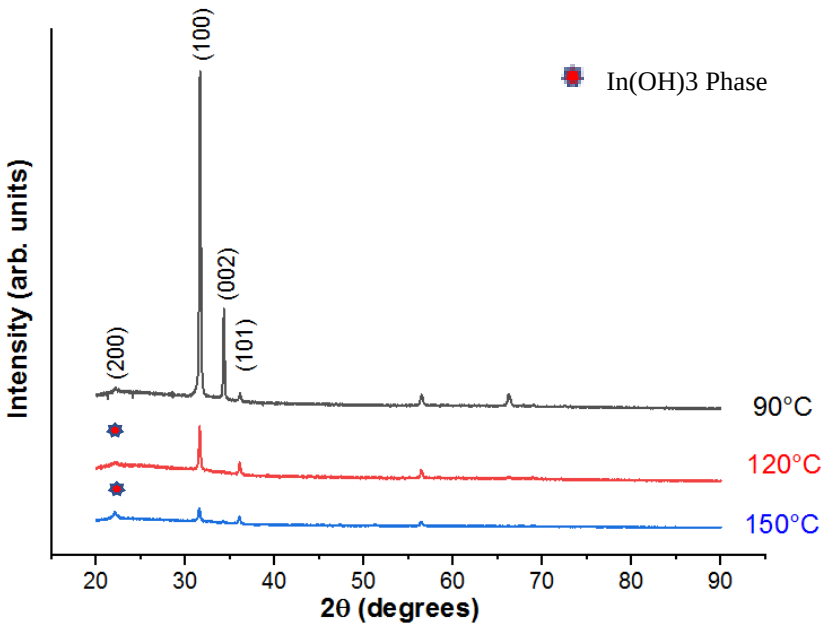

Figure 3. 8 The XRD patterns of IZO thin films at 90°C, 120°C and 150°C growth temperatures

The Figure 3.8 shows the X-ray diffraction patterns of the 0.03M, %5 In doped IZO thin films for 5 hours which grown at different growth temperatures.

The predominantly preferred growth orientation for each growth temperatures was been along the (100) plane and the growth temperature did not change the preferred growth orientation of ZnO thin films. It is obvious that the appearance of prominent XRD peak is related to hexagonal wurtzite ZnO and in all the samples [160,161].

The peak intensities of preferred (100) growth planes in all the films are 22691, 3928 and 1451 for 90°C, 120°C and 150°C growth temperatures, respectively (in Table 3.3). The peak intensities of the growth planes decreased with growth temperature. It can be said that increasing growth temperature cause the films poorly crystalline.

An extra peak appeared at 2θ = 22,24 and 22,16 for 120℃ and 150℃ growth temperatures, respectively. It was thought that these extra peaks because of the formation of new In(OH)3 phase. When the detected extra XRD peaks compared with values in the JCPDS PDF Card No: 85-1338, they are compatible with the cubic phase of indium hydroxide [162]. The existence of In(OH)3 can be explained as that the most of the adjoined indium ions (In^{+3}) formed theirs oxide form from the solution and it remained as a separate phase rather than being doped into ZnO nanostructures [31,25].

According to results, following chemical reaction for formation of In(OH)3 nanorods was suggested: [162,163]

$$C_6H_{12}N_4 + 6H_2O \rightarrow 6HCHO + 4NH_3 \quad \textbf{(3.2a)}$$

$$In^{3+} + 3\,NH_3 + 3H_2O \rightarrow In(OH)_3 + 3NH_4^{+} \quad \textbf{(3.2b)}$$

Full Width Half Maximum (FWHM), Dislocation density (δ), Crystallite size (D), Microstrain (ε) and Peak intensity values are given in Table 3.3 and the changing crystal quality of films with growth temperature can be seen in Figure 3.9.

Table 3. 3 The structural parameters of the IZO thin films obtained at 5h and different temperatures

Growth Temperature for IZO Thin Film	2θ (100)	d (nm)	FWHM (β)	D (nm)	δ $(nm)^{-2}$	ε x 10^{-3}	Peak Intensity
0.03M- 5h-In %5- 90℃	31.64	0.282	0.2231	37.0031	0.000730	0.936	22691
0.03M- 5h-In %5- 120℃	31.60	0.282	1.5960	5.1724	0.0373	6.701	3928
0.03M- 5h-In %5- 150℃	31.56	0.283	1.7739	4.6533	0.0461	7.448	1451

The lowest FWHM, dislocation density and microstrain values were obtained at the IZO thin film which grown at 90℃ growth temperature. Also, the highest peak intensity and crystallite size were observed at this temperature (in Figure 3.9).

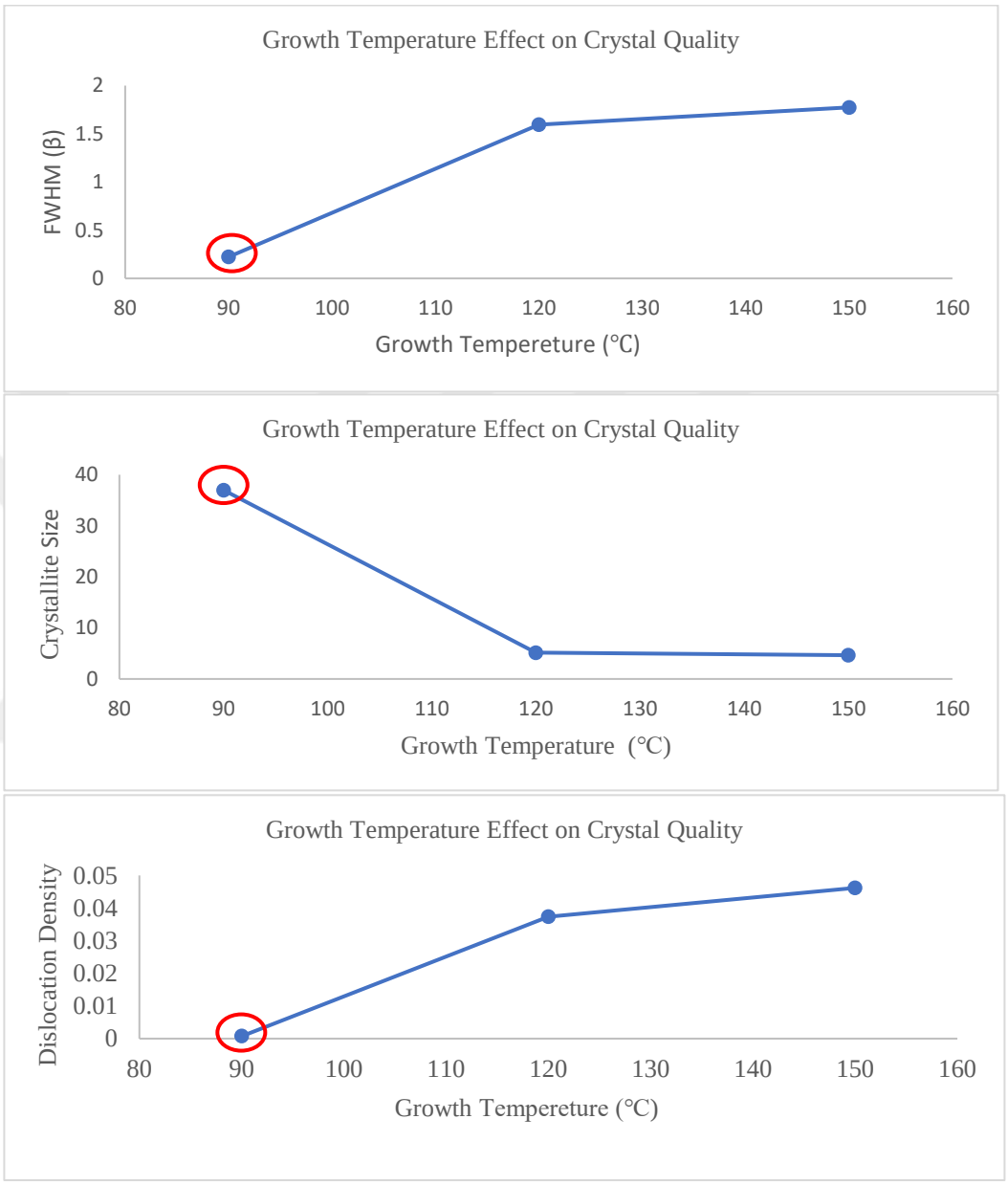

Figure 3. 9 (Continuing): Crystal quality change with growth temperature a) crystal size b) FWHM c) dislocation density d) microstrain e) peak intensity

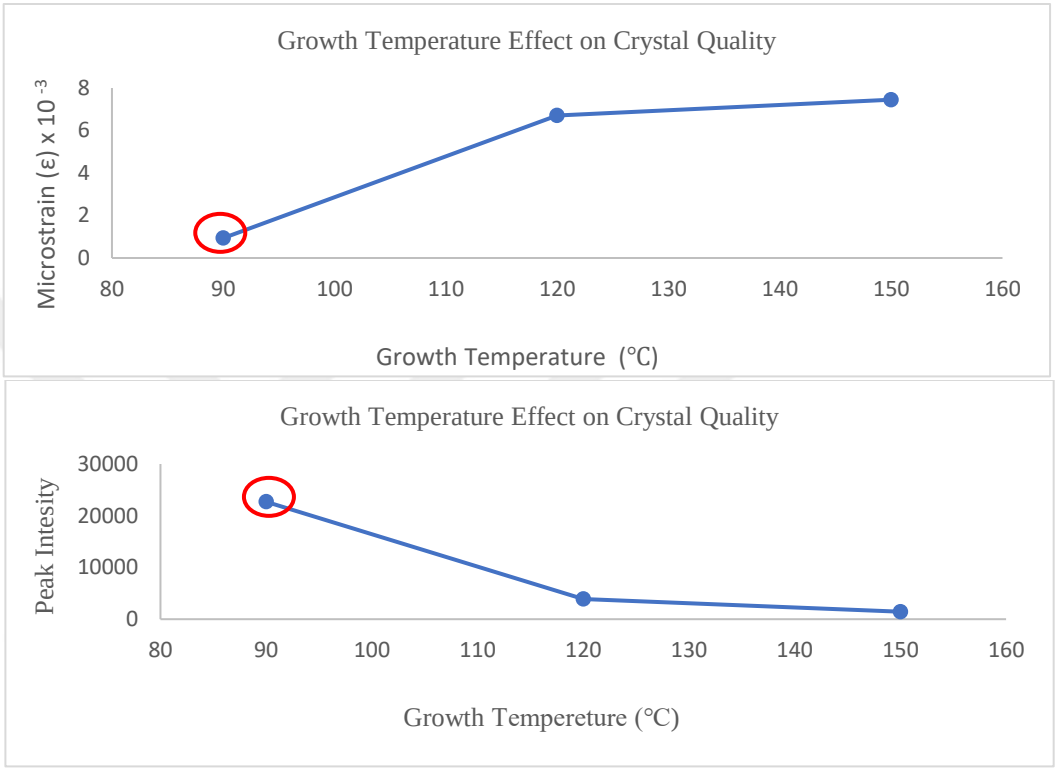

Figure 3. 9 Crystal quality change with growth temperature a) crystal size b) FWHM c) dislocation density d) microstrain e) peak intensity

In addition, with the increasing temperature, the background in XRD graph and tendency to amorphous structure were observed. According to the structural parameters, it can be said that 90°C growth temperature is the best for IZO thin film.

3.3 Surface Properties

3.3.1 Growth Time Effect

SEM images (x500 magnification) of the ZnO thin films grown on the glass substrates at different growth time are given in Figure 3.10.

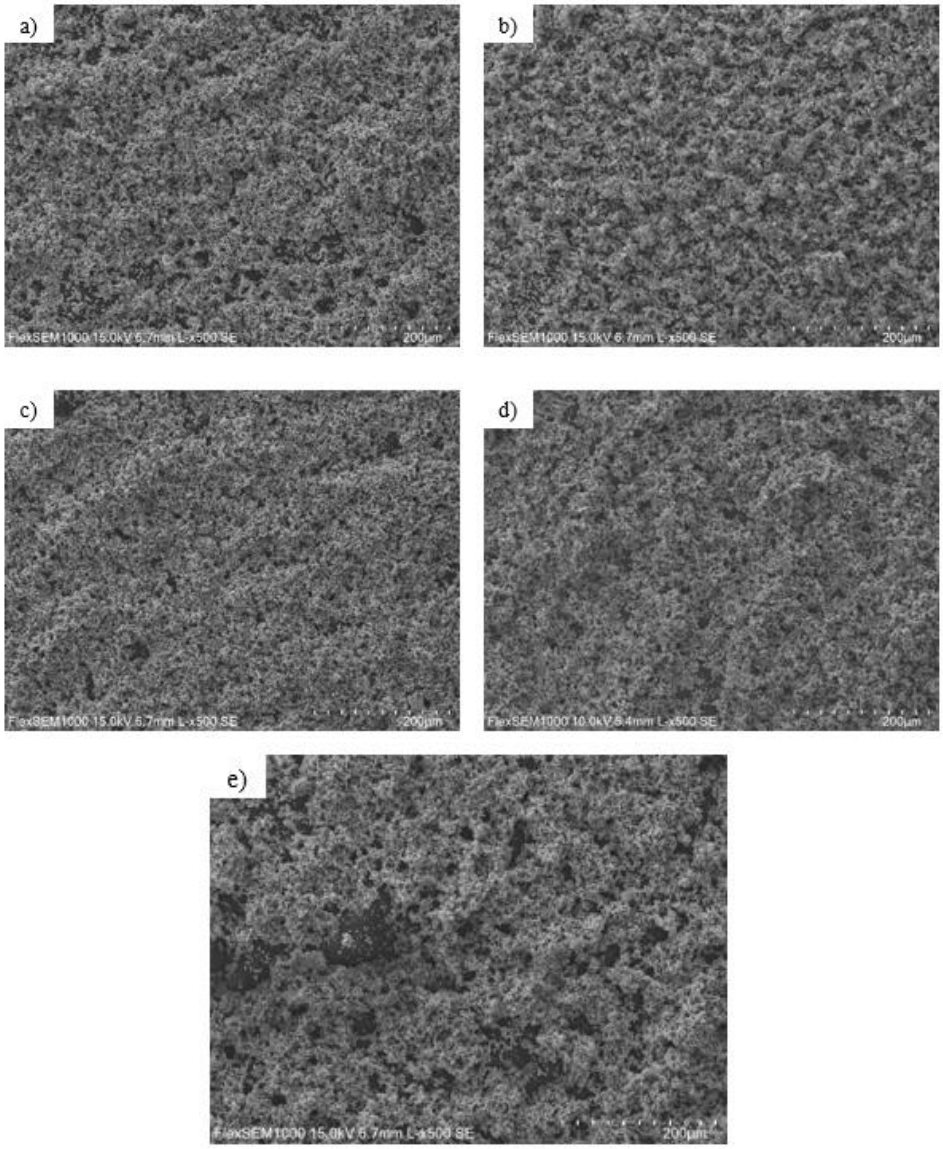

Figure 3. 10 SEM images of ZnO films for a)3h, b)5h, c)7h d)9h e)24h growth time [x500 magnification]

As seen in the Figure 3.10, with increasing growth time, the uniformity, particle distribution, smoothness, packing density, and adhesion to the glass substrates were increased with increasing growth time but at 24h they showed a dramatic decreasing. As can be seen that the ZnO particles more homogeneously covered the substrate at 9h.

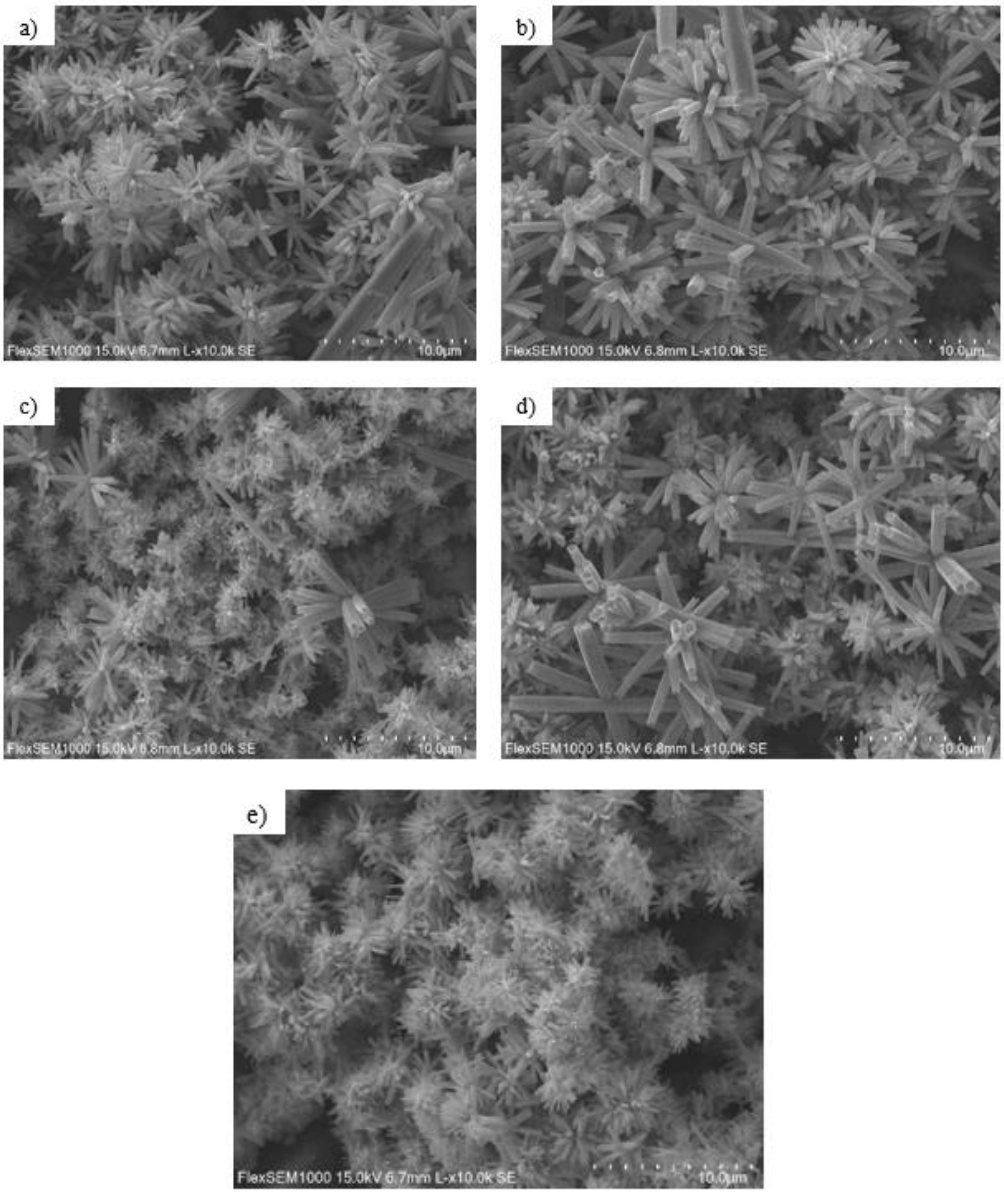

Figure 3. 11 SEM images of ZnO films for a)3h, b)5h, c)7h, d)9h, e)24h growth time [x10000 magnification]

With higher magnification (in Figure 3.11), the morphologies of ZnO nanoparticles became clear. All the film contains ZnO nanorods which have flower-like branched structures. Similar structures have been seen in previous studies [77,152,164].

Also, in Figure 3.12 it is seen clearly, these structures consist of hexagonal nanorods and the most of these nanorods assembled each other from their midpoint [2,142]. The rod shape of ZnO nanoparticles is due to anisotropic growth with different growth rates of each faces. The growth rates rankings of the faces are (0 0 0 1), (1 0 $\bar{1}$ 0), (1 0 $\bar{1}$ $\bar{1}$), (1 0 $\bar{1}$ 0) and (0 0 0 $\bar{1}$), respectively from the high to low rate. When the energy minimization principle is considered, a vertical growth to (0001) plane is more convenient which cause formation of rod shape ZnO [141].

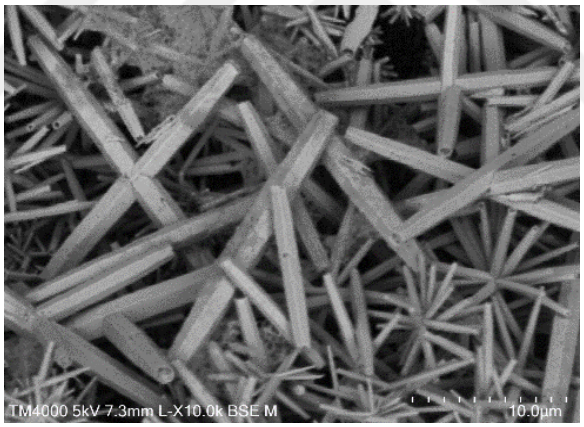

Figure 3. 12 ZnO hexagonal nanorods which have flower-like branched structures [x10000] (0.03M-5h-90°C)

In conclusion, the growth time significantly affected the surface properties of the hydrothermally grown ZnO films. The grown films' uniformity, smoothness, density, and adhesion to the glass substrates enhanced with increasing growth time. However, at a higher growth time (24h), these surface properties worsened [89].

3.3.2 Indium Doping Effect

SEM images of the IZO thin films grown on glass substrates with different doping percentages (1%, 3%, 5%, 7%In) are given in Figure 3.13.

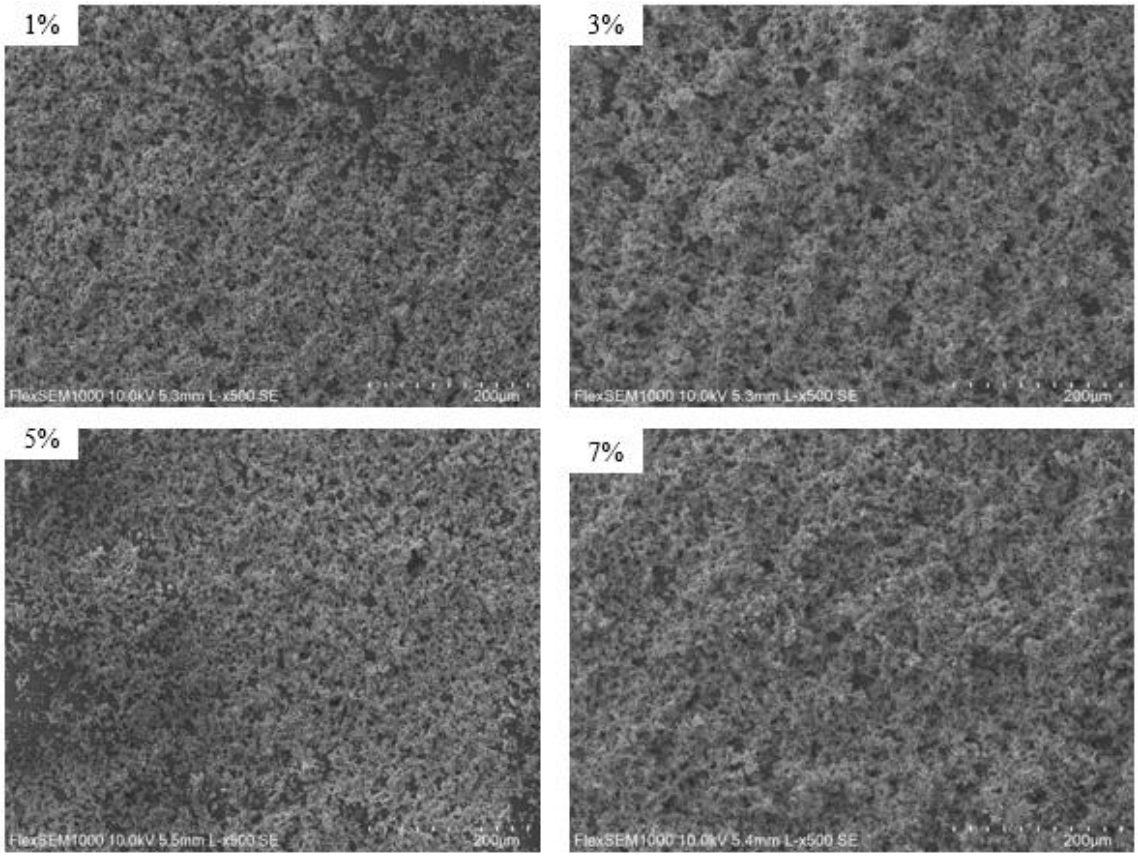

Figure 3. 13 SEM images of IZO films doped by a)1%, b)3%, c)5%, d)7%In [x500 magnification]

At 3% and 7% In doping percentage, the uniformity, particle distribution, packing density, and adhesion to the glass substrate of the IZO films were better than the others. At 1% and 5% In doped films, there are empty areas where adhesion of film on glass substrate was not successful.

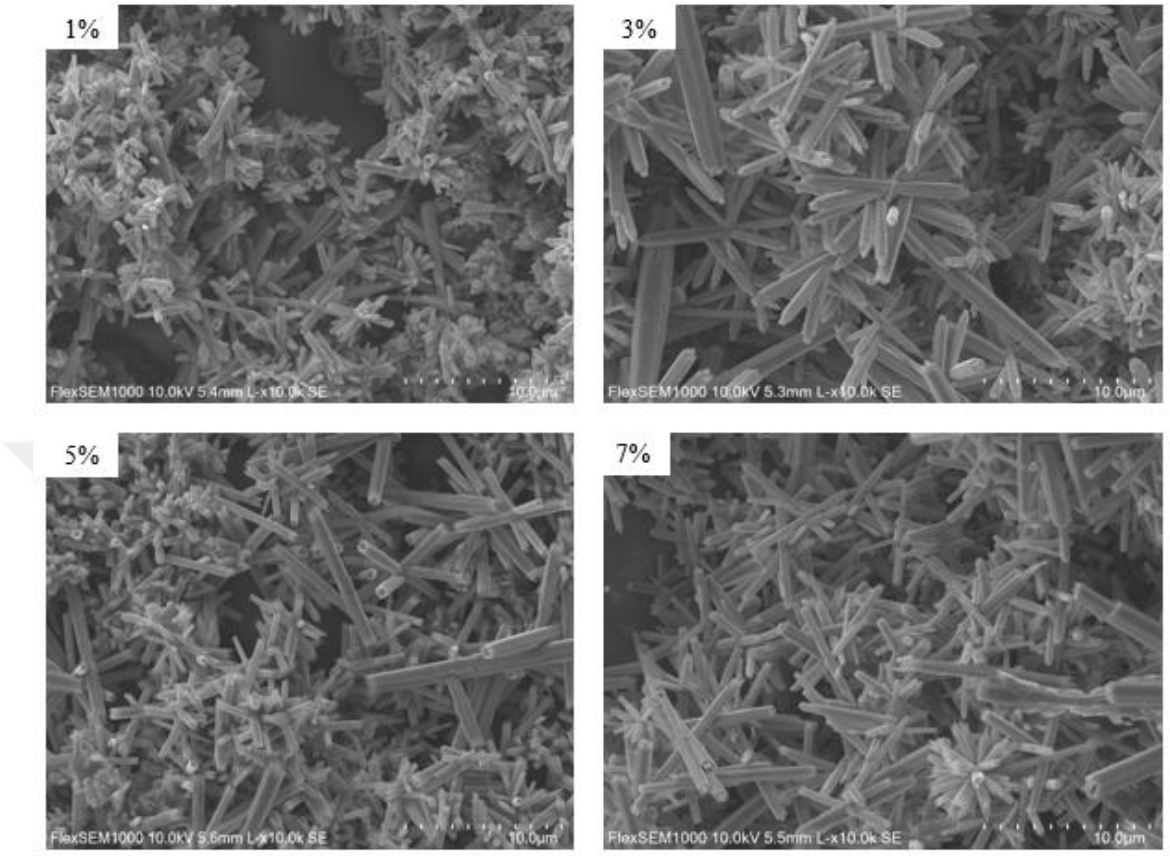

Figure 3. 14 SEM images of IZO films doped by a)1%, b)3%, c)5%, d)7%In [x10000 magnification]

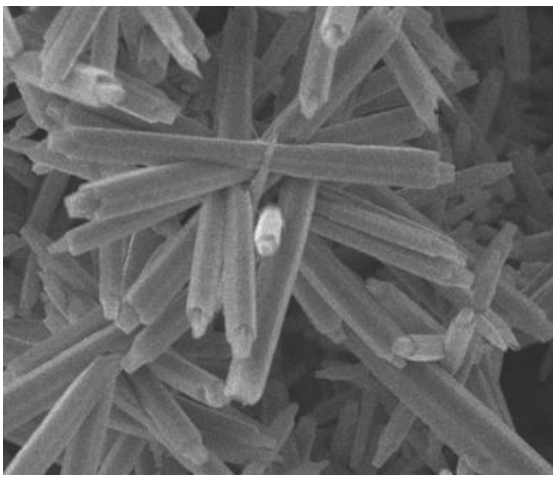

Figure 3. 15 SEM images of pipette like structure of indium doped ZnO

When the Figure 3.11 and 3.14 compared, it was observed that nanoflower structures tend to separate with indium doping. While the nanoflower structures separated slightly, the number of single nanorod increased. Also, despite In doping process, the nanostructures continued to preserve their hexagonal nanorod structures.

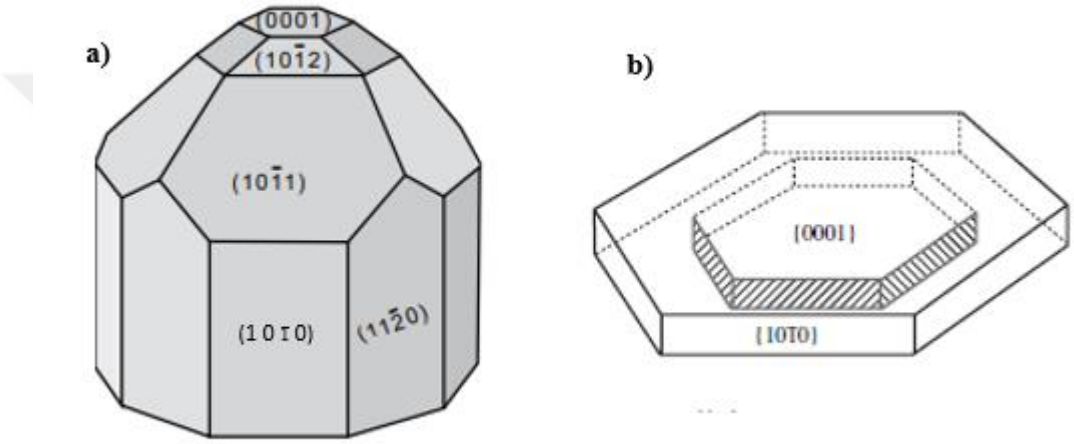

Figure 3. 16 a) Miller indices of nanorods b) Illustration of crystal grown in the presence of In +3 ions. (initial seed were hatched) [165,166]

With the indium doping, formation of hillocks at the ends of rods were seen (in Figure 3.15). The morphological changes of ZnO nanorods is due to the presence of In $^{+3}$ ions. In hydrothermal conditions growth kinetic is affected from the In^{3+} and NH^{4+} impurities. With the presence of In^{+3} ions, the hexagonal prism's growth rate at (1 0 $\bar{1}$ 0) and (1 1 $\bar{2}$ 0) faces greatly increasing. On the other hand, monohedral (0 0 0 $\bar{1}$) and (0 0 0 1) and pyramid faces (1 0 $\bar{1}$ 1) and (1 0 $\bar{1}$ 2) are strongly decreasing. The crystal's faces were given in the Figure 3.16-a and the change of ZnO crystal grown in the presence of In $^{+3}$ ions illustrated in Figure 3.16-b [100,166-168].

These hillocks produced by In $^{+3}$ impurities which hinder the growth of {0 0 0 1} planes. Therefore, both (0 0 0 1) and (0 0 0 $\bar{1}$) faces are smooth for undoped ZnO crystals (in

Figure 3.12), whereas indium doped ZnO (in Figure 3.15) is seen as pipette like nanoparticles on these faces.

As a result, the best homogeneity was obtained at 3% IZO film. Good particle distribution, high packing density, and well adhesion to the glass substrate were observed for 3% In. Also, the particle size of 3% IZO film is bigger which can be seen from Figure 3.14-b. Based on these comparisons, the best indium doping amount was defined as 3% In.

3.4 Optical Properties

3.4.1 Defect Types and Crystallization Quality

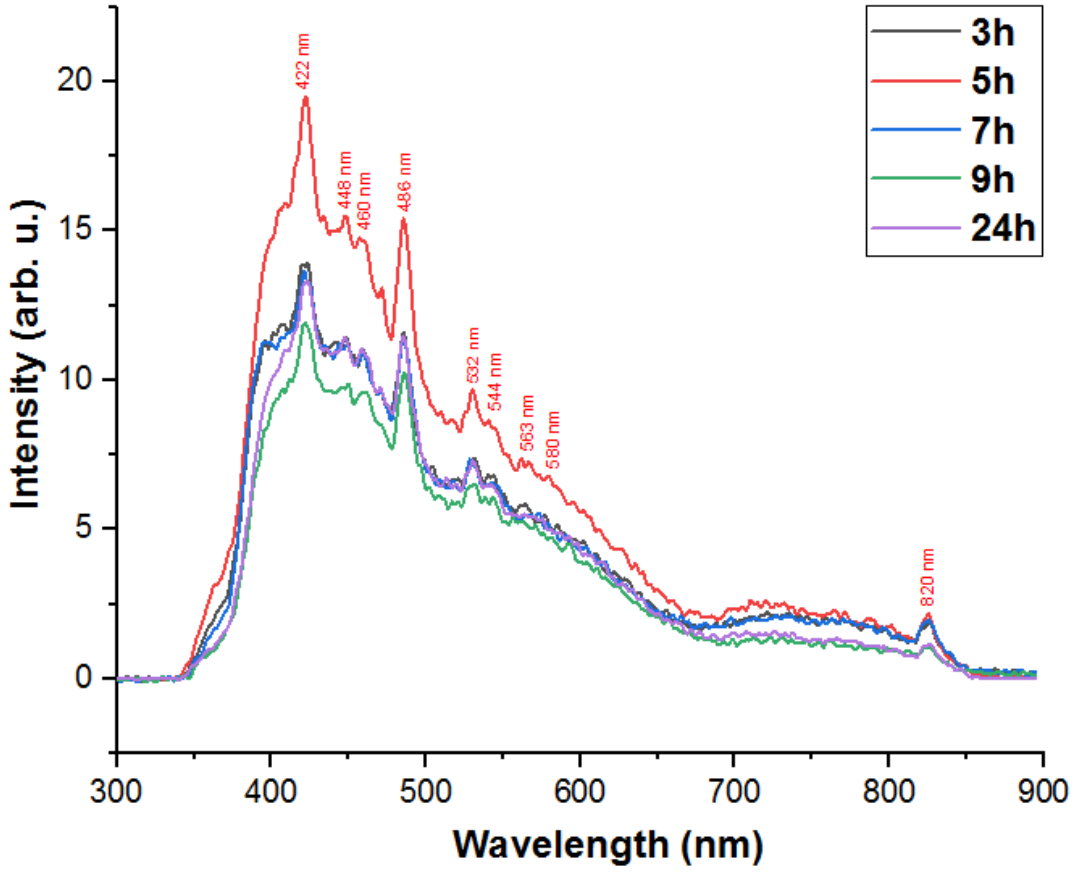

Figure 3. 17 PL graph of ZnO films

From the PL graph (in Figure 3.17). the nine emission bands for ZnO thin films can be seen at 422, 448, 460 486, 532, 544, 563, 580 and 820nm. With the 300nm excitation light which energy is higher that the bandgap energy, ZnO films gave broad and powerful signal at between 400 – 550nm range. The two PL peaks at 422 and 486 were considerably predominant. However, the near band emission (NBE) region can not be seen. According to Zhang et all. (2003) [169], with the 300nm excitation wavelength, UV emission of ZnO

film on various substrate would disappear. Also, it may due to that while generally semiconductor nanoparticles show the excitonic PL signal with higher excitation energy, band to band signal can be obtained rarely [125]. Probably, due to one of these reasons, band to band emission is not exist.

In hydrothermally synthesized materials, red and green emission are mostly observed which are the visible emissions [170-173].

Many researchers suggest that, while generally oxygen vacancy defects in ZnO materials causes the green emission, oxygen interstitial defects and oxygenic species adsorbed on the surface of ZnO leads to red emissions [170,174].

In addition to this common hypothesis, the reason for the low UV and the high visible (green and yellow) emission can probably due to the presence of Zn(OH)2 at the surface [175,176].

Schematic energy band diagram and defect levels for ZnO thin film were given in Figure 3.18.

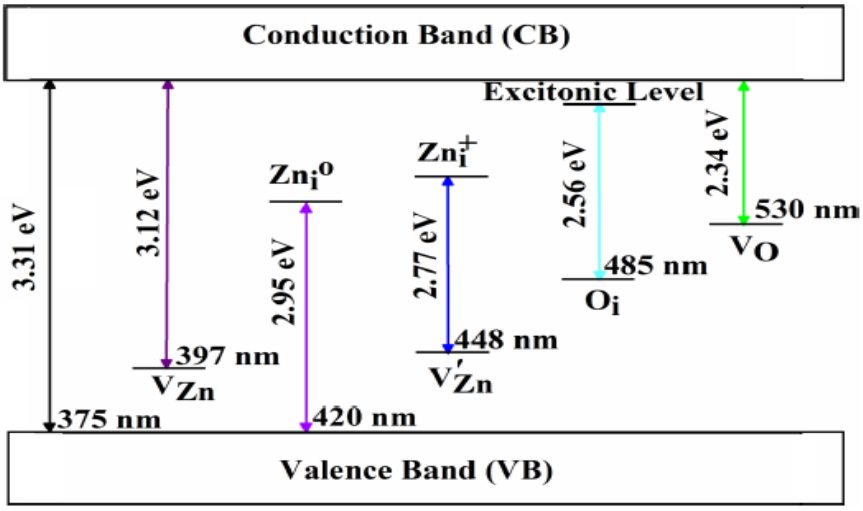

Figure 3. 18 Schematic energy band diagram and defect levels for ZnO thin film [153]

- According to Ahn et all., (2009) [177] the violet emissions are due to the Zni interstitial shallow donor levels. The 422nm which is violet emission band is related with electrons transition from neutral Zni (Zni°) to valance band VB [178].
- The blue emission band at 448nm is represents the transition between Vzn as deep acceptor (Vzn´) and Zni as a shallow donor (Zni^{+}) [179].
- The small peak centered at 460nm originated because of recombination of electron and hole in between Zni and shallow acceptor VZn [180].
- The other blue emission band is 486nm which is due to the transition between Oi and exciton level [153].
- Previous studies present that green emission in ZnO is mostly cause of the oxygen related defects [180,181]. The other considerations for the green emission are the surface defects like electrons adjusted to the conduction band and hole trapped at Vo [121] or singly ionized oxygen vacancy [182].
- The green emission at 532nm is attributed to recombination of hole and ionized oxygen and formation deep Oi state [183].
- For the emission at 544nm it has been suggested that it is generated by conduction band (CB) to Oi transition [177,184,185].
- Also, Vlasenko et al. (2005) [186], Ahn et al. (2009) [177] and Cao et al. (2006) [184] identify contributions to the green emission at 554 nm Zni to Vo transition.
- The deep level involved in the yellow luminescence peak (563) was likely interstitial oxygen which is originated due to antisite oxygen (Ozn) defect state [187].
- During production of ZnO with the low temperature hydrothermal method, stable OH ions may be supported at the ZnO surface and generally forms $Zn(OH)_2$ [188]. It was believed that by some researchers, the yellow emission band for

hydrothermally grown nanorods due to the presence of OH groups on the surface. [175,185] On the other hand, according to some reports, for the produced ZnO from zinc nitrate hydrate and HMTA aqueous solution, the yellow emission is attributed to Oxygen interstitial [182,187,189,190].

- Based on these, it is thought that the yellow emission band which peak at 580nm is related to oxygen interstitials or OH groups on the surface.

- The very broad but low intensity of red PL band which centered at around 730nm was associated with the oxygen interstitials (O_i) which mostly observed in hydrothermal method [191,192].

- According to PL studies, a new near infrared (NIR) PL band emission is observed in addition to visible and UV bands. This band is in the 815-886nm range. Studies showed that it is related to excess oxygen content and unreacted metallic Zn in the ZnO structure. Based on this, the peaks at 820 nm is attributed to neutral oxygen interstitial (Oi) or Zinc interstitial (Zni) defects in ZnO film [193,194].

3.4.1.1 Growth Time Effect

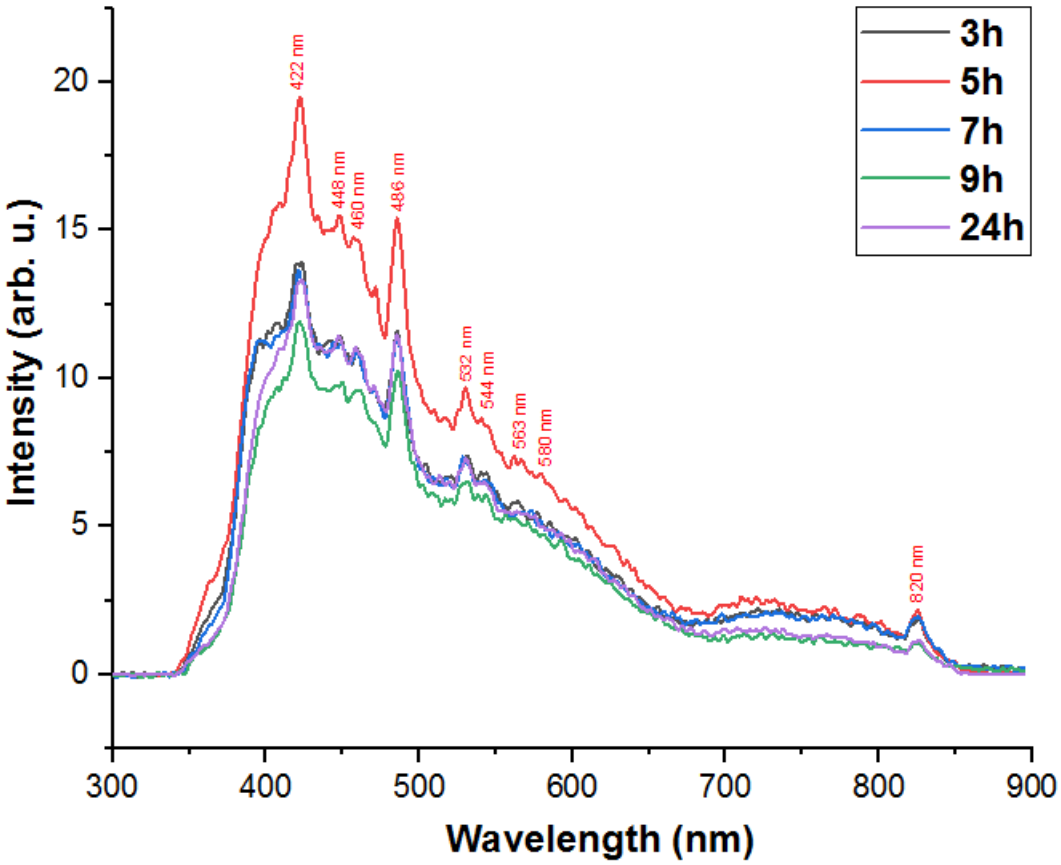

Figure 3. 19 PL graph of ZnO films which are grown at different growth temperature

The photoluminescence spectra for different growth time are given in Figure 3.19. It can be clearly seen the change of visible emission intensity. As mentioned above, the visible emission intensity is related to point defects of ZnO thin films which can be oxygen vacancy, zinc interstitial and impurities [117-122,195].

According to PL spectra (Figure 3.19), when the growth time increased from 3h to 5h the visible light emission peak intensities at 422, 448, 486, 532, 544, 563, and 580 nm increased. After that point it can be said that, with the increasing growth time, the visible light emission peak intensities at these wavelengths quenched. This result can be

explained that the increasing growth time, causes removing of contained defects and gradual improvement on the crystallization quality of the ZnO thin films. Similar results were detected by following researches [99,196]. The lowest PL peaks in visible range was obtained for 9h growth time. Due to high crystallization quality and optical quality 9h have been decided as best growth time. That result is in agreement with the XRD and SEM results.

3.4.1.2 Indium Doping Effect

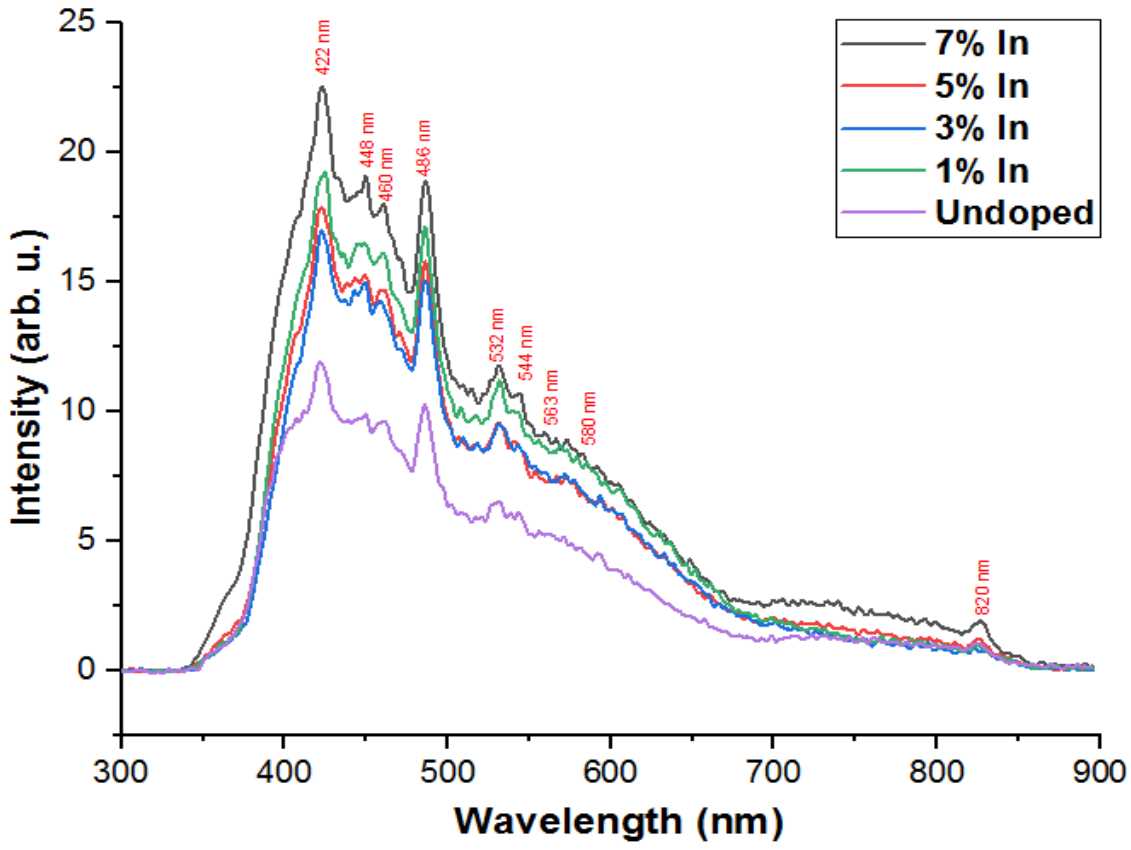

Figure 3. 20 PL graph of IZO films which were doped with different indium percentages

The photoluminescence spectra of IZO films with different dope percentages are given in Figure 3.20 where the change of visible emission intensity can be clearly seen. According to PL spectra, when the dope percentage increased from 1% to 3% the visible light

emission peak intensities at 422, 448, 486, 532, 544, 563, and 580 nm showed a strong decreasing and FWHM values of the peaks were narrowed. After that point, with the increasing indium doping percentage, the visible light emission peak intensities at were gradually increased. This result can be explained that the increasing indium doping percentage, causes new defects states and gradual deterioration on the crystallization quality of the ZnO thin films. Basically, extensive In concentration increased the distortion of the crystal lattice. Similar results were detected by following researchers [36,197].

While the highest PL peaks intensity in visible range was obtained for 7% In, the lowest PL peaks intensity in visible range was obtained for 3% In doping percent. Due to low defect concentration, high crystallization quality, less defect and high optical quality 3% In have been decided as best doping percent. That result is in agreement with the XRD and SEM results.

In addition, when PL spectra of the doped and undoped ZnO films are compared from the Figure 3.20, it can be seen clearly that Indium doping did not cause any new emission and In doping increased the defect intensities. Hence, it can be said that, by controlling the indium dopant amount, the optical properties of ZnO thin films can be adjusted for various purposes [153].

3.4.1.3 Growth Temperature Effect

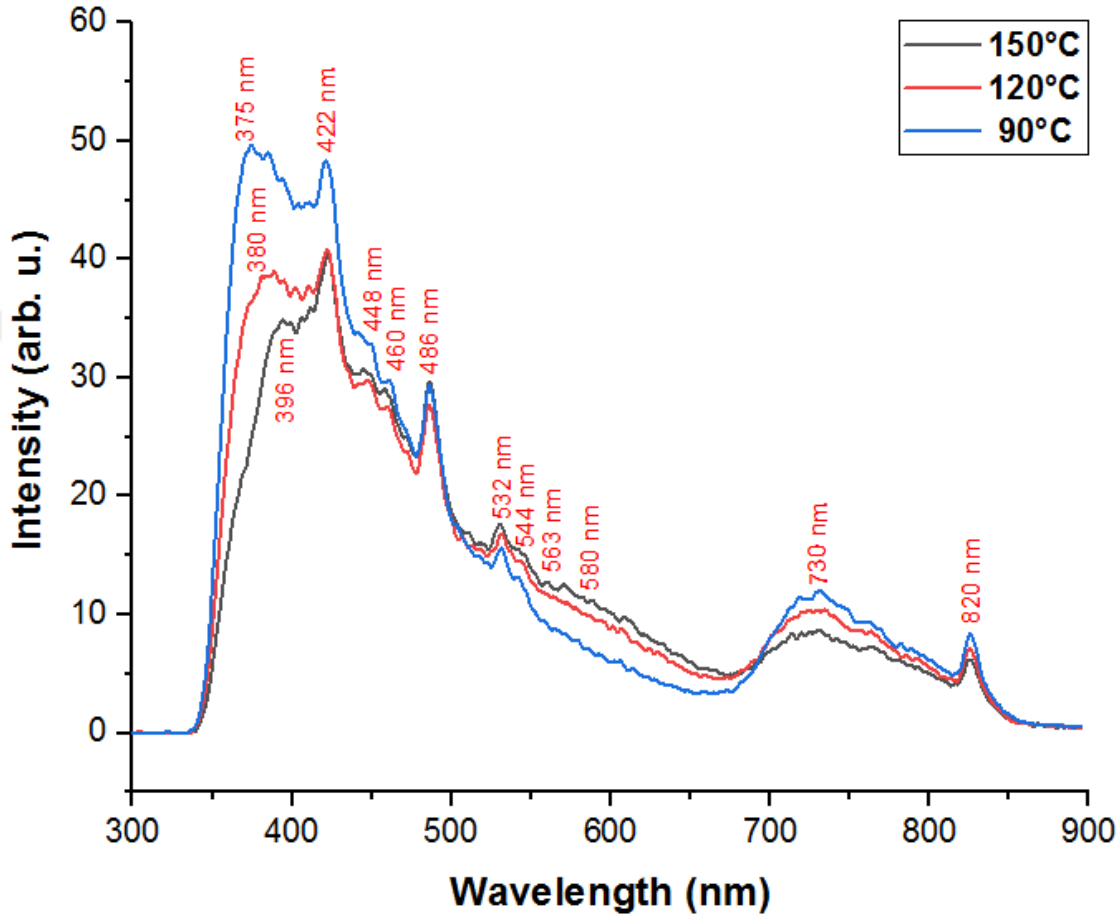

Figure 3. 21 PL graph of IZO thin films with different growth temperature

The PL spectra of IZO film for 90℃, 120℃ and 150℃ growth temperatures were shown in Figure 3.21. UV emission peak was observed at around 380 nm for 90℃, 120℃ and 150℃ growth temperature of IZO films and a broad emission bands obtained at between 400 – 550nm range. The peaks at around 380nm are ultraviolet emission and they occur because of recombination of excitons [185].

For ZnO films, while the green emission is related to deep levels of point defects like oxygen vacancy [195], the UV emission is caused by exciton related activity [198]. The growth temperature of ZnO films correlate with the relative PL intensity ratio of

ultraviolet emission (IUV) to deep level emission (IDLE) of ZnO films. It can be seen from Figure 3.21, with the increasing growth temperature, IUV/ IDLE values are decreased gradually. It was accepted that the crystal quality of ZnO samples values are associated with the of IUV/IDLE [199]. It can be said that with the increasing growth temperature, the crystal quality of ZnO films deteriorated. It may be due to that, with increasing temperature, crystal size decreased; oxygen vacancies and defects increased. Similar results were detected by another researcher [149,200].

With the increasing growth temperature, the excitonic emission peak of the films shifted higher wavelength [33,34,36,201]. The redshift phenomenon can be related to various intrinsic or extrinsic defects or different exciton- phonon interaction which depends on the surface defects [202].

According to photoluminescence spectroscopy results, the best growth temperature for IZO film was chosen as 90°C because of high crystallization and optical quality. These results are in agreement with the XRD results.

3.4.2 Absorption and Energy Bandgap

3.4.2.1 Growth Time Effect

The optical absorption spectra of the ZnO films with different growth time was measured at visible and ultraviolet region and given in the Figure 3.22-a. The observed absorption peaks for different growth time was around 381nm in Figure 3.22-b. Similar results have also been reached by other studies [31,203,204]. Absorption peaks of all the films were lower than that of bulk ZnO (388 nm) [203].

It is obvious from the absorption spectra, there is high absorbance in UV region whose wavelength is below the 400nm. Also, low absorbance is shown in the visible region which means high transparency at this range. This is the optical characteristic of ZnO [205]. Also, at long wavelengths, the low absorption values are observed which is related to the defects on ZnO nanorods that are constituent of film such as oxygen vacancies and interstitial Zn atoms, which act as donor impurities [206].

To determine the energy bandgap (Eg) values of the ZnO films with different growth time measured by Tauc's relation by plotting $(\alpha h\nu)^2$ versus photon energy ($h\nu$) graph in Figure 3.23.

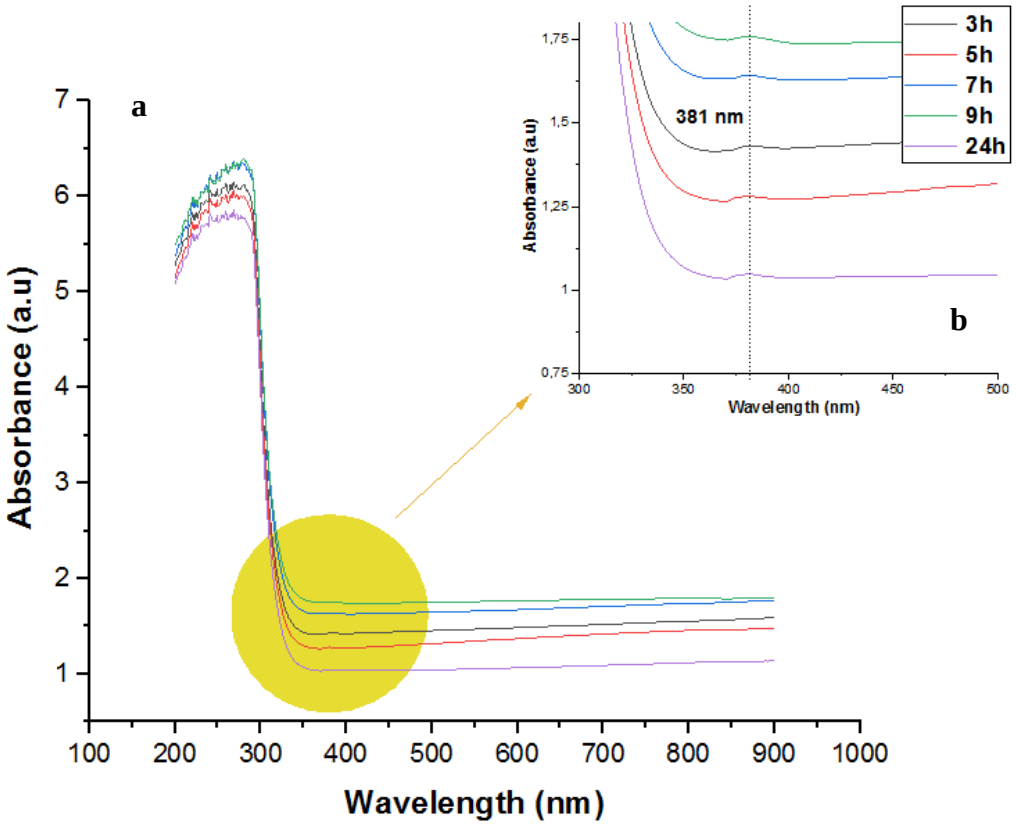

Figure 3. 22 The optical absorption spectra of the ZnO films with different growth time

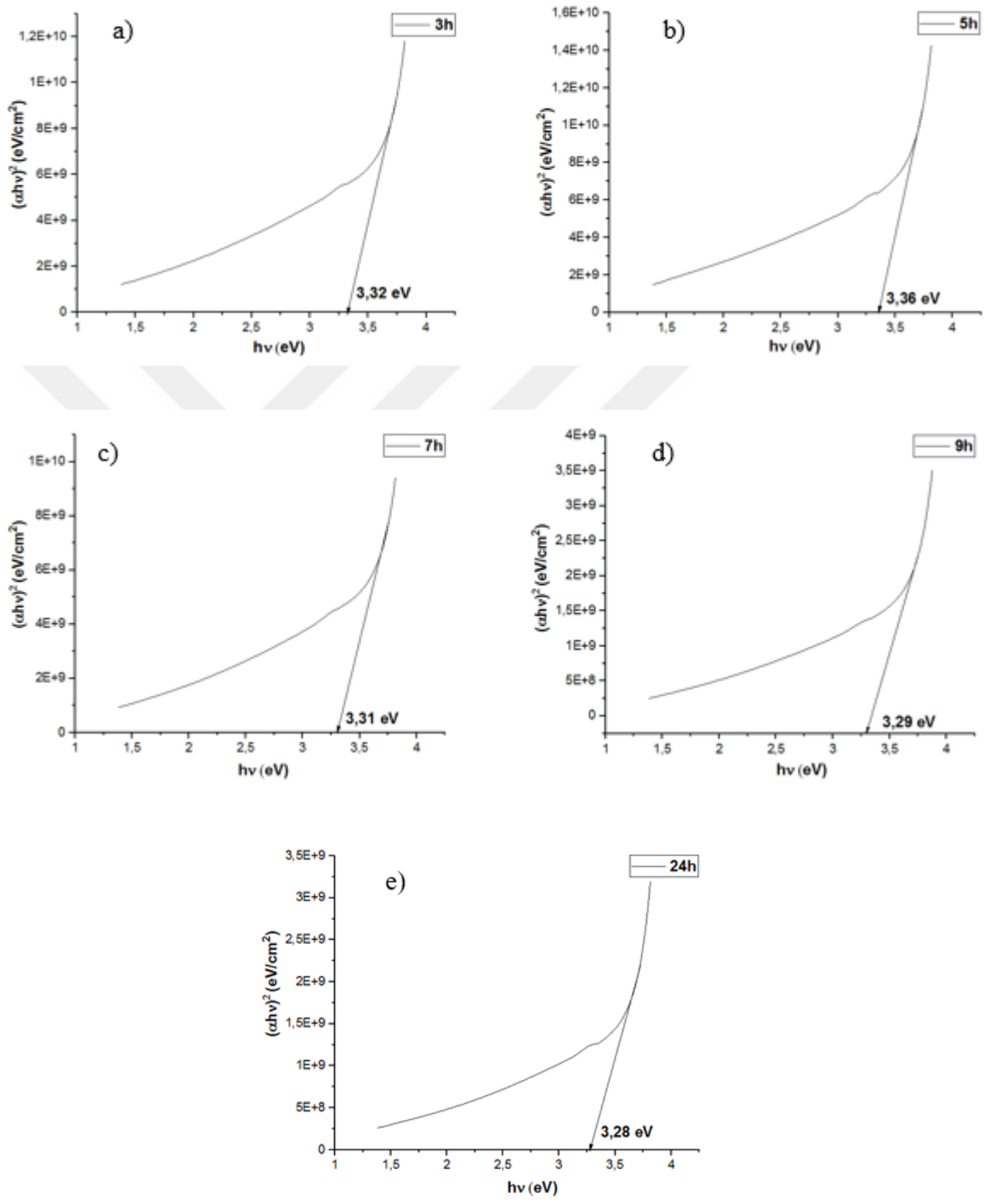

Figure 3. 23 Plot of (αhν)2 versus (hν) for ZnO films grown at various growth times a) 3h b)5h c)7h d)9h e)24h

It can be said that, the transition region is around 3.3 eV. This is related to the direct transition between valance band and conduction band and it shows the optical energy band gap of the ZnO semiconductor [205]. The obtained energy band gap (Eg) values of ZnO thin films are 3.32, 3.36, 3.31, 3.29 and 3. 28eV for different growth times that 3h, 5h, 7h, 9h and 24h, respectively. This band gap value ranges are compatible with the literature [7,207]. The optical energy band gap of bulk ZnO is about 3.37 eV and it is higher than the ZnO films because of the optical confinement effect of the formation of ZnO nanorods [208,209].

Bandgap energy shows a decreasing trend with increasing growth time except 5h. The bandgap changing with growth time was illustrated in Figure 3.24 [210]. Grain size, stress state and carrier concentration of the films affects the energy band gap (Eg) value [211].

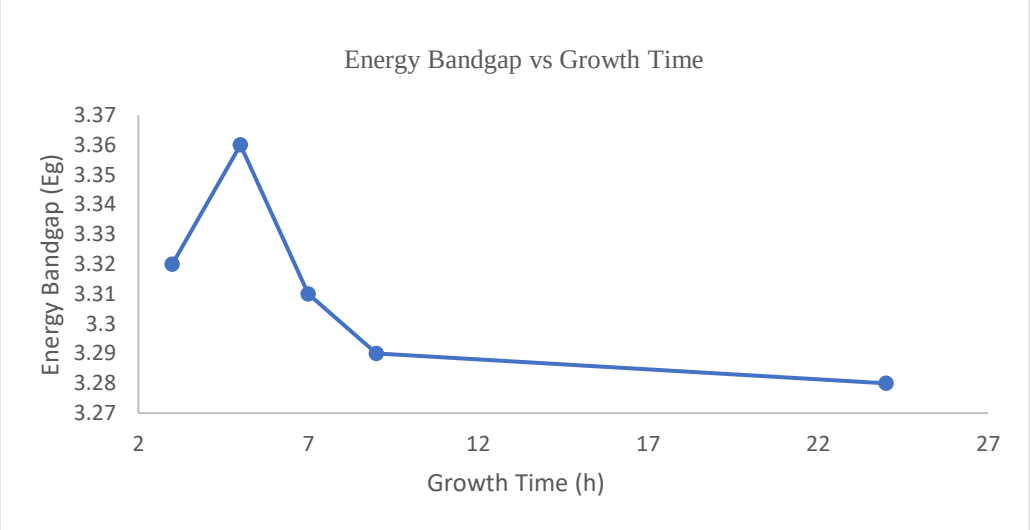

Figure 3. 24 Bandgap changing with the growth time

The increasing grain size, decreasing defect, tensile stress and oxygen vacancies can lead to lower carrier concentration in conduction band. As a result of the lowered carrier concentration, the energy band gap narrows [212,213].

The equation (3.3), proves that the narrowing optical energy gap is because of the decrease of carrier concentration [214].

$$\Delta Eg = \left(\frac{\hbar^2}{2m*_{cv}}\right)(3\pi^2 N)^{2/3} \quad \textbf{(3.3)}$$

where the ΔEg is the shift in the optical energy gap, $\hbar$ is Planck's constant, m_{cv} is the electron's effective mass, and N is the carrier concentration [215].

The decrease in the bandgap of ZnO thin films can be associated with the grain size. The increasing crystallite size of films with the increasing time caused the decrease in the bandgap values. The crystallite size of the ZnO film was 33.93, 31.99, 34.06, 34.51 and 34.55nm for 3h, 5h, 7h, 9h and 24h, respectively which are in direct proportion to bandgap change. This relationship can be seen from Figure 3.25 [213,216,217].

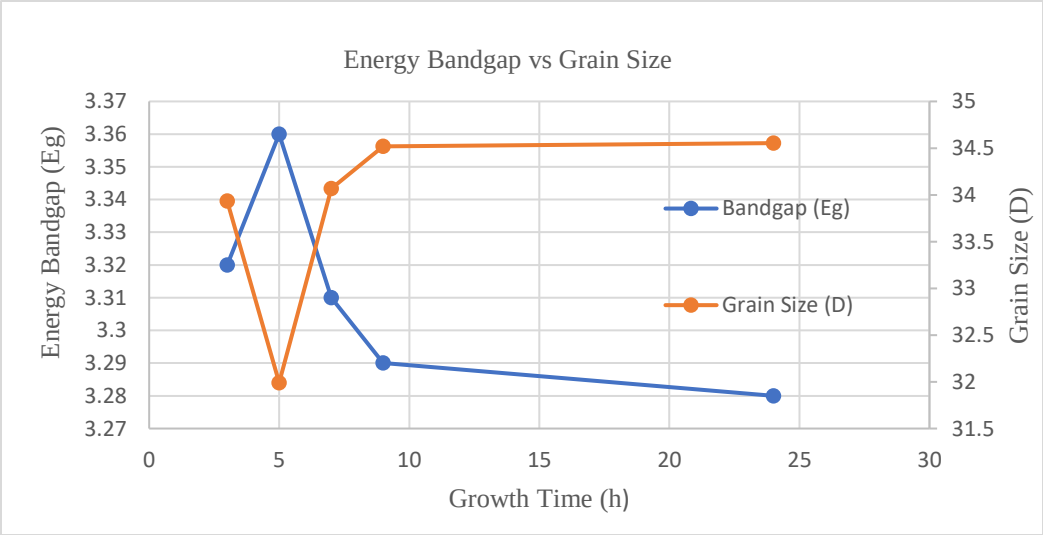

Figure 3. 25 Relation between energy bandgap and grain size

3.4.2.2 Indium Doping Effect

The optical absorption spectra of the IZO films with different doping percent was measured at visible and ultraviolet region and given in the Figure 3.26-a. The observed absorption peaks for various doping amount around 381 nm in Figure 3.26-b which means there is high absorbance in UV region below the 400nm wavelength [203].

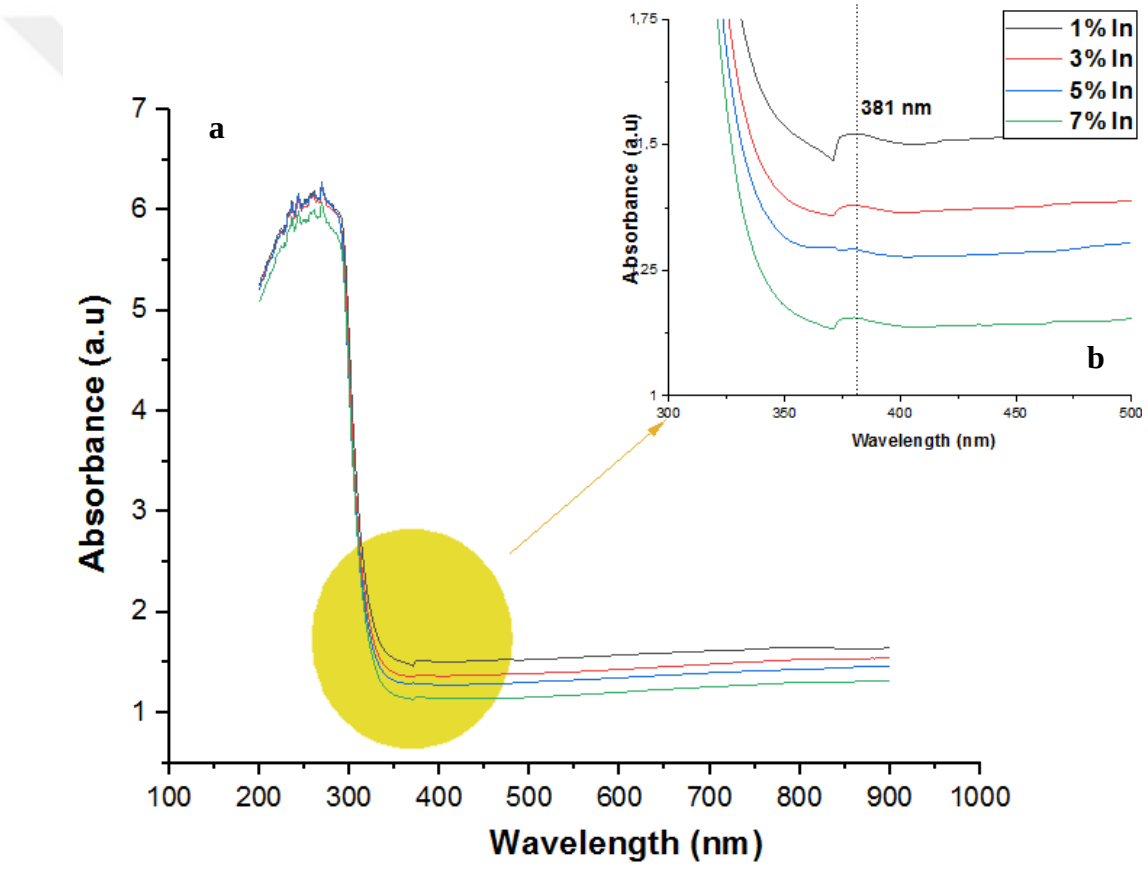

Figure 3. 26 The optical absorption spectra of the IZO films with doping percentage

UV- Vis spectrum of IZO films shows well defined absorption peak at 380nm. This peak is related to hexagonal wurtzite phase ZnO and characteristic peak for bandgap of ZnO [218-220]. No extra absorption peak was observed in the UV- Vis spectrum which is

related to any impurity. Based on this information, it can be said that, the grown IZO thin films have good optical properties [221].

The plot of $(\alpha h\nu)^2$ versus photon energy ($h\nu$) are given in the Figure 3.27, to determine the bandgap values of IZO films with changing dopant amount.

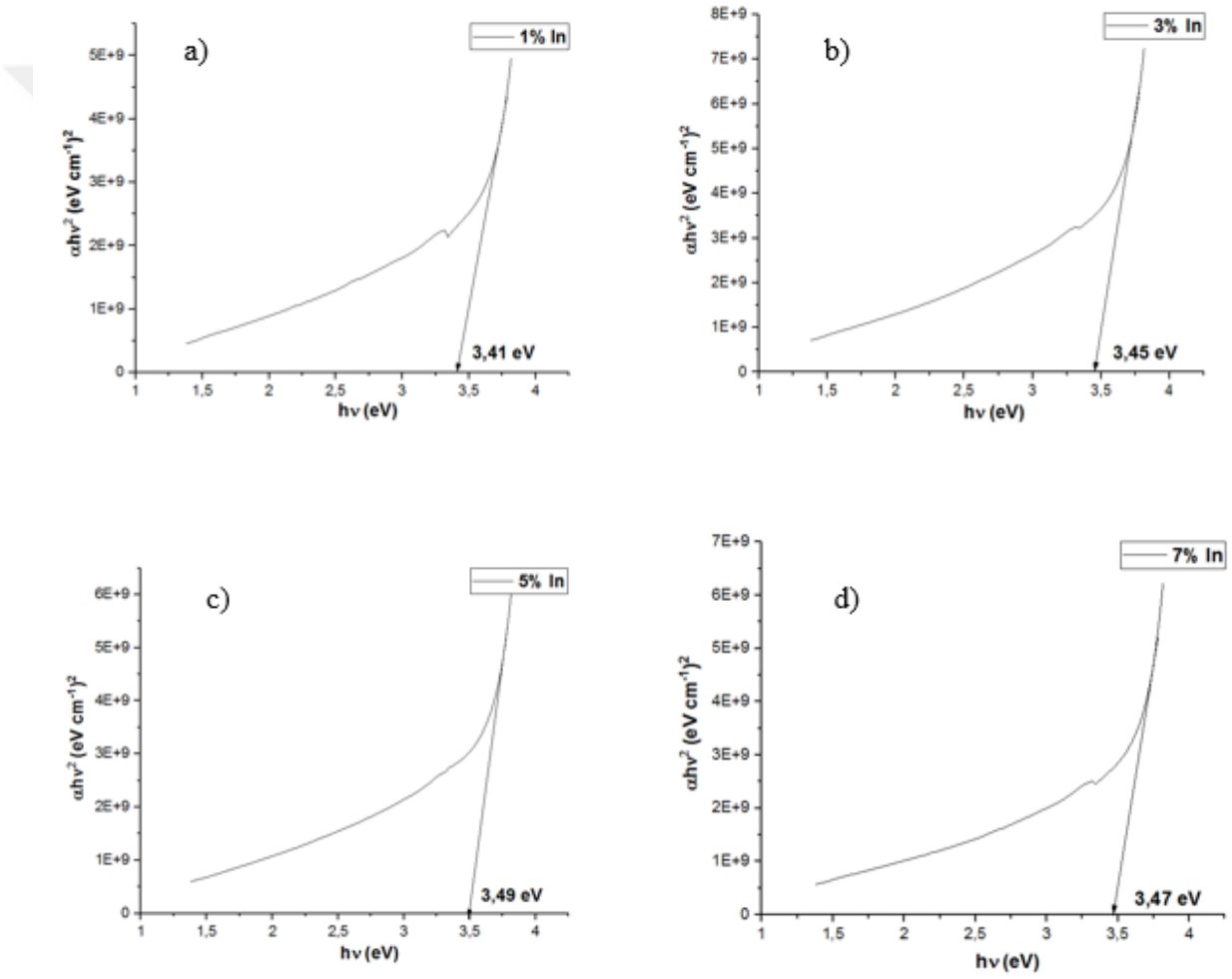

Figure 3. 27 Plot of (αhν)2 versus (hν) for IZO films doped with various percentages a) 1% b) 3% c) 5% d) 7%In

The impurity addition to wide bandgap semiconductors like ZnO, mostly causes dramatic changes in optical properties. Doping process concluded with the replacing Zn^{+2} ions with

higher valency atoms. The performance of impurities is related to the ionic radius and electronegativity of atoms [28].

The dopants can be used in ZnO lattice for the controlled application of ZnO as various impurity. The significant aim of the doping with various dopant is tailoring and modifying the bandgap of ZnO [221].

Generally, group III, IV, and V elements are used as a dopant material to enhance the optical and electrical behaviors of ZnO. Indium is a positively charged substitution group III elements and indium dopants gives free electrons to the ZnO structure. By this way, it increases the optical band gap and n-type conductivity [222-224].

The transition region of indium doped ZnO films is around 3.4 eV. This is related to the direct transition between valance band and conduction band. It shows the ZnO semiconductor's optical energy band gap [205]. The obtained energy band gap (Eg) values of IZO thin films are 3.41, 3.45, 3.49 and 3. 47eV for different indium doping percentage of 1%, 3%, 5%, and 7%, In, respectively. The bandgap values are in agreement with the other IZO film researches [25,225-227]. The Eg changing with In concentration was given in Figure 3.28.

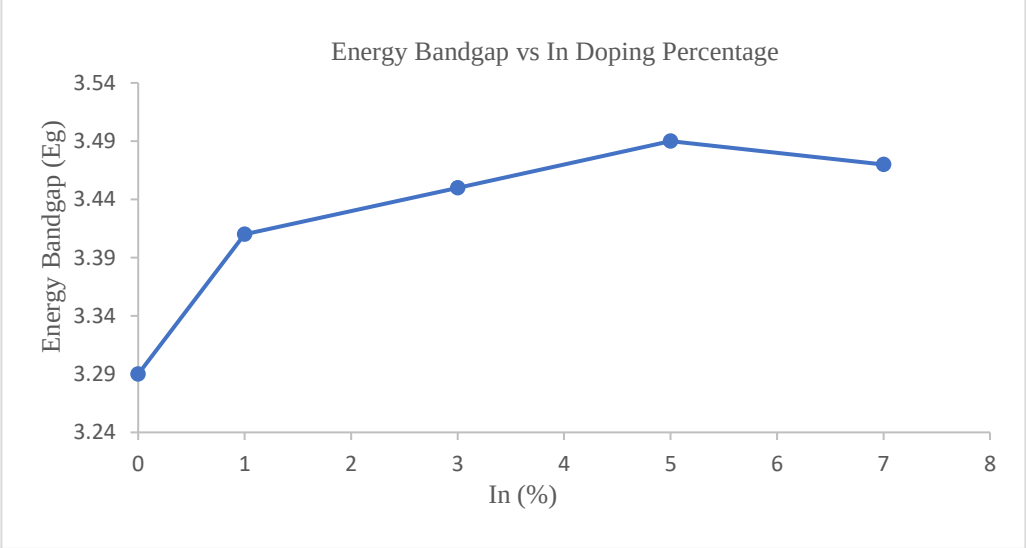

Figure 3. 28 Bandgap changing with the indium percentage

The energy band gap (Eg) of the IZO films increased with increasing indium concentration up to 5%In and slightly decreased at 7%In. The same phenomenon was reported in another IZO thin film study in which %5In doped IZO film's bandgap was found as 3.46eV then it decreased at 7%In [225]. Also, for Al doped ZnO thin films showed the same behavior. [228]. The bandgap of all indium doped IZO films are higher than intrinsic ZnO film Similar bandgap change with indium doping was indicated in the other studies [229-232].

With indium doping, in the ZnO crystal lattice stresses and defects were produced due to the replacement of In^{+3} ions and Zn^{+2} ions. The lattice distortion from the stress and defects caused some changes in the structural and optical properties of ZnO [228].

With increasing indium percentage, the blue shift in the band gap was continued to rise up to 5%. The addition of indium dopant was caused increasing of band gap of films which is most probably due to degenerated semiconductor [228] and increasing in the carrier concentration by doping [225,233-235].

This widening of optical band gap with indium doping attributed to the Burstein–Moss shift. Following researches also support this idea [230,231,233,236-238]. The Burstein–Moss effect can be explained as that, in the degenerated semiconductor, conduction band is highly filled with carrier concentration. While the lowest valance band is blocked, Fermi level lifted into conduction band. Hence, the increasing Fermi level in conduction bands causes widening of apparent band gap energy by way of high carrier concentration. However, the apparent band gap is not actual band gap energy. While the apparent optical energy band gap is related to the excitation of the electrons from the valance band to the Fermi level in the conduction band, the actual band gap of the material is related to the excitation of the electrons from the top of the valence band to the bottom of the conduction band. In conclusion, the widening energy band due to the increasing carrier concentration which causes elevate the fermi level and degenerate the semiconductor [228,231,233,239-241].

On the other hand, narrowing of optical band gap after 5%In doping, is generally caused by energy shift in conduction and valance band. Which is resulted due to some effects like

electron impurity and electron - electron interaction [227,242]. It can be said that the shrinkage effect is became more dominant over the Burstein Moss effect at higher than 5%In [225,243].

3.4.2.3 Growth Temperature Effect

The optical absorption spectra of the IZO films with different growth temperature was measured at visible and ultraviolet region and given in the Figure 3.29-a. The observed absorption peaks for various growth temperatures around 380 nm in Figure 3.29-b.

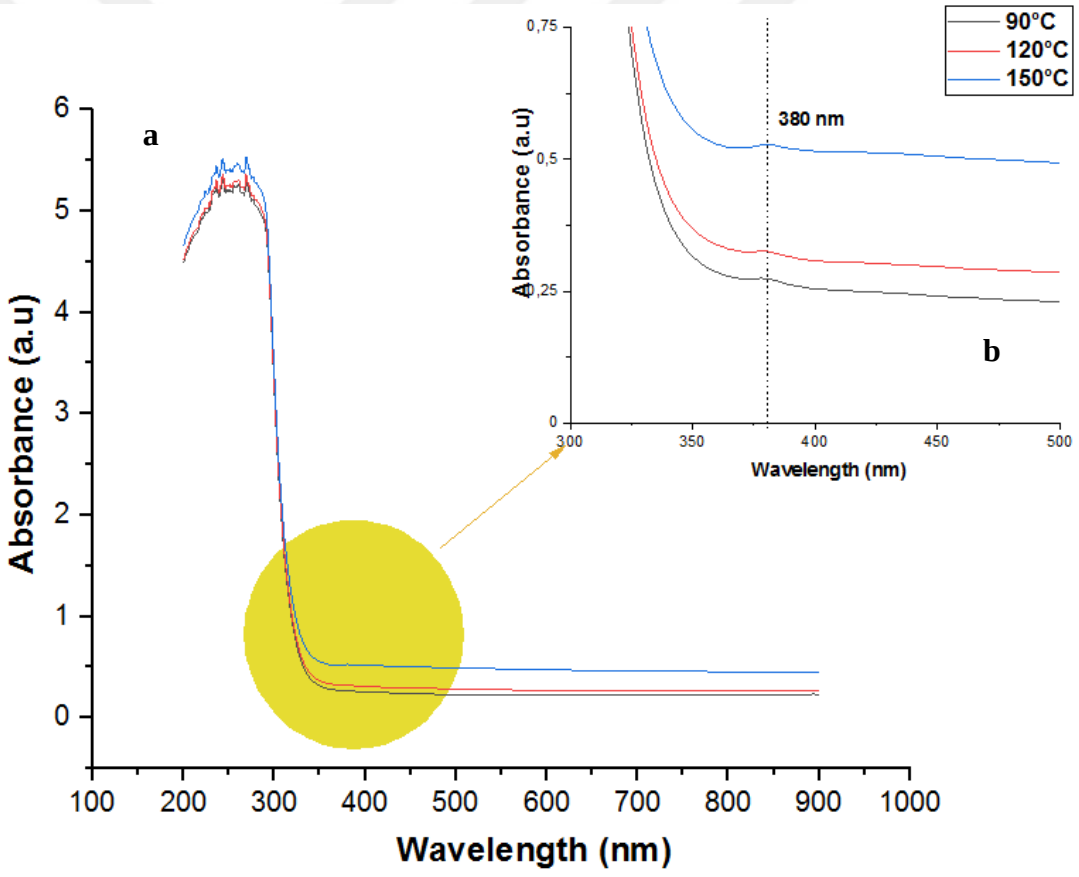

Figure 3. 29 The optical absorption spectra of the IZO films with different growth time

The plot of $(\alpha h\nu)^2$ versus photon energy ($h\nu$) are given in the Figure 3.30, to determine the bandgap values of IZO films with changing dopant amount.

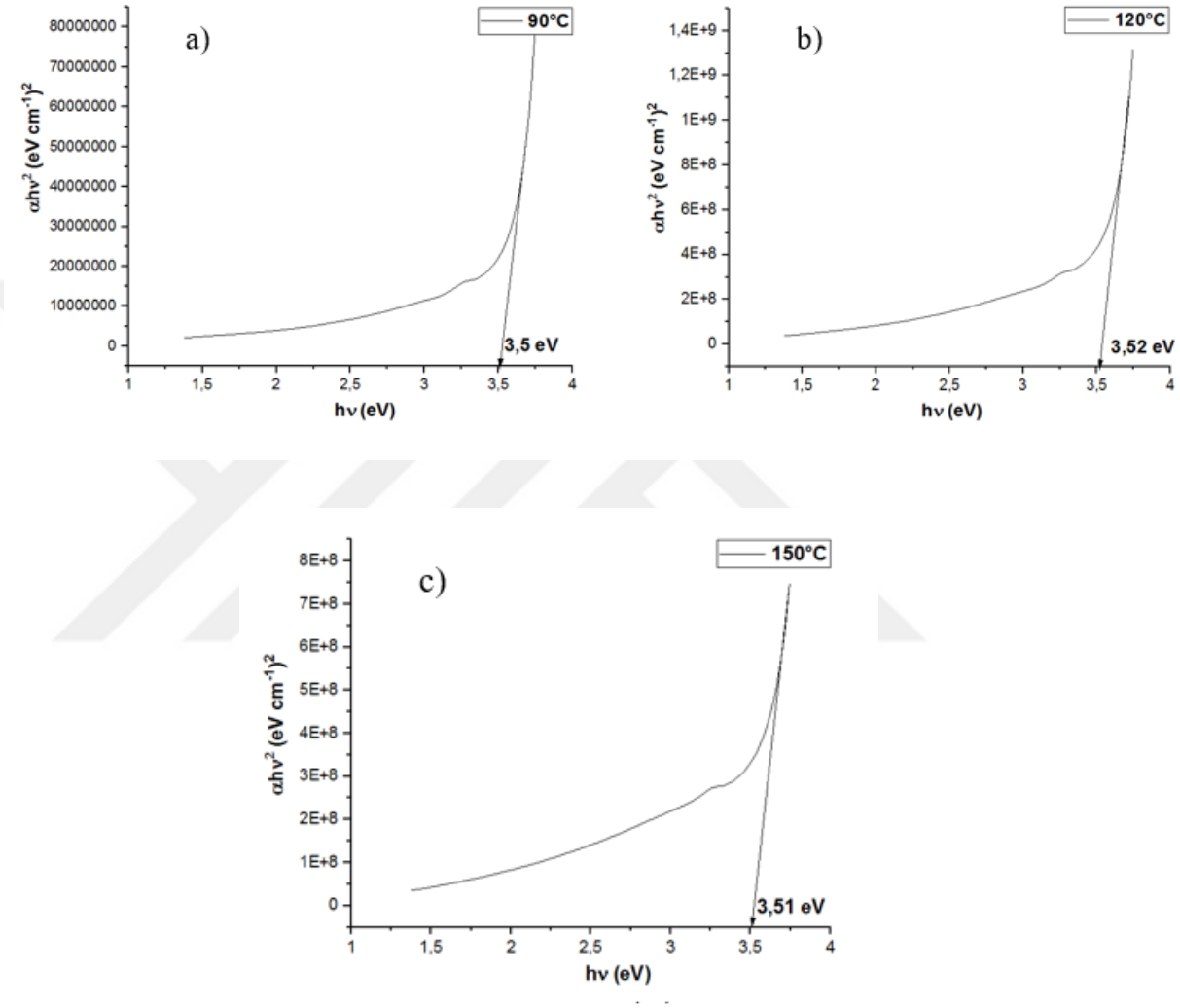

Figure 3. 30 Plot of (αhν)2 versus (hν) for IZO films grown at various growth temperature a) 90℃ b)120℃ c)150℃

It can be said that, the transition region is around 3.5 eV. This is related to the direct transition between valance band and conduction band and it shows the optical energy band gap of the produced ZnO semiconductor [205]. The obtained energy band gap (Eg) values of thin films are 3.50, 3.52 and 3.51eV for different growth temperature that 90℃, 120℃

and 150℃, respectively. The bandgap changing with growth temperature was illustrated in Figure 3.31.

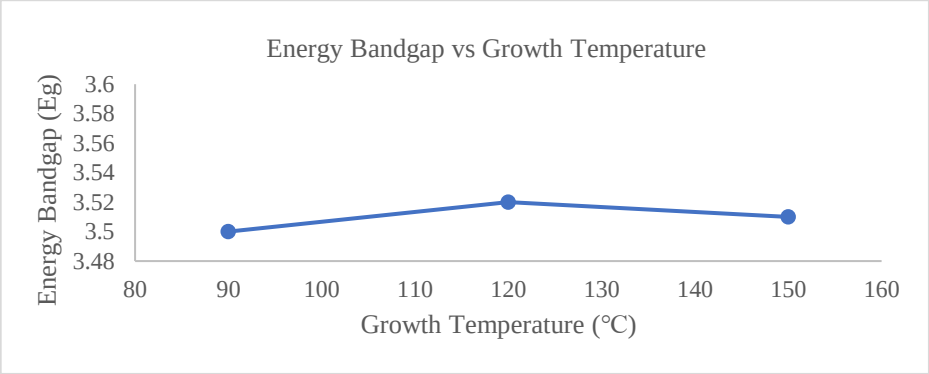

Figure 3. 31 Bandgap changing with the growth temperature

The energy band gap (Eg) of the films very slightly increased, after that decreased with increasing growth temperature. There was no considerable change in the bandgap values with the growth temperature. Similar results were indicated in different researches [180].

3.4.3 Refractive Index and Dielectric Constant

The dielectric constant (ε) and refractive index (n) of semiconductors is very substantial for determining the optical and electrical properties of the crystals. Refractive index is necessary for optoelectronic devices and solar cell applications. The refractive index of the films was calculated using Herve and Vandamme and Moss Relation Equ (2.10) and (2.9), respectively. Also, dielectric constant and static dielectric constant calculated by Equ (2.11) and Equ (2.12), respectively. Table 3.4 shows the refractive index and dielectric constant changes for different growth time.

Table 3. 4 Refractive index, optical and static dielectric constant changes for different growth time

	Herve and Vandamme		Moss Relation		Static Dielectric
Growth Time for ZnO Thin Films	**n**	**ε_∞**	**n**	**ε_∞**	**ε_0**
3h	2.257	5.09	2.388	5.70	8.29
5h	2.246	5.04	2.381	5.66	8.17
7h	2.260	5.10	2.390	5.71	8.32
9h	2.265	5.13	2.393	5.72	8.38
24h	2.268	5.14	2.395	5.73	8.41

Refractive index of ZnO films behaves the opposite way with the energy band gap. It can be said that, if the material has larger band gap energy, it has lower refractive index or vice versa. It can be seen from Equ (2.9) and (2.10) [244]. Also, according to the Equ (2.11), the dielectric function is directly proportional to square of refractive index.

With the increasing growth time, the refractive index, dielectric constant, and static dielectric constant values not much changed but slowly increased. This behavior is parallel with the bandgap energy change of ZnO films with growth time. It was supposed that with the increasing growth time the crystal size increased which caused decrease of carrier concentration therefore, the refractive index of films increased [213,225].

According to Herve and Vandemme equation, the lowest refractive index value was 2.246 and the highest value was 2.268 for different growth time. While the lowest dielectric constant was 5.04, the highest one 5.14. On the other hand, according to Moss relation, the lowest refractive index value was 2.381 and the highest value was 2.395 for different growth time. While the lowest optical dielectric constant was 5.66, the highest one 5.73. The lowest static dielectric constant was measured as 8.17 and the highest one as 8.41. The dielectric constant range of ZnO films are compatible with the fallowing reports [245,246].

The refractive index and dielectric constant changing with different In doping percentages were given in Table 3.5.

Table 3. 5 Refractive index, optical and static dielectric constant changes for In doping percentages

	Herve and Vandamme		**Moss Relation**		**Static Dielectric**
Doping Percentage of IZO Thin Films	**n**	**ε_∞**	**n**	**ε_∞**	**ε_0**
1%	2.233	4.98	2.372	5.62	8.01
3%	2.223	4.94	2.365	5.59	7.89
5%	2.212	4.89	2.358	5.56	7.77
7%	2.217	4.91	2.361	5.57	7.83

While the highest refractive index, optical dielectric constant, and static dielectric constant values were calculated for 1% In doping, the lowest values were calculated for 5%In doping.

With the increasing doping percentage, the refractive index, dielectric constant, and static dielectric constant values decreased. This behavior is parallel with the bandgap energy change of IZO films and the decrease of refractive index can be attributed to increased carrier concentration [247-249].

The refractive index and dielectric constant changing for different growth temperature were given in Table 3.6.

Table 3. 6 Refractive index, optical and static dielectric constant changes for different temperatures

	Herve and Vandamme		**Moss Relation**		**Static Dielectric**
Growth Temperature for IZO Thin Films	**n**	**ε_∞**	**n**	**ε_∞**	**ε_0**
90°C	2.21	4.88	2.372	5.55	7.74
120°C	2.205	4.86	2.365	5.53	7.67
150°C	2.207	4.87	2.358	5.54	7.70

According to Herve and Vandemme equation, the lowest refractive index value was 2.205 and the highest value was 2.21 for different growth temperature. While the lowest optical dielectric constant was 4.86, the highest one 4.88. On the other hand, according to Moss relation, the lowest refractive index value was 2.358 and the highest value was 2.372 for different growth time. While the lowest optical dielectric constant was 5.53, the highest one 5.55. The lowest static dielectric constant was measured as 7.67 and the highest as 7.74. These static dielectric constant values are in agreement with the following reports [245,250].

With the increasing growth temperature, the refractive index, optical dielectric constant, and static dielectric constant values decreased. This decreasing with the increasing growth temperature was attributed to decreasing crystal size and increasing carrier concentration [213,225,251].

CHAPTER 4

CONCLUSION

Zinc oxide (ZnO) and Indium doped zinc oxide (IZO) thin films were successfully grown on the glass substrate by hydrothermal method with different growth time, indium doping percentage, and growth temperature. The effects of In doping and hydrothermal method parameters; growth time and growth temperature on the structural, surface and optical properties of ZnO films were investigated. For this aim X-Ray Diffraction (XRD), Scanning Electron Microscopy (SEM), Photoluminescence spectroscopy (PL) and UV-VIS Spectroscopy measurements were carried out.

The undoped ZnO films were grown for different growth time (3h, 5h, 7h, 9h, and 24h) at 90℃ to analyze the growth time effect on the films' characteristics. According to XRD results, the films for all growth time showed polycrystalline and hexagonal wurtzite structure. The peak intensities of preferred (101) growth planes in all the films are 6529, 8614, 8809, 11909 and 4221 for 3 h, 5 h, 7 h, 9 h, and 24 h growth times, respectively. The FWHM, crystallite size, dislocation density and microstrain values for 9h were calculated as 0.2421, 34.5186nm, $0.000839nm^{-2}$ and $1.004x10^{-3}$, respectively. With the SEM imaging, it was observed that, all films consist of ZnO hexagonal nanorods which have flower-like branched structures. High homogeneity, uniformity and well adhesion to substrate was observed for 9h growth time. In the PL spectroscopy, emission bands observed at 422, 448, 460 486, 532, 544, 563, 580 and 820nm wavelengths which are related oxygen vacancy and interstitial defects. The lowest PL intensity at visible region was shown for 9h. Therefore, lowest defect and highest crystallization quality were obtained for 9h growth time. Finally, from the UV-VIS spectroscopy, absorption peak was seen at around 381nm, energy band gap (Eg) values of ZnO thin films were found as 3.32, 3.36, 3.31, 3.29 and 3. 28eV for 3h, 5h, 7h, 9h and 24h, growth times respectively. The decreasing in energy band gap was associated with the increasing grain size and decreasing carrier concentration of the films. The refractive index and static dielectric

constant of the films are 2.388, 2.381, 2.390, 2.393, 2.395 and 8.29, 8.17, 8.32, 8.38, 8.41, for 3h, 5h, 7h, 9h and 24h, growth times, respectively.

ZnO films were doped with different indium percentages (1% 3%, 5% and 7%) at 90℃ for 9h to analyze the doping effect on the films' characteristics. The XRD peak intensities of preferred (101) growth planes in all the films are 9563, 9119, 7753, and 7354 for 1%, 3%, 5% and %7 In doping percentages, respectively. Although 1% IZO film has highest XRD peak intensity, its SEM image showed that 3% IZO has better uniformity and well adhesion. Also, PL spectra proved that, 3% IZO film has less defect and better crystallization than 1% IZO film. FWHM, crystallite size, dislocation density and microstrain values of 3% IZO were found as 0.2345, 35.6403nm, 0.000787nm $^{-2}$ and 0.972 x10^{-3}, respectively. From the SEM imaging it was reached that, the indium doping caused a morphological change on the ZnO rods and pipette like formation occurred at the end of rods. It was thought that, this morphological change is due to In^{+3} ions which hider the growth of {0 0 0 1} plane. In the PL characterization the lowest intensity in the visible range was observed for 3% IZO which represents the lowest defect and higher crystallization. From the UV-VIS spectrum, the absorption peaks were found around 380 nm for all doping percentage of IZO films. The energy band gap (Eg) values of IZO thin films were calculated as 3.41, 3.45, 3.49 and 3.47 eV for percentage of 1%, 3%, 5%, and 7% IZO films, respectively. The refractive index values were calculated as 2.372, 2.365, 2.358, 2.361 and the static dielectric constant were calculated as 8.01, 7.89, 7.77, 7.83 for 1% 3%, 5%, 7% doped IZO films.

To investigate the growth temperature effect, 5% In doped IZO films were grown at 90℃, 120℃ and 150℃. The predominantly preferred growth orientation for each growth temperatures was been along the (100) plane and the peak intensities at this plane are 22691, 3928 and 1451 for 90℃, 120℃ and 150℃ growth temperatures, respectively. An extra peak appeared at 2θ = 22,24 and 22,16 for 120℃ and 150℃ growth temperatures, respectively. It was thought that these extra peaks because of the formation of new In(OH)3 phase. This phase became due to the In^{+3} ions remained as separate phase and undoped into ZnO structures. The lowest FWHM, crystallite size, dislocation density and microstrain values were obtained at the IZO thin film which grown at 90℃ growth

temperature which are 0.2231, 37.0031nm, 0.000730nm^{-2} and 0.936 x10^{-3}, respectively. The highest XRD peak intensity and crystallite size were observed at this temperature. In the PL characterization, UV emission peak was observed at around 380 nm for 90℃, 120℃ and 150℃ growth temperature of IZO films and a broad emission bands obtained at between 400 – 550nm range. With the increasing growth temperature, IUV/ IDLE values decreased gradually. The highest IUV/ IDLE value was observed for 90℃. At UV-Vis spectroscopy absorption peaks were found around 380 nm for different temperatures. The obtained energy band gap (Eg) values of thin films were calculated as 3.50, 3.52 and 3.51eV for different growth temperature that 90℃, 120℃ and 150℃, respectively. While the refractive index values are 2.372, 2.365, 2.358, the static dielectric constants were calculated as 7.74, 7.67, 7.70 for the 90℃, 120℃ and 150℃ growth temperature, respectively.

As a result, for this work, 9 h growth time, 90 ℃ growth temperature and % 3 In doping concentration were defined as the optimal growth parameters. The thin films showed highest crystallization and good crystal quality when these parameters used for growth of ZnO and IZO film by hydrothermal method.

The produced and optimal growth parameters determined ZnO and IZO films can be used in optoelectronic applications with further developments. Films were produced by low cost and less energy consumed hydrothermal method which allows to modify and control the properties of films. Due to advantageous properties of hydrothermal method, it can be available for industry. Also, indium doped ZnO can be alternative material to transparent electrodes which currently made from tin doped indium oxide (ITO). Thank to IZO films, consumption of the expensive element indium can be decreased and the utilization of cheap and abundant ZnO can be extended.

FUTURE STUDIES

- Detailed characterization of microstructures and optical properties of IZO film.

- Investigating the effects of the other hydrothermal parameters;
  -Precursor concentration
  -PH effect

- Applications of the IZO thin films onto devices;
  -Display and lighting devices
  -Gas sensors

REFERENCES

[1] Lee, J.-H., & Park, B.-O., "Transparent Conducting ZnO:Al, In and Sn Thin Films Deposited by The Sol–gel Method", Thin Solid Films, 426(1-2), 94–99, 2003.

[2] Kahraman, S., Çakmak, H. M., Çetinkaya, S., Bayansal, F., Çetinkara, H. A., & Güder, H. S., "Characteristics of ZnO thin films doped by various elements", Journal of Crystal Growth, 363, 86–92, 2013.

[3] Ozgur, U., Alivov, Y. I., Liu, C., Teke, A., Reshchikov, M. A., Dogan, S., Avrutin, V., Cho, S. J., Morkoc, H., "A Comprehensive Review of ZnO Materials and Devices", Journal of Applied Physics, 98, 041301, 2005.

[4] Özgür, Ü., Avrutin, V., & Morkoç, H., "Molecular Beam Epitaxy (2nd Edition), Zinc Oxide Materials and Devices Grown by Molecular Beam Epitaxy", pp. 343-375, Oxford, Elsevier, 2018.

[5] Xu, L., Zheng, G., Xian, F., Su, J., "The Morphological Evolution of ZnO Thin Films by Sn ions Doping and Its Influence on The Surface Energy and Photocatalytic Activity", Mater. Chem. Phys, 229, pp. 215–225, 2019.

[6] Shinde, S.S., Shinde, P.S., Oh, Y.W., Haranath, D., Bhosale, C.H., Rajpure, K.Y., "Structural Optoelectronic, Luminescence and Thermal Properties of Ga-doped Zinc Oxide Thin Films", Appl. Surf. Sci, 258, 9969–9976, 2012.

[7] Kuo, S., Chen, W., Lai, F., Cheng, C., Kuo, H., Wang, S. and Hsieh, W., "Effects of Doping Concentration and Annealing Temperature on Properties of Highly-Oriented Al-Doped ZnO Films", Journal of Crystal Growth, 287, 78-84, 2006.

[8] Bouderbala, M., Hamzaoui, S., Amrani, B., Reshak, A. H., Adnane, M., Sahraoui, T. and Zerdali, M., "Thickness Dependence of Structural, Electrical and Optical Behaviour of Undoped ZnO Thin Films", Physica B, 403, 3326–3330, 2008.

[9] Huang, J., Li, B., Hu, Y., Zhou, X., Zhang, Z., Ma, Y., Tang, K., Wang, L., Lu, Y., "Transparent p-NiO/n-ZnO Heterojunction Ultraviolet Photodetectors Prepared on Flexible Substrates", Surf. Coat. Technol. 362, 57–61, 2019.

[10] Wu, D., Wang, Y., Ma, N., Cao, K, Zhang, W., Chen, J., Wang, D., Gao, Z., Xu, F., Jiang, K., "Single-crystal-like ZnO Mesoporous Spheres Derived from Metal Organic Framework Delivering High Electron Mobility for Enhanced Energy Conversion and Storage Performance", Electrochimica Acta, 305, 474-483, 2019.

[11] Ginley, D. S., Hosono, H., & Paine, D.C., "Handbook of Transparent Conductors", Springer, New York, 2010.

[12] Muchuweni, E., Sathiaraj, T. S., & Nyakotyo, H., "Synthesis and Characterization of Zinc Oxide Thin Films For Optoelectronic Applications", Heliyon, 3(4), e00285, 2017.

[13] Muchuweni, E., Sathiaraj, T. S., & Nyakotyo, H., "Physical Properties of Gallium and Aluminium co-doped Zinc oxide Thin films Deposited at Different Radio Frequency Magnetron Sputtering Power", Ceram. Int. 42, 17706–17710, 2016.

[14] Cooray, N. F., Kushiya, K., Fujimaki, A., Sugiyama, I., Miura, T., Okumura, D., … Yamase, O., "Large Area ZnO Films Optimized for Graded band-gap Cu(InGa)Se2 Based Thin film mini modules", Solar Energy Materials and Solar Cells, 49(1-4), 291–297, 1997.

[15] Nunes, P., Fortunato, E., Tonello, P., Braz Fernandes, F., Vilarinhob, P. and Martins, R., "Effect of Different Dopant Elements on The Properties of ZnO Thin Films", Vacuum. 64, 281–285, 2002.

[16] Xu, Z.Q., Deng, H., Li, Y., Guo, Q.H., Li, Y.R., "Characteristics of Al-doped C-Axis Orientation ZnO Thin Films Prepared by The Sol-Gel Method", Materials Research Bulletin, 41, 354–358, 2006.

[17] Gümüş, C., Özkendir, O.M., Kavak, H., Ufuktepe, Y., "Structural and Optical Properties of Zinc Oxide Thin Films Prepared by Sprey Pyrolysis Method", Journal of Optoelectronics and Advenced Materials, 8, 299-303, 2006.

[18] Suvaci, E. and Özer, G.Ö., "Processing of Textured Zincoxide Varistors via Templated Grain Growth", Journal of the European Ceramic Society, 25, 1663–1673, 2005.

[19] Saito, N., Haneda, H., Sekiguchi, T., Ohashi, N., Sakaguchi, I. and Koumoto, K., "Low-Temperature Fabrication of Light-Emitting Zinc Oxide Micropatterns Using Self-Assembled Monolayers", Advanced Materials, 14, 418–421, 2002.

[20] Huang, M.H., Mao, S., Feick, H., Yan, H., Wu, Y., Kind, H., Weber, E., Russo, R. and Yang, P., "Room-Temperature Ultraviolet Nanowire Nanolasers", Science, 292 (5523), 1897 – 1899, 2001.

[21] Lampert, C. M., "Heat Mirror Coatings for Energy Conserving Windows", Solar Energy Materials, 6(1), 1–4, 1981.

[22] Dayan, N. J., Sainkar, S., Karekar, R., & Aiyer, R., "Formulation and Characterization of ZnO:Sb Thick-film Gas Sensors", Thin Solid Films, 325(1-2), 254–258, 1998.

[23] Yoshino, Y., Makino, T., Katayama, Y., & Hata, T., "Optimization of Zinc Oxide Thin Film for Surface Acoustic Wave Filters by Radio Frequency Sputtering", Vacuum, 59(2-3), 538–545, 2000.

[24] Edwards, P P., Porch, A., Jones, M. O., Morgan, D. V., & Perks, R .M., "Basic Materials Physics of Transparent Conducting Oxides", Dalton Transaction, 19, 2995–3002, 2004.

[25] Sugumaran, S., Ahmad, M. N. B., Jamlos, M. F., Bellan, C. S., Pattiyappan, S., Rajamani, R., & Sivaraman, R. K., "Transparent with Wide Band Gap InZnO Nano Thin Film: Preparation and Characterizations", Optical Materials, 49, 348–356, 2015.

[26] Fathollahi, V., & Amini, M. M., "Sol–gel Preparation of Highly Oriented Gallium-doped Zinc Oxide Thin Films", Materials Letters, 50(4), 235–239, 2001.

[27] Edinger, S., Bansal, N., Bauch, M., et. al, "Highly Transparent and Conductive Indium-doped Zinc oxide Films Deposited at Low Substrate Temperature by Spray Pyrolysis from Water-based Solutions", Journal of Materials Science, 52(14), 8591–8602, 2017.

[28] Kumar, P. M. R., Kartha, C. S., Vijayakumar, K. P., Abe, T., Kashiwaba, Y., Singh, F., & Avasthi, D. K., "On The Properties Of Indium Doped ZnO Thin Films", Semiconductor Science and Technology, 20(2), 120–126, 2004.

[29] Jagadish, C., Pearton, S., "Zinc Oxide Bulk, Thin Films and Nanostructures: Processing, Properties, and Applications", Elsevier Science, Hong Kong, 2006.

[30] Banerjee, S. K., and Streetman, B. G., "Solid State Electronic Devices (6th Edition)", Phi Learning, New Delhi, 2009.

[31] Escobedo Morales, A., Herrera Zaldivar, M., & Pal, U., "Indium Doping in Nanostructured ZnO Through Low-Temperature Hydrothermal Process", Optical Materials, 29(1), 100-104, 2006.

[32] Morkoc, H., & Özgür, Ü., "Zinc Oxide: Fundamentals, Materials and Device Technology", Wiley-VCH, Weinheim, 2009.

[33] Jie, J., Wang, G., Han, X., Yu, Q., Liao, Y., Li, G., Hou, J.G., "Indium-Doped Zinc Oxide Nanobelts", Chem. Phys. Lett. 387, 466–470, 2004.

[34] Xu, L., Su, Y., Chen, Y., Xiao, H., Zhu, L., Zhou, Q., Li, S., "Synthesis and Characterization of Indium-Doped ZnO Nanowires with Periodical Single-Twin Structures", J. Phys. Chem. B. 110, 6637–6642, 2006.

[35] Liu, J., Zhang, Y., Qi, J., Huang, Y., Zhang, X., Liao, Q., "In-Doped Zinc Oxide Dodecagonal Nanometer Thick Disks", Mater. Lett. 60, 2623–2626, 2006.

[36] Pál, E., Hornok, V., Oszkó, A., & Dékány, I., "Hydrothermal Synthesis of Prism-Like And Flower-Like ZnO And Indium-Doped ZnO Structures", Colloids and Surfaces A: Physicochemical and Engineering Aspects, 340(1-3), 1–9, 2009.

[37] Jilani, A., Abdel-wahab, M. S., & Hammad, A. H., "Advance Deposition Techniques for Thin Film and Coating, Modern Technologies for Creating the Thin-Film Systems and Coatings", InTech, pp.137-149, 2017.

[38] Martin, P.M., "Handbook of Deposition Technologies for Films and Coatings (3rd Edition)", William Andrew Publishing, USA, pp. 1-31, 2010.

[39] Purica, M., "Optical And Structural Investigation of ZnO Thin Films Prepared by Chemical Vapor Deposition (CVD)", Thin Solid Films, 403-404, 485–488, 2002.

[40] Kaflé, B. P., "Chemical Analysis and Material Characterization by Spectrophotometry", Elsevier, pp.156, 2019.

[41] Singh, T. R. R., Mcmillan, H., Mooney, K., Alkilani, A. Z., & Donnelly, R. F., "Microneedles for Drug Delivery and Monitoring", Microfluidic Devices for Biomedical Applications, Woodhead Publishing, pp. 185-230, 2013.

[42] Rossnagel, S. M., "Thin film Deposition with Physical Vapor Deposition And Related Technologies", Journal of Vacuum Science & Technology A: Vacuum, Surfaces, and Films, 21(5), S74–S87, 2003.

[43] Gonçalves, R.S., Barrozo, P., Brito, G.L., Viana, B.C., Cunha, F., "The Effect of Thickness on Optical, Structural and Growth Mechanism of ZnO Thin Film Prepared By Magnetron Sputtering", Thin Solid Films 661, 40–45, 2018.

[44] Selloum, D., Henni, A., Karar, A., Tabchouche, A., Harfouche, N., Bacha, O., Tingry, S., Rosei, F., "Effects of Fe Concentration on Properties of ZnO Nanostructures and Their Application to Photocurrent Generation", Solid State Sci., 92, 76–80, 2019.

[45] Fernandez, L., Alkan, G., Milosevic, O., Rabanal, M.E., Friedrich, B., "Synthesis and Characterisation of Spherical Core-Shell Ag/ZnO Nanocomposites Using

Single and Two Steps Ultrasonic Spray Pyrolysis (USP)", Catal. Today 321–322, 26–33, 2019.

[46] Kennedy, O.W., Coke, M.L., White, E.R., Shaffer, M.S.P., Warburton, P.A., "MBE Growth and Morphology Control of ZnO Nanobelts with Polar Axis Perpendicular to Growth Direction", Mater. Lett, 212, 51–53, 2018.

[47] Kumar Sharma, H., Archana, R., Sankar ganesh, R., Pal Singh, B., Ponnusamy, S., Hayakawa, Y., Muthamizhchelvan, C., Raji, P et all., "Substitution of Al+3 to Zn+2 sites of ZnO Enhanced The Photocatalytic Degradation of Methylene Blue Under Irradiation of Visible Light", Solid State Science, 94, 45-53, 2019.

[48] Ivanova, T., Harizanova, A., Koutzarova, T., Vertruyen, B., "Optical Characterization of Sol–gel ZnO:Al Thin Films", Superlattice Microstruct. 85, 101–111, 2015.

[49] Hachigo, A., Nakahata, H., Higaki, K., Fujii, S., & Shikata, S., "Heteroepitaxial Growth of ZnO Films on Diamond (111) Plane by Magnetron Sputtering", Applied Physics Letters, 65(20), 2556–2558, 1994.

[50] Tiku, S. K., Lau, C. K., and Lakin, K. M., "Chemical Vapor Deposition of ZnO Epitaxial Films on Sapppire", Applied Physics Letters, 36, 4, 1980.

[51] Kim, K.-K., Song, J.-H., Jung, H.-J., Choi, W.-K., Park, S.-J., & Song, J.-H., The "Grain Size Effects on The Photoluminescence of ZnO/α-Al2O3 Grown by Radio-Frequency Magnetron Sputtering", Journal of Applied Physics, 87(7), 3573–3575, 2000.

[52] Fons, P., Iwata, K., Niki, S., Yamada, A., & Matsubara, K., "Growth of High-Quality Epitaxial ZnO Films on α-Al2O3", Journal of Crystal Growth, 201-202, 627–632, 1999.

[53] Vispute, R. D., Talyansky, V., Choopun, S., Sharma, R. P., Venkatesan, T., He, M., … Jones, K. A., "Heteroepitaxy of ZnO on GaN and Its Implications For Fabrication Of Hybrid Optoelectronic Devices", Applied Physics Letters, 73(3), 348–350, 1998.

[54] Liu, Y., Gorla, C. R., Liang, S., Emanetoglu, N., Lu, Y., Shen, H., & Wraback, M., "Ultraviolet Detectors Based on Epitaxial ZnO Films Grown by MOCVD", Journal of Electronic Materials, 29(1), 69–74, 2000.

[55] Byrappa, K., & Yoshimura, M., "Handbook of Hydrothermal Technology (2nd Edition)", Chapter 10, William Andrew, pp.617-737, 2012.

[56] Feng, S.H., & Li, G.H., "Hydrothermal and Solvothermal Syntheses Modern Inorganic, Synthetic Chemistry (2nd Edition)", Elseiver, pp73-104, 2017.

[57] Ay, B., "Dikarboksilik Asit Grupları İçeren Geçiş Metal Komplekslerinin Hidrotermal Sentezi, UV Etkileşimlerinin ve Katalitik Aktivitelerinin İncelenmesi", Thesis (Msc), Çukurova Üniversitesi Fen Bilimleri, 2011.

[58] Byrappa, K., Yoshimura, M., "Handbook of Hydrothermal Technology, A Technology for Crystal Growth and Materials Processing", William Andrew , New Jersey, 2001.

[59] Laudise, R.A., "The Growth of Single Crystals, Prentice-Hall", Englewood Cliffs, NJ, pp. 261-265, 1970.

[60] Rabenau, A., "The Role Hydrothermal Synthesis in Preparative Chemistry", Angew. Chem. Int. Eng. Ed., 24(12), 1026-1040, 1985.

[61] Byrappa, K., "Hydrothermal Growth of Crystals", Pergamon Press, Oxford, UK, pp. 1–365, 1992.

[62] Yoshimura, M., Suda, H., "Hydrothermal Processing of Hydroxyapatite: Past,Present and Future, in: Hydroxyapatite and Related Materials", P.W. Brown and B. Constanz,Eds., CRC Press, pp. 45-72, 1994.

[63] Vayssieres, L., "Growth of Arrayed Nanorods and Nanowires of ZnO from Aqueous Solutions", Advanced Materials, 15(5), 464–466, 2003.

[64] Kim, Y.J., Lee, C-H., Hong, Y.J., Yi, G-C., Kim, S.S., and Cheong H., "Controlled Selective Growth of ZnO Nanorod And Microrod Arrays on Si Substrates by a Wet Chemical Method", Appl. Phys. Lett. 89, 163128, 2006.

[65] Yuhas, B.D., Zitoun, D.O., Pauzauskie, P.J., He, R., &Yang, P., "Transition-metal-doped Zinc Oxide Nanowires", Angew. Chem. Int. Ed., 45, 420, 2006.

[66] Gao, P-X., Liu, J., Buchine, B.A., Weintraub, B., Wang, Z.L., and Lee, J.L., "Bridged ZnO Nanowires Across Trenched Electrodes", Appl. Phys. Lett, 91, 142108, 2007.

[67] Schäf, O., Ghobarkar, H., Knauth, P., "Hydrothermal Synthesis of Nanomaterials. In: Knauth P., Schoonman J. (eds) Nanostructured Materials", Electronic Materials: Science & Technology, vol 8. Springer, Boston, MA, 2004.

[68] Knauth, P., & Schoonman, J., "Nanostructured Materials: Selected Synthesis Methods Properties and Applications", Kluwer, Boston, pp 23-41, 2002.

[69] Yoshimura, M., & Byrappa, K., "Hydrothermal Processing of Materials: Past, Present and Future", Journal of Materials Science, 43(7), 2085–2103, 2007.

[70] Byrappa, K., "Hydrothermal Processing of Advance Materials", Kirk-Othmer Encyclopedia of Chemical Technology, John Wiley & Sons, London, 2005.

[71] Morita, T., Wagatsuma, Y., Cho, Y., Morioka, H. et al., "Ferroelectric Properties Of An Epitaxial Lead Zirconate Titanate Thin Film Deposited By A Hydrothermal Method Below The Curie temperature", Applied Physics Letters, 84(25), 5094–5096, 2004.

[72] Byrappa, K., & Yoshimura, M., "Handbook of Hydrothermal Technology (2nd Edition)", Chapter 1, William Andrew, pp.1-49, 2012.

[73] Navaneethan, M., Archana, J., Arivanandhan, M., & Hayakawa, Y., Functional "Properties of Amine-Passivated ZnO Nanostructures and Dye-Sensitized Solar Cell Characteristics", Chemical Engineering Journal, 213, 70–77, 2012.

[74] Navaneethan, M., Nisha, K. D., Ponnusamy, S., & Muthamizhchelvan, C., "Optical and Surface Morphological Properties of Triethylamine Passivated Lead Sulphide Nanoparticles", Materials Chemistry and Physics, 117(2-3), 443–447, 2009.

[75] Nose, K., Fujita, H., Omata, T., Otsuka-Yao-Matsuo, S., Nakamura, H., & Maeda, H., "Chemical Role of Amines In The Colloidal Synthesis of Cdse Quantum Dots and Their Luminescence Properties", Journal of Luminescence, 126(1), 21–26, 2007.

[76] Rahman, M. Y. A., Umar, A. A., Roza, L., & Salleh, M. M., "Effect of Hexamethylenetetramines (HMT) Surfactant Concentration on the Performance of TiO2 Nanostructure Photoelectrochemical Cells", Russian Journal of Electrochemistry, 50(10), 974–980, 2014.

[77] Narayanan, G. N., & Annamalai, K., "Role of Hexamethylenetetramine Concentration on Structural, Morphological, Optical and Electrical Properties of Hydrothermally Grown Zinc Oxide Nanorods", Journal of Materials Sci. Mat. in Elec., 27(11), 12209-12215, 2016.

[78] Byrappa, K., Yoshimura, M., "Handbook of Hydrothermal Technology (2nd Edition)", William Andrew Publishing, Chapter 3, pp. 75-137, 2013.

[79] Yoshitake, M., "Nanocrystals. InTech", Rijeka. pp.33-34, 2010.

[80] Khachatryan, H., Lee, S.-N., Kim, K.-B., Kim, H.-K., & Kim, M., "Al Thin Film: The Effect of Substrate Type on Al Film Formation and Morphology", Journal of Physics and Chemistry of Solids, 122, 109–117, 2018.

[81] Guo, M., Diao, P., & Cai, S., "Hydrothermal Growth of Well-Aligned ZnO Nanorod Arrays: Dependence Of Morphology and Alignment Ordering Upon Preparing Conditions", Journal of Solid State Chemistry, 178(6), 1864–1873, 2005.

[82] Zhao, X., Lee, J. Y., Kim, C.-R., Heo, J., Shin, C. M., Leem, J.-Y et al., "Dependence of The Properties of Hydrothermally Grown ZnO on Precursor Concentration", Physica E: Low-Dimensional Systems and Nanostructures, 41(8), 1423–1426, 2009.

[83] Mahmood, M. A., Jan, S., Shah, I. A., & Khan, I., "Growth Parameters for Films of Hydrothermally Synthesized One-Dimensional Nanocrystals of Zinc Oxide", International Journal of Photoenergy, 1–12, 2016.

[84] Le, H. Q., Chua, S. J., Koh, Y. W., Loh, K. P., and Fitzgerald, E. A., "Systematic Studies of The Epitaxial Growth Of Single-Crystal ZnO Nanorods on Gan Using Hydrothermal Synthesis", Journal of Crystal Growth, 293(1), pp. 36–42, 2006.

[85] Li, Q., Bian, J., Sun, J., Wang, J., Luo, Y., Sun, K., & Yu, D., "Controllable Growth of Well-Aligned ZnO Nanorod Arrays By Low-Temperature Wet Chemical Bath Deposition Method", Applied Surface Science, 256(6), 1698–1702, 2010.

[86] Wang, S.-F., Tseng, T.-Y. ,. Wang, Y.-R., Wang, C.-Y., Lu, H.-C., & Shih, W.-L., "Effects of Preparation Conditions on the Growth of ZnO Nanorod Arrays Using Aqueous Solution Method", Int. Jurnal of Applied Ceramic Technology, 5 (5), 419–429, 2008.

[87] Lee, K. M., Park, K. H., et al., "Synthesis of High Quality ZnO Nanorods by Low Temperature Wet Chemical Process", 2nd IEEE International Conference on Nano/Micro Engineered and Molecular Systems (IEEE NEMS '07), Bankok, pp. 775-778, 2007.

[88] Xu, S., Lao, C., Weintraub, B., & Wang, Z. L., "Density-controlled Growth of Aligned ZnO Nanowire Arrays by Seedles Chemical Approach on Smooth Surfaces", Journal of Materials Research, 23(8), 2072–2077, 2008.

[89] Akhiruddin, M., Sugianto, S., & Irmansyah, I., "The Influence of Hydrothermal Duration on Structures and Optical Properties of ZnO Nanoparticles", Journal of Materials Physics and Chemistry, 2(2), 34-37, 2014.

[90] Baruah, S., and Dutta, J., “PH-Dependent Growth of Zinc Oxide Nanorods”, Journal of Crystal Growth, 311 (8), 2549– 2554, 2009.

[91] Pei, L.Z., Zhao, H.S., Tan W., et al., “Hydrothermal Oxidization Preparation of ZnO Nanorods on Zinc Substrate”, Physica E:Low-Dimensional Systems and Nanostructures, 42(5), 1333–1337, 2010.

[92] Polsongkram, D., Chamninok, P., Pukird, S., Chow, L., Lupan, O., Chai, G., … Schulte, A., “Effect of Synthesis Conditions on the Growth of ZnO Nanorods via Hydrothermal Method”, Physica B: Condensed Matter, 403(19-20), 3713–3717, 2008.

[93] Tang, L., Bao, X-B, Zhou, H., & Yuan, A. H., “Synthesis and Characterization of ZnO Nanorods by a Simple Single -Source Hydrothermal Method”, Physica E: Low-Dimensional Systems and Nanostructures, 40(4), 924–928, 2008.

[94] Li, F, Hu, L., Li, Z., & Huang, Z., “Influence of Temperature on the Morphology and Luminescence of ZnO Micro and Nanostructures Prepared by CTAB-assisted Hydrothermal Method”, Journal of Alloys and Compounds, 465(1-2), L14–L19, 2008.

[95] Wahab, R., Ansari, S.G., Seo, H-K., Kim, Y.S., Suh, E.K., & Shin, H-S., “Low Temperature Synthesis and Characterization of Rosette-like Nanostructures of ZnO Using Solution Process”, Solid State Sciences, 11(2) ,439–443, 2009.

[96] Alshehri, N. A., Lewis, A. R., Pleydell-Pearce, C., & Maffeis, T. G. G., “Investigation of The Growth Parameters of Hydrothermal ZnO Nanowires for Scale up Applications”, Journal of Saudi Chemical Society, 22(5), 538–545, 2018.

[97] Kumaresan, N., Ramamurthi, K., Ramesh Babu, R., Sethuraman, K., & Moorthy Babu, S., “Hydrothermally Grown ZnO Nanoparticles for Effective Photocatalytic Activity”, Applied Surface Science, 418, 138–146, 2017.

[98] Ellmer, K., & Bikowski, A., “Intrinsic and Extrinsic Doping of ZnO and ZnO Alloys”, Journal of Physics D: Applied Physics, 49(41), 413002, 2016.

[99] Xu, L., Wang, X., Qian, L., Zhu, Y., Luo, X., Wang, W., … Xu, J., “The Dependence of The Optical Properties of ZnO Nanorod Arrays on Their Growth Time”, Optik, 202, 163634, 2020.

[100] Wang, B., Callahan, M. J., Xu, C., Bouthillette, L. O., Giles, N. C., & Bliss, D. F. “Hydrothermal Growth and Characterization of Indium-doped-conducting ZnO Crystals”, Journal of Crystal Growth, 304(1), 73–79, 2007.

[101] Guohong, C., “Nanostructures and Nanomaterials”, World Scientific Publishing Company, Singapore, 2004.

[102] Vashista, M., & Paul, S., “Correlation Between Full Width at Half Maximum (FWHM) of XRD Peak With Residual Stress On Ground Surfaces”, Philosophical Magazine, 92(33), 4194–4204, 2012.

[103] Bushroa, A. R., Rahbari, R. G., Masjuki, H. H., & Muhamad, M. R., “Approximation of Crystallite Size and Microstrain via XRD Line Broadening Analysis in TiSiN thin films”, Vacuum, 86(8), 1107–1112, 2012.

[104] Ashraf, M., Akhtar, S. M. J., Khan, A. F., Ali, Z., & Qayyum, A., “Effect of Annealing on Structural and Optoelectronic Properties of Nanostructured ZnSe Thin Films”, Journal of Alloys and Compounds, 509(5), 2414–2419, 2011.

[105] Mohamad Zaidi, U. Z., Bushroa, A. R., Ghahnavyeh, R. R., & Mahmoodian, R., Crystallite Size and Microstrain: XRD Line Broadening Analysis of AgSiN Thin Films”, Pigment & Resin Technology, 48 (6), 473-480, 2019.

[106] Yıldırım, M. A., Ates A., “Influence of Films Thickness and Structure on The Photo-Response of ZnO Films”, Optics Communications, 283(7), 1370-1377, 2010.

[107] Callister, W.D., “Materials Science and Engineering: An Introduction”, John Wiley and Sons, New York, 1997.

[108] Saleem, M., Fang, L., Ruan, H.B., Wu, F., Huang, Q.L., Xu, C.L., Kong, C.Y, “Effect of Zinc Acetate Concentration On The Structural and Optical Properties of ZnO Thin Films Deposited By Sol-Gel Method”, Intl. J. Phy. Sci. 7(23), 2971–2979, 2012.

[109] Suryanarayana, C., Norton, M.G., “X-ray Diffraction: A Practical Approach”, Plenum Press Publishing, New York, 1998.

[110] Kim, J.M., & Chung, H.T, “Electrochemical Characteristics of Orthorhombic LiMnO2 with Different Degrees of Stacking Faults”, Journal of Power Sources, 115 (1), 125-130, 2003.

[111] Tung, H. M., Huang, J. H., Tsai, D. G., Ai, C. F., Yu, G. P., “Hardness and Residual Stress in Nanocrystalline ZrN films: Effect of Bias Voltage and Heat Treatment”, Mater. Sci. Eng. A, 500(1–2), 104–108, 2009.

[112] Rai, S., Choudhary, B.K., Jayakumar, T.,. Rao K.B.S., & Raj, B., "Characterization of Low Cycle Fatigue Damage in 9Cr–1Mo Ferritic Steel Using X-ray Diffraction Technique", Int. J. Pres. Ves. Pip. 76 (5), 275-281,1999.

[113] Bindu, P., & Thomas, S., "Estimation of Lattice Strain in ZnO Nanoparticles: X-ray Peak Profile Analysis", Journal of Theoretical and Applied Physics, 8(4), 123–134, 2014.

[114] Dulgheru (Nedelcu), N., Anastasescu, et al., "Surface Topography And Optical Properties of Ge-Sb(As)-S-Te Thin Films By Atomic-Force Microscopy and Variable Angle Spectroscopic Ellipsometry", Journal of Physics: Conference Series, 356, 012019, 2012.

[115] Narayanan, N., Deepak, N.K., "Realizing Luminescent Downshifting in ZnO Thin Films by Ce Doping with Enhancement of Photocatalytic Activity", Solid State Sci. 78, 144–155, 2018.

[116] Bagnall, D. M., Chen, Y.F., Zhu, Z., & Yao, Y., "Optically Pumped Lasing of ZnO at Room Temperature", Appl. Phys. Lett. 70, 2230,1997.

[117] Choi, B. K., Chang, D. H., Yoon, Y. S., & Kang, S. J., "Optical Characterization of ZnO Thin Films Deposited by Sol-gel Method", J. Mater. Sci. 17, 1011–1015, 2006.

[118] Wan, X., Liang, X., Zhang, C., Li, X., Liang, W., Xu, H., Lan, S., Tie, S., "Morphology Controlled Syntheses of Cu-doped ZnO, Tubular Zn(Cu)O and Ag Decorated Tubular Zn(Cu)O Microcrystals For Photocatalysis", Chem. Eng. J., 272, 58–68, 2015.

[119] Sahu, D., Panda, N., Acharya, B., "Effect of Gd Doping on Structure and Photoluminescence Properties of ZnO nanocrystals", Mater. Res. Express 4 (11), 114001, 2017.

[120] Lai, Y.L., Meng, M., Yu, Y.F., Wang, X.T., "Photoluminescence and Photocatalysis of the Flower-Like Nano-ZnO Photocatalysts Prepared by a Facile Hydrothermal Method with or without Ultrasonic Assistance", Appl.Catal.B-Environ., 105(3-4), 335-345, 2011.

[121] Zeng, H., Duan, G., Li, Y., Yang, S., Xu, X., Cai, W., "Blue Luminescence of ZnO Nanoparticles Based on Non-Equilibrium Processes: Defect Origins and Emission Controls", Adv.Funct.Mater. 20(4), 561, 2010.

[122] Djurišić, A. B., Choy, W. C. H., Roy, V. A. L., Leung, Y. H., Kwong, C. Y., Cheah, K. W., … Surya, C., "Photoluminescence and Electron Paramagnetic Resonance

of ZnO Tetrapod Structures. Advanced Functional Materials", 14(9), 856–864, 2004.

[123] Wang, Y., Hou, Z., Guo, H., Shen, L., Wang, G., Cui, F., Zhang, Q., "Preparation of ZnO Nanorods via Aqueous Solution Process and Their PL Properties", Materials Letters, 91, 107-110, 2013.

[124] Amari, R., Mahroug, A., Boukhari, A., Deghfel, B., Selmi, N., "Structural, Optical and Luminescence Properties of ZnO Thin Films Prepared by Sol-Gel Spin-Coating Method: Effect of Precursor Concentration", Chin. Phys. Lett. 35(1), 016801, 2018.

[125] Liqiang, J., Yichun, Q., Baiqi, W., et al., "Review of Photoluminescence Performance of nano-Sized Semiconductor Materials and Its Relationships with Photocatalytic Activity", Solar Energy Materials and Solar Cells, 90(12), 1773–1787, 2006.

[126] Virk, H. S., "Nanomaterials: Basic Concepts and Applications", Trans Tech Pubn, Pfaffikon, pp.20-21, 2015.

[127] Thomas, S., Didier, R., Ponnamma, D., "Spectroscopy of Polymer Nanocomposites", William Andrew Publushing, Oxford, pp. 130-157, 2016.

[128] Tauc, J., Grigorovici, R., Vancu, A., "Optical Properties and Electronic Structure of Amorphous Germanium", Phys. Status Solid, 15, 627–637, 1966.

[129] Holi, A.M., Zainal, Z., et al., "Hydrothermal Deposition of CdS on Vertically Aligned ZnO Nanorods for Photoelectrochemical Solar Cell Application", J. Mater. Sci. Mater. Electron., 27, 7353–7360, 2016.

[130] Yıldırım, M. A., "The Effect of Copper Concentration on Structural, Optical and Dielectric Properties of CuxZn1 − xS Thin Films", Optics Communications, 285(6), 1215–1220, 2012.

[131] Rosencher, E., and Vinter, B., "Optoelectronics", Cambridge University Press, p. 304, 2002.

[132] Amin, G., Asif, M.H., Zainelabdin, A., Zaman, S., Nur, O., Willander, M., "Influence of pH, Precursor Concentration, Growth Time, And Temperature on The Morphology of ZnO Nanostructures Grown by the Hydrothermal Method", J. Nanomater, 5 (2011), 2011.

[133] Akaltun, Y., Yıldırım, M. A., Ates, A., Yıldırım, M., "The Relationship Between Refractive Index-Energy Gap and The Film Thickness Effect on The Characteristic Parameters of CdSe Thin Films", Opt. Commun. 284, 2307-2311, 2011.

[134] Hannachi, L., Bouarissa, N., "Band Parameters for Cadmium and Zinc Chalcogenide Compounds", Physica B: Condensed Matter, 404, 3650-3654, 2009.

[135] Mezrag, F., Mohamed, W.K., Bouarissa, N., "The Effect of Zinc Concentration Upon Optical and Dielectric Properties of Cd1-xZnxSe", Physica B, 405, 2272–2276, 2010.

[136] Herve, P., Vandamme, L.K.J., "General Relation Between Refractive Index and Energy Gap in Semiconductors", Infrared Phys. Technol., 35, 609-615, 1994.

[137] Hannachi, L., Bouarissa, N., "Band Parameters for Cadmium and Zinc Chalcogenide Compounds", Physica B 404, Pages 3650-3654, 2010.

[138] Adachi, S., "Properties of Group IV, III-V and II-VI Semiconductors", John Wiley & Sons, Ltd, Chishester, 2005.

[139] Boryorysiewicz, M.A., "ZnO as a Functional Material, A Review, Crystals", 9(10), 505, 2019.

[140] Wang H., Xie J., Yan K., Duan M., "Growth Mechanism of Different Morphologies of ZnO Crystals Prepared by Hydrothermal Method", J. Mater. Sci. Technol., 2011, 27, 153–158.

[141] Krasovska, M., Gerbreders, V., Sledevskis, E., Gerbreders, A., Mihailova, I., Tamanis, E., & Ogurcovs, A., "Hydrothermal Synthesis of ZnO Nanostructures with Controllable Morphology Change", Cryst. Eng. Comm, 22(8), 1346-1358 , 2020.

[142] Perillo, P. M., Atia, M. N., & Rodríguez, D. F., "Studies on the Growth Control of ZnO Nanostructures Synthesized by the Chemical Method", Matéria (Rio de Janeiro), 23(2), 2018.

[143] Guillemin, S., Rapenne, L., Roussel, H., Sargiannidou, E., Bremond, G., Consonni, V., "Formation Mechanisms of ZnO Nanowires: The Crucial Role of Crystal Orientation and Polarity", The Journal of Physical Chemistry C, 117(40), 20738-20745, 2013.

[144] Wahab, R., Kim, Y., Lee, K., & Shin, H., "Fabrication and Growth Mechanism of Hexagonal Zinc Oxide Nanorods via Solution Process", Journal of Materials Science 45(11), 2967-2973, 2010.

[145] Hafdallah, A., Yanineb, F., Aida, M. S., & Attaf, N., “In Doped ZnO Thin Films”, Journal of Alloys and Compounds, 509(26), 7267–7270, 2011.

[146] Ilıcan, S, Caglar, Y, Caglar, M, Demirci, B., “Polycrystalline Indium-doped ZnO Thin Films: Preparation And Characterization”, Journal of Optoelectronics and Advanced Materials 10 (10), 2592 – 2598, 2008.

[147] Shannon, R. D., “Revised Effective Ionic Radii and Systematic Studies of Interatomic Distances in Halides and Chalcogenides”, Acta Crystallographica Section A, 32(5), 751–767, 1976.

[148] Kim, D. L., Jeong, W. H., Kim, G. H., & Kim, H. J., “Solution-Processed Indium–Zinc Oxide With Carrier-Suppressing Additives”, Journal of Information Display, 13(3), 113–118, 2012.

[149] Yu, H., & Dong, Y., “Investigation of ZnO Nanostructures Synthesized From Different Zinc Salts”, ChemXpress, 9(1), 091-097, 2016.

[150] Prabhu, Y. T., Rao, K. V., Kumar, V. S. S., & Kumari, B. S., “Synthesis of ZnO Nanoparticles by a Novel Surfactant Assisted Amine Combustion Method”, Advances in Nanoparticles, 02(01), 45–50, 2013.

[151] Wasly, H. S., El-Sadek, M. S. A., & Henini, M., “Influence of Reaction Time And Synthesis Temperature on the Physical Properties of ZnO Nanoparticles Synthesized by the hydrothermal Method”, Applied Physics A, 124(1), 2018.

[152] Urgessa, Z. N., Talla, K., Dobson, S. R., Oluwafemi, O. S., Olivier, E. J., Neethling, J. H., & Botha, J. R., “Mechanisms of Self-assembly in Solution Grown ZnO Nanorods”, Materials Letters, 108, 280–284, 2013.

[153] Osali, S., Esfahani, H., Dabir, F., & Tajaslan, P., “Structural and Electro-Optical Properties of Electrospun Cu-Doped ZnO Thin Films”, Solid State Sciences, 98, 106038, 2019.

[154] Singh, A., & Vishwakarma, H. L., “Study of Structural, Morphological, Optical and Electroluminescent Properties of Undoped ZnO Nanorods Grown by a Simple Chemical Precipitation”, Materials Science-Poland, 33(4), 751–759, 2015.

[155] Tuyen, V., & Long, N., & Hoa, T., & Nghia, X., & Chi, H., Higashimine, K., “Indium-doped Zinc Oxide Nanometre Thick Disks Synthesised by a Vapour-Phase Transport Process”, Journal of Experimental Nanoscience, 4(3), 243-252, 2009.

[156] Akgun, M. C., Kalay, Y. E., & Unalan, H. E., "Hydrothermal Zinc Oxide Nanowire Growth Using Zinc Acetate Dihydrate Salt", Journal of Materials Research, 27(11), 1445–1451, 2012.

[157] Yoshida, M., Delgado, F., Lopez, W., Andrade, E., "Structure and Morphology of High Quality Indium-doped ZnO Films Obtained by Spray Pyrolysis", Thin Film Solids, 376 (1-2), 99-109, 2000.

[158] Paraguay, F., Morales, J., Estrada, L., Andrade, E., Yoshida, M., "Influence of Al, In, Cu, Fe and Sn Dopants in the Microstructure of Zinc Oxide Thin Films Obtained by Spray Pyrolysis", Thin Solid Films, 336, 16-17, 2000.

[159] Bae, S. Y., Na, C. W., Kang, J. H., & Park, J., "Comparative Structure and Optical Properties of Ga-, In-, and Sn-Doped ZnO Nanowires Synthesized via Thermal Evaporation", The Journal of Physical Chemistry B, 109(7), 2526–2531, 2005.

[160] Rusu, D., Rusu, G., & Luca. D., "Structural Characteristics and Optical Properties of Thermally Oxidized Zinc Films", Acta Physica Polonica A, 119 (6), 2011.

[161] Rusu, G., Rusu, D., & Apetroaei, N., "On The Structural Changes During Thermal Oxidation of Evaporated Zn Thin Films, Thin Solid Films", 515(24), 8699-8704, 2007.

[162] Yang, H., Yang, Z., Liang, H., Liu, L., Guo, J., & Yang, Y., "Solvothermal Synthesis of In(OH)3 Nanorods and Their Conversion to In2O3", Materials Letters, 64(13), 1418–1420, 2010.

[163] Chen, L.-Y., & Zhang, Z.-D., "Biomolecule-Assisted Synthesis of In(OH)3 Hollow Spherical Nanostructures Constructed with Well-Aligned Nanocubes and Their Conversion into C−In2O3", The Journal of Physical Chemistry C, 112(48), 18798–18803, 2008.

[164] Yuan, W., Lu, Z., & Li, C. M., "Self-assembling Microsized Materials To Fabricate Multifunctional Hierarchical Nanostructures on Macroscale Substrates", Journal of Materials Chemistry A, 1(21), 6416, 2013.

[165] Liou, K.-N., & Yang, P., "Ice in the Earth's Atmosphere, Light Scattering by Ice Crystals", Cambridge University Press, Cambridge, 1–57, 2016.

[166] Demianets, L. N., Kostomarov, D. V., Kuz'mina, I. P., & Pushko, S. V., "Mechanism of Growth of ZnO Single Crystals from Hydrothermal Alkali Solutions", Crystallography Reports, 47(S1), 86–98, 2002.

[167] Laudise, R. A., Kolb, E. D., & Caporaso, A. J., “Hydrothermal Growth of Large Sound Crystals of Zinc Oxide”, Journal of the American Ceramic Society, 47(1), 9–12, 1964.

[168] Kolb, E. D., & Laudise, R. A., “Hydrothermally Grown ZnO Crystals of Low and Intermediate Resistivity”, Journal of the American Ceramic Society, 49(6), 302–305, 1966.

[169] Zhang, D. H., Wang, Q. P., & Xue, Z. Y., “Photoluminescence of ZnO Films Excited with Light of Different Wavelength”, Applied Surface Science, 207(1-4), 20–25, 2003.

[170] Ginting, R.T, Lee, H.B., Tan, S.T., Tan, C.H., et al., “A Simple Approach Low-Temperature Solution Process for Preparation of Bismuth Doped ZnO Nanorods and Its Application In Hybrid Solar Cells”, J. Phys. Chem. C, 120 (2016), 771–780, 2016.

[171] Shen, P., Tong, Y., Sheng, D., Tang, X., Shao, L., Duan, H., “Modulating the Morphology of ZnO Nanorod Arrays on SiOx-maskpatterned GaN Template”, Mater. Lett. 195, 22-25, 2017.

[172] Fan, J., Li, T., Heng, H., “Hydrothermal Growth of ZnO Microrods on ITO-coated Glass Substrate”, Appl. Phys. A 119 (2015) 185–192, 2015.

[173] Barnett, C.J., Mourgelas, V., McGettrick, J.D., Maffeis, T.G.G., Barron, A.R., & Cobley, R.J., “The Effects of Vacuum Annealing on the Conduction Characteristics of ZnO Nanorods”, Mater. Lett. 243 (2019) 144–147, 2019.

[174] Neykova, N., Chang, Y., Buryi, M., Davydova, M., Kucerkova, R., Simek, D., Remes, Z., Pop-Georgievski, O., “Study of ZnO Nanorods Grown Under UV Irradiation”, Appl. Surf. Sci., 472 (2019), 105–111, 2019.

[175] Djurišić, A. B., Leung, Y. H., Tam, K. H., Hsu, Y. F., Ding, L., Ge, W. K., … Phillips, D. L., “Defect Emissions in ZnO Nanostructures”, Nanotechnology, 18(9), 095702, 2007.

[176] Zhou, H., Alves, H., Hofmann, D.M., Kriegseis, W., Meyer, B K., Kaczmarczyk, G., and Hoffmann, A., “Behind The Weak Excitonic Emission of ZnO Quantum Dots: ZnO/Zn(OH)2ZnO/Zn(OH)2 Core-shell Structure”, Appl. Phys. Lett., 80(2), 210, 2002.

[177] Ahn, H.A., Kim, Y.Y., Kim, D.C., Mohanta, S.K., Cho, H.K.,, “A Comparative Analysis of Deep Level Emission in ZnO Layer Deposited by Various Methods”, J. Appl. Phys. 105(1), 013502, 2009.

[178] Kuriakose, S., Satpati, B., Mohapatra, S., "Highly Efficient Photocatalytic Degradation of Organic Dyes by Cu Doped ZnO Nanostructures", Chem. Phys., 17 (38), 25172–25181, 2015.

[179] Srinatha, N., Raghu, P., Mahesh, H., Angadi, B., "Spin-coated Al-doped ZnO Thin Films for Optical Applications: Structural, Micro-structural, Optical and Luminescence Studies", J. Alloy. Comp., 722, 88–895, 2017.

[180] Das, R., Kumar, A., Kumar, Y., Sen, S., & Shirage, P. M., "Effect of Growth Temperature on the Optical Properties of ZnO Nanostructures Grown by Simple Hydrothermal Method", RSC Advances, 5(74), 60365–60372, 2015.

[181] Zhang, S.B., Wei, S.H., and Zunger, A., "Intrinsic n-type Versus p-type Doping Asymmetry And The Defect Physics of ZnO", Phys. Rev. B, 63(7), 075205, 2001.

[182] Djurisic, A.B., Leung, Y.H., "Optical Properties of ZnO Nanostructures", Nanomicro Small, 2(8-9), 944-961, 2006.

[183] Sajjad, M., Ullah, I., Khan, M.I., Khan, J., Khan, M.Y., Qureshi, M.T., "Structural and Optical Properties of Pure and Copper Doped Zinc Oxide Nanoparticles", Results Phys., 9, 1301–1309, 2018.

[184] Cao, B., Cai, W., & Zeng, H., "Temperature-dependent Shifts of Three Emission Bands for ZnO Nanoneedle Arrays", Appl Phys Lett 2006, 88(16), 161101, 2006.

[185] Vempati, S., Mitra, J., & Dawson, P., "One-step Synthesis of ZnO nanosheets: a Blue-white Fluorophore", Nanoscale Res Lett 7, 470, 2012.

[186] Vlasenko, LS., & Watkins, G.D., "Optical Detection of Electron Paramagnetic Resonance in room-Temperature Electron-Irradiated ZnO", Phys Rev B, 71(12), 125210, 2005.

[187] Li, D., Leung, Y. H., Djurišić, A. B., Liu, Z. T., Xie, M. H., Shi, S. L., … Chan, W. K., "Different Origins of Visible Luminescence in ZnO Nanostructures Fabricated by the Chemical and Evaporation Methods", Applied Physics Letters, 85(9), 1601–1603, 2004.

[188] Norberg, NS., Gamelin, DR., Cheah, KW., Kwok, WM., Phillips, D.L., "Influence of Surface Modification on The Luminescence of Colloidal ZnO Nanocrystals", J. Phys. Chem. B, 109(44), 20810–20816, 2005.

[189] Greene, L.E., Law, M., Goldberger. J., Kim, F., Johnson, J.C., Zhang, Y., Saykally, R.J., Yang, P., "Low-temperature Wafer-scale Production of ZnO Nanowire Arrays", Angew Chem Int Ed Engl, 42(26), 3031-3034, 2003.

[190] Heo, Y. W., Norton, D. P., & Pearton, S. J., “Origin of Luminescence in ZnO Thin Film Grown by Molecular-Beam Epitaxy”, Journal of Applied Physics, 98(7), 073502, 2005.

[191] Raji, R., & Gopchandran, K. G., “ZnO Nanostructures with Tunable Visible Luminescence: Effects of Kinetics of Chemical Reduction and Annealing”, Journal of Science: Advanced Materials and Devices, 2(1), 51–58, 2017.

[192] Reynolds, D.C., Look, D.C., Jogai, B., “Fine Structure On The Green Band in ZnO”, J. Appl. Phys., 89 (2001), 6189-6191, 2001.

[193] Biroju, R. K., & Giri, P. K., “Strong Visible and Near Infrared Photoluminescence from ZnO Nanorods/Nanowires Grown on Single Layer Graphene Studied Using Sub-Band Gap Excitation”, Journal of Applied Physics, 122(4), 044302., 2017.

[194] Gomi, M., Oohira, N., Ozaki, K., Koyano, M., “Photoluminescent and Structural Properties of Precipitated ZnO Fine Particles”, Jpn. J. Appl. Phys., 42(2A), 481-485, 2003.

[195] Vanheusden, K., Seager, C.H., Warren, W.L., Tallant, D., Voigt, J.A., “Corrolation Between Photoluminescence and Oxygen Vacancies in ZnO Phosphors”, Appl. Phys. Lett., 68, 403-405, 1996.

[196] Yang, J. H., Zheng, J. H., Zhai, H. J., & Yang, L. L., “Low Temperature Hydrothermal Growth and Optical Properties of ZnO Nanorods”, Crystal Research and Technology, 44(1), 87–91, 2009.

[197] Fang, T.-H., & Kang, S.-H., “Optical and Physical Characteristics of In-doped ZnO Nanorods”, Current Applied Physics, 10(4), 1076–1086, 2010.

[198] Kurudirek, S. V., Pradel, K. C., & Summers, C. J., “Low-temperature Hydrothermally Grown 100 μm Vertically Well-Aligned Ultralong and Ultradense ZnO Nanorod Arrays With Improved PL Property”, Journal of Alloys and Compounds, 702, 700–709, 2017.

[199] Bagnall, D. M., Chen, Y. F., Zhu, Z., Yao, T., Shen, M. Y., & Goto, T., “High Temperature Excitonic Stimulated Emission From ZnO”, Applied Physics Letters, 73(8), 1038–1040, 1998.

[200] Zheng, Z., Lin, J., Song, X., & Lin, Z., “Optical Properties of ZnO Nanorod Films Prepared by CBD Method”, Chemical Physics Letters, 712, 155-159, 2018.

[201] Xia, C., Hu, C., & Zhou, P., "Low-temperature Growth and Optical Properties of Ce-doped ZnO Nanorods", Journal of Experimental Nanoscience, 8(1), 69–76, 2013.

[202] Chen, T., & Liu, Y., "Semiconductor Nanocrystals and Metal Nanoparticles: Physical Properties and Device Applications", CRC Press, Boca Raton, p.56, 2016.

[203] Jay Chithra, M., Sathya, M., & Pushpanathan, K., "Effect of pH on Crystal Size and Photoluminescence Property of ZnO Nanoparticles Prepared by Chemical Precipitation Method", Acta Metallurgica Sinica (English Letters), 28(3), 394–404, 2015.

[204] Khorsand Zak, A., Razali, R., Abd Majid, W. H. B., & Darroudi, M., "Synthesis and Characterization of a Narrow Size Distribution of Zinc Oxide Nanoparticles", International Journal of Nanomedicine, 6 ,1399-1403, 2011.

[205] Roza, L., Rahman, M. Y. A., Umar, A. A., & Salleh, M. M., "Direct Growth of Oriented ZnO Nanotubes by Self-selective Etching at Lower Temperature for Photo-Electrochemical (PEC) Solar Cell Application", Journal of Alloys and Compounds, 618, 153–158, 2015.

[206] Shabannia, R., Hassan, H.A., "Characteristics of Photoconductive UV Photodetector Based on ZnO Nanorods Grown on Polyethylene Naphthalate Substrate by Chemical Bath Deposition Method", Electron. Mater. Lett., 10(40), 837–843, 2014.

[207] Silva-Lopez, H. E., Marcelino, B. S., Guillen-Cervantes, A., Zelaya-Angel, O., & Ramirez-Bon, R., "Physical Properties of Sputtered Indium-doped ZnO Films Deposited on Flexible Transparent Substrates", Materials Research, 21(6), 2018.

[208] Foo, K.L., Hashim, U., Muhammad, K., et al., "Sol–gel Synthesized Zinc Oxide Nanorods and Their Structural and Optical Investigation for Optoelectronic Application", Nanoscale Res Lett., 9, 429, 2014.

[209] Singh, A. V., Mehra, R. M., Wakahara, A., & Yoshida, A., "P-Type Conduction in Codoped ZnO Thin Films", Journal of Applied Physics, 93(1), 396–399, 2013.

[210] Fudzi, M. L., Zainal, Z., Lim, H.N., Chang, S. K., Holi, A. M, Ali, S.M., "Effect of Temperature and Growth Time on Vertically Aligned ZnO Nanorods by Simplified Hydrothermal Technique for Photoelectrochemical Cells", Materials (Basel), 11(5), 704, 2018.

[211] Zhu, B. L., Sun, X. H., Guo, S. S., Zhao, X. Z., Wu, J., Wu, R., and Liu, J., "Effect of Thickness on the Structure and Properties of ZnO Thin Films Prepared by Pulsed Laser Deposition", Jpn. J. Appl. Phys., 45, 7860, 2006.

[212] Caglar, M., Ilican, S., Caglar, Y., & Yakuphanoglu, F., "Electrical Conductivity and Optical Properties of ZnO Nanostructured Thin Film", Applied Surface Science, 255(8), 4491–4496, 2009.

[213] Abdulrahman, A. F., Ahmed, S. M., & Almessiere, M. A., "Effect of The Growth Tıme on The Optıcal Properties of ZnO Nanorods Grown By Low Temperature Method, Digest Journal of Nanomaterials and Biostructures", 12(4), 1001-1009, 2017.

[214] Jeong, C., Kim, H.S., Chang, D.R., Kamisako, K., "Effect on Al2O3 Doping Concentration of RF Magnetron Sputtered ZnO:Al Films for Solar Cell Applications", Jpn. J. Appl. Phys., 47(7), 5656-5658, 2008.

[215] Wei, T., Lan, P., Yang, Y., Zhang, X., Tan, R., Li, Y., & Song, W., "Tailoring The Refractive Index of Aluminum Doped Zinc Oxide Thin Films by Co-Doping With Titanium", Applied Surface Science, 263, 210–214, 2012.

[216] Sivapriya, S., & Balasubramanian, K., "Preparation and Characterization of ZnO Thin Films by Using Two Different Techniques", IOSR Journal of Applied Physics, 02, 42-44, 2017.

[217] Idiawati, R., Mufti, N., Taufiq, A., Wisodo, H., Laila, I.K.R., Sunaryono, S., Fuad, A., "Effect of Growth Time on the Characteristics of ZnO Nanorods", IOP Conf. Series: Materials Science and Engineering, 202, 012050, 2017.

[218] Umar, A., Rahman, M., Alhajry, A., & Hahn, Y., "Highly-sensitive Cholesterol Biosensor Based on Well-Crystallized Flower-Shaped ZnO Nanostructures", Talanta, 78(1), 284–289, 2009.

[219] Nyquist, R.A., and Kagel, R.O., "Infrared Spectra of Inorganic Compounds", Academic Press, Inc., New York, London, 1971.

[220] Ni, Y., Wei, X., Hong, J., & Ye, Y., "Hydrothermal Preparation and Optical Properties of ZnO Nanorods", Materials Science and Engineering: B, 121(1-2), 42–47,2005.

[221] Khayyat, S. A., Abaker, M., Umar, A., Alkattan, M. O., Alharbi, N. D., & Baskoutas, S., "Synthesis and Characterizations of Cd-Doped ZnO Multipods for Environmental Remediation Application", Journal of Nanoscience and Nanotechnology, 12(11), 8453–8458, 2012.

[222] Elfakir, A., Tlemçani, T. S., Benamar, E. B., Belayachi, A., Gutierrez-Berasategui, E., Schmerber, G., "Structural, electrical and optical properties of sprayed Nd–F codoped ZnO thin films", Journal of Sol-Gel Science and Technology, 73(3), 557–562, 2014.

[223] Shettigar, N., Pramodini, S., Kityk, I. V., Abd-Lefdil, M., et al., "Tuning the Third-Order Nonlinear Optical Properties of In:ZnO Thin Films by 8 MeV Electron Beam İrradiation", Journal of Physics and Chemistry of Solids, 110, 260–265. 2017.

[224] Shan, F. K., & Yu, Y. S., "Band Gap Energy of Pure and Al-doped ZnO Thin Films", Journal of the European Ceramic Society, 24(6), 1869–1872, 2004.

[225] Xie, G. C., Fanga, L., Peng, L. P., Liu, G. B., Ruan, H. B., Wu, F., & Kong, C. Y., "Effect of In-doping on the Optical Constants of ZnO Thin Films", Physics Procedia, 32, 651–657, 2012.

[226] Benouis, C.E., Sanchez-Juarez, A., and Aida, M.S., "Physics Properties Comparison Between Undoped ZnO and AZO, IZO Doped Thin Films Prepared By Spray Pyrolysis", Journal of Applied Sciences, 7, 220-225, 2007.

[227] Major, S., Banerjee, A., Chopra, K. L., & Nagpal, K. C., "Thickness-Dependent Properties of Indium-doped ZnO Films", Thin Solid Films, 143(1), 19–30, 1986.

[228] Bharti, G. P., & Khare, A., "Structural and Linear and Nonlinear Optical Properties of Zn1-x AlxO ($0 \leq x \leq 010$) Thin Films Fabricated via Pulsed Laser Deposition Technique", Optical Materials Express, 6(6), 2063, 2016.

[229] Medjaldi, M., Touil, O., Boudine, B., et al,. "Study of Undoped and Indium Doped ZnO Thin Films Deposited by Sol Gel Method", Silicon 10, 2577–2584, 2018.

[230] Tokumoto, M., Smith, A., Santilli, C., Pulcinelli, S., et al, "Structural Electrical and Optical Properties of Undoped and Indium Doped ZnO Thin Films Prepared by The Pyrosol Process at Different Temperatures", Thin Solid Films, 416(1-2), 284–293, 2002.

[231] Shinde, S. S., Shinde, P. S., Bhosale, C. H., & Rajpure, K. Y., "Optoelectronic Properties of Sprayed Transparent and Conducting Indium Doped Zinc Oxide Thin Films", Journal of Physics D: Applied Physics, 41(10), 105109, 2008.

[232] Saw, K. G., Aznan, N. M., Yam, F. K., Ng, S. S., & Pung, S. Y., "New Insights on the Burstein-Moss Shift and Band Gap Narrowing in Indium-Doped Zinc Oxide Thin Films", PLOS ONE, 10(10), e0141180, 2015.

[233] Burstein, E., “Anomalous Optical Absorption Limit in InSb”, Physical Review, 93(3), 632–633, 1954.

[234] Benouis, C.E., Benhaliliba, M., Sanchez Juarez, A., Aida, M.S., Chami, F., et al., “The Effect of Indium Doping on Structural, Electrical Conductivity, Photoconductivity and Density of States Properties of ZnO Films”, J. Alloys Compd., 490, 62, 2010.

[235] Gupta, R.K., Ghosh, K., Patel, R., Mishra, S.R., Kahol, P.K., “Band Gap Engineering of ZnO Thin Films by In2O3 Incorporation”, J. Crystal Growth, 310, 3019, 2008.

[236] Xue, S.W., Zu, X.T., Zheng, W.G., Deng, H.X., Xiang, X., “Effects of Annealing and Dopant Concentration on the Optical Characteristics of ZnO:Al Thin Films by Sol–Gel Technique”, Physica B, 382, 201, 2006.

[237] Sernelius, B.E., Berggren, K.-F., Jin, Z.-C., Hamberg, I., and. Graqvist, C.G., “Band-gap Tailoring of ZnO by Means of Heavy Al Doping”, Phys. Rev. B, 37, 10244–10248, 1998.

[238] Ghosh, A., & Choudhary, R. N. P., “Optical Emission and Absorption Spectra of Zn–ZnO Core-shell Nanostructures”, Journal of Experimental Nanoscience, 5(2), 134–142, 2010.

[239] Abdolahzadeh Ziabari, A., and Rozati, S.M., “Carrier Transport and Band Gap Shift in N-type Degenerate ZnO Thin Films: The Effect of Band Edge Non Parabolicity”, Physica B, 407(23), 4512–4517, 2012.

[240] Ferro, R., “Some Physical Properties of F-doped CdO Thin Films Deposited by Spray Pyrolysis”, Thin Solid Films, 347(1-2), 295–298, 1999.

[241] Ferro, R., & Rodríguez, J., “Influence of F-doping on the Transmittance and Electron Affinity of CdO Thin Films Suitable for Solar Cells Technology”, Solar Energy Materials and Solar Cells, 64(4), 363–370, 2000.

[242] Joseph, B., Manoj, P. K., & Vaidyan, V. K., “Studies on Preparation and Characterization of Indium Doped Zinc Oxide films by Chemical Spray Deposition”, Bulletin of Materials Science, 28(5), 487–493, 2005.

[243] Hamberg, I., Granvist, C.G., “Evaporated Sn-doped In2O3 films: Basic Optical Properties and Applications to Energy-Efficient Windows”, J. Appl. Phys. 60, 123, 1986.

[244] Yıldırım, M. A., Akaltun, Y., Ates, A., "Characteristics of SnO2 Thin Films Prepared by SILAR", Solid State Sciences, 14(9), 1282-1288, 2012.

[245] Alexander, T. P., Bukowski, T. J., Uhlmann, D. R., Teowee, G., et. al., "Dielectric Properties of Sol-Gel Derived ZnO Thin Films", ISAF '96. Proceedings of the 9th IEEE International Symposium on Applications of Ferroelectrics, USA, pp. 585-588, 1996.

[246] Hutson, A. R., "Piezoelectricity and Conductivity in ZnO and CdS", Physical Review Letters, 4(10), 505–507, 1960.

[247] Caglar, M., Ilican, S., Caglar, Y., et al. "The effects of Al Doping on The Optical Constants of ZnO Thin Films Prepared by Spray Pyrolysis Method", J Mater Sci: Mater Electron, 19(8-9), 704–708, 2008.

[248] Kim, H., Pique, A., Horwitz, J.S., Murata, H., Kafafi, Z.H., Gilmore, C.M., & Chrisey, D.B., "Effect of Aluminum Doping on Zinc Oxide Thin Film Grown by Pulsed Laser Deposition for Organic Light Emitting Devices", Thin Solid Films, 377–378, 798–802, 2000.

[249] Qiao, Z., Agashe, C., and Mergel, D., "Dielectric Modeling of Transmittance Spectra of Thin ZnO:Al films", Thin Solid Films, 496(2), 520–525, 2006.

[250] Hickernell, F.S., "ZnO Processing for Bulk and Surface-Wave Devices", Ultrasonics Symposium, 1980, Boston, MA, USA, pp. 785-794, 1980.

[251] Shrisha, B. V., Bhat, S., Kushavah, D., & Gopalakrishna Naik, K., "Hydrothermal Growth and Characterization of Al-doped ZnO Nanorods", Materials Today: Proceedings, 3(6), 1693–170, 2016.

CURRICULUM VITAE

PERSONAL INFORMATION

Name Surname : Tuğçe BAYRAKTAR

Date of Birth : 18/03/1994

E-mail : tuci.bayraktar@gmail.com

EDUCATION

2018-ongoing : **Ankara Yıldırım Beyazıt University**, Ankara, Turkey

M.Sc., Materials Engineering

Thesis: "**Growth and Characterization of Undoped and Indium Doped Zinc Oxide Thin Films Grown by Hydrothermal Method**"

2013-2018 : **Ankara Yıldırım Beyazıt University**, Ankara, Turkey

B.Sc., Metallurgical and Materials Engineering, June 2018

Graduation Project: "**Production and Characterization of Alumina - Glass Composites**"

INTERNSHIPS

August-September 2017 : **ODAK Kompozit Teknolojileri A.Ş**

July – August 2016 : **TUSAŞ Türk Havacılık ve Uzay Sanayii A.Ş**